Lipid transfer proteins and a PI 4-kinase initiate nuclear phosphoinositide signaling

Noah D. Carrillo[1,2,4], Mo Chen[1,3,4], Tianmu Wen[1], Poorwa Awasthi[1], Trevor J. Wolfe[1], Colin Sterling[1,2], Vincent L. Cryns[1,2,5,*] and Richard A. Anderson[1,5,*]

[1]University of Wisconsin Carbone Cancer Center, University of Wisconsin-Madison, School of Medicine and Public Health; 1111 Highland Avenue, Madison, WI 53705, USA
[2]Department of Medicine, University of Wisconsin-Madison, School of Medicine and Public Health; 1111 Highland Avenue, Madison, WI 53705, USA
[3]Current Address: Department of Pharmacology, Joint Laboratory of Guangdong-Hong Kong Universities for Vascular Homeostasis and Diseases, School of Medicine, Southern University of Science and Technology, Shenzhen 518055, China
[4]Co-first authors
[5]These authors contributed equally to this work
[*]Correspondence: vlcryns@medicine.wisc.edu; raanders@wisc.edu

Summary 150 max

Phosphoinositide (PIP_n) messengers are present in non-membranous regions of nuclei, where they are assembled into a phosphatidylinositol (PI) 3-kinase (PI3K)/Akt pathway that is distinct from the cytosolic membrane-localized pathway. In the nuclear pathway, PI kinases/phosphatases bind the p53 tumor suppressor protein (wild-type and mutant) to generate p53-PIP_n complexes that regulate Akt activation. However, this pathway is dependent on poorly characterized nuclear PIP_n pools. Here we report that PI transfer proteins (PITPs), which transport PI between membranes to enable membrane-localized PIP_n synthesis, accumulate in the nucleoplasm in response to stress and supply nuclear PIP_n pools. PITPα/β and the PI 4-kinase PI4KIIα bind p53 and are required to generate p53-PI4P, which is further phosphorylated to synthesize p53-PIP_n complexes that regulate nuclear Akt activation and stress-resistance. Remarkably, PITPα/β and PI4KIIα initiate PIP_n-linkage to multiple proteins that are detectable by immunoblotting and [^{3}H]*myo*-inositol metabolic labeling and are resistant to denaturation, suggesting a posttranslational modification.

Key words

Phosphoinositide; phosphatidylinositol transfer protein; PIP_n-linked proteins, p53; PI4,5P_2; PI3,4,5P_3; nucleus; cell stress; Akt

In brief

Phosphatidylinositol transfer proteins initiate the nuclear PIP_n-linked protein network in membrane-free regions.

59 **Main text**
60

61 Phosphoinositide (PIP_n) lipids are synthesized from phosphatidylinositol (PI) in
62 membranes by PIP kinases to produce a second messenger network comprised of seven
63 distinct isomers that play key roles in many cellular pathways[1]. Cytosolic class I PI 3-
64 kinases (PI3Ks) catalyze the synthesis of PI3,4,5P_3, which leads to the recruitment and
65 activation of the serine/threonine kinases phosphoinositide-dependent kinase 1 (PDK1),
66 mTOR Complex 2 (mTORC2), and Akt at membranes[2-8]. Akt in turn phosphorylates many
67 substrates, such as forkhead box O (FOXO) proteins, tuberous sclerosis complex 2
68 (TSC2), and BCL2-associated agonist of cell death (BAD), to promote cell growth and
69 inhibit apoptosis[4]. This membrane-localized PI3K/Akt pathway is often hyperactivated in
70 cancer and class I PI3K inhibitors are currently in the clinic[9, 10].

71 Akt is also activated in the nucleus[11-16]. Recent studies have identified a non-
72 membranous nuclear PI3K/Akt pathway that is dependent on p53[17, 18], a tumor
73 suppressor that is frequently mutated in cancer, resulting in gain-of-function oncogenic
74 acitivities[19, 20]. In this nuclear pathway, wild-type and mutant p53 are sequentially modified
75 by PIP_ns and their associated PIP kinases/phosphatases. The type I PI4P 5-kinase α
76 (PIPKIα) directly interacts with p53 and generates the p53-PI4,5P_2 complex (p53-PIP_n
77 signalosome) in response to stress[18]. PI5P4Kβ has also been functionally linked to p53
78 as deletion of both genes is lethal in mice, but the mechanism is poorly defined[21]. The
79 nuclear PI 3-kinase IPMK acts on p53-PI4,5P_2 to synthesize p53-PI3,4,5P_3 complexes,
80 which then recruit and activate Akt in the non-membranous nucleoplasm[17, 18]. The nuclear

81 Akt pathway is insensitive to PI3K inhibitors currently in the clinic[17], highlighting its
82 therapeutic importance.

83 Although multiple PIP_ns and PIP kinases/phosphatases are present in the nucleoplasm[16,
84 22-24], the mechanism by which the pool of nuclear PIP_ns is established and its molecular
85 characteristics are unknown. Unlike the most abundant nuclear phospholipid,
86 phosphatidylcholine (PC), which is synthesized *in situ* in the nucleus[25-27], PI represents a
87 minor fraction of free nuclear phospholipids and is synthesized in the endoplasmic
88 reticulum (ER)[28] which is contiguous with the nuclear envelope[29], suggesting that PI is
89 transported into the nucleoplasm. In the cytosol, PI is transported from the ER to
90 membranes and between membranes by a family of lipid transfer proteins, the
91 phosphatidylinositol transfer proteins (PITPs). To date, research has focused on cytosolic
92 PITP function[30-32]. Intriguingly, PITPβ interacts with p53[33], prompting us to investigate the
93 functional role for PITPs in regulating the synthesis of p53-PIP_n complexes and nuclear
94 PIP_n signaling. Here we demonstrate that the class I PITPs are specifically required to
95 generate the non-membranous nuclear PIP_n pools in the nucleus. In addition, the class I
96 PITPs and a PI 4-kinase, PI4KIIα, function together to generate the nuclear PIP_n pools.
97 Both class I PITPs and PI4KIIα bind to p53 and to each other and are necessary to
98 synthesize the nuclear p53-PIP_n complexes that regulate nuclear Akt activation.
99 Strikingly, the PIP_ns on p53 and in these nuclear pools are coupled to proteins.

100 **The nuclear localization of PITPs is regulated by cellular stress**

101 The PITP family is composed of five members that are subdivided into two classes that
102 exchange PI for PC (Class I, the single domain PITPα and PITPβ isoforms) or PI for

103 phosphatidic acid (PA) (Class II, the single domain PITP cytoplasmic 1 (PITPNC1) and
104 multi-domain PITP membrane associated 1 (PITPNM1), and PITP membrane associated
105 2 (PITPNM2) isoforms with C-terminal extensions)[34] (Fig. 1a). The most homologous
106 members within the PITP family, PITPα/β/NC1, were expressed in the nucleus under
107 basal conditions, and the nuclear levels of each isoform and PI4,5P_2 were increased by
108 cisplatin as determined by immunofluorescence (IF) (Fig. 1b,c and Extended Data Fig.
109 1a-c). The PITPα and PITPβ antibodies are specific for IF staining as KD of the PITPs
110 eliminated staining (Extended Data Fig. 1d-e). The PITPα antibody had partial cross
111 reactivity for PITPβ by Western blot (Extended Data Fig. 1f) but was specific for these
112 PITPs. Nuclear fractionation (Extended Data Fig. 1g) and confocal 3D sectioning
113 (Extended Data Fig. 2a-d) confirmed the enhanced nuclear levels of PITPα/β in response
114 to genotoxic stress, which were observed in all cell lines tested regardless of tissue of
115 origin or p53 mutational status (Extended Data Fig. 3a,b). Multiple cellular stressors
116 (genotoxic, oxidative and ferroptotic) increased the nuclear levels of PITPα/β, indicating
117 a fundamental nuclear role for the PITPs in the cellular stress-response (Extended Data
118 Fig. 4a,b). Moreover, cell stress induced the targeting of PITPs to the non-membranous
119 nucleoplasm in all cell lines examined (Fig. 1d and Extended Data Fig. 4c-e).

120 **PITPs regulate the nuclear PIP_n pool**

121 All PIP_n isomers except PI3,5P_2 have been detected in the nucleus by multiple methods[16-
122 18, 22, 23, 27, 35]. Among these, PI4,5P_2 forms distinctive nuclear foci that colocalize with
123 nuclear speckle markers in regions devoid of membranes[16-18, 23, 36]. PI is the precursor of
124 all PIP_ns[37] and together with our observation that cellular stress induces the nuclear

125 localization of PITPs, we investigated the role of PITPs in regulating the nuclear PIP_n pool.
126 Silencing PITPα or PITPβ reduced basal and stress-induced nuclear $PI4,5P_2$ levels, while
127 combined knockdown (KD) of both PITPα and PITPβ further decreased nuclear $PI4,5P_2$
128 levels compared to the individual KD (Fig. 1e,f and Extended Data Fig. 5a). In contrast,
129 PITPNC1 KD had no effect on basal nuclear $PI4,5P_2$ levels and minimal effect on stress-
130 induced $PI4,5P_2$ levels (Fig. 1e,f). Combined KD of PITPα and PITPβ also suppressed
131 stress-induced nuclear levels of PI4P and $PI3,4,5P_3$ (Fig. 1g and Extended Data Fig. 5b).
132 Combined KD of PITPα and PITPβ robustly inhibited stress-induced nuclear $PI4,5P_2$
133 generation in transformed and untransformed cells independent of p53 mutational status
134 (Fig. 1h,i and Extended Data Fig. 5c,d). These results demonstrate that PITPs are
135 necessary to generate the nuclear PIP_n pools that are detected by specific PIP_n antibodies
136 (Fig. 1j).

137 **PITPα/β bind p53 and their interaction is regulated by cellular stress**

138 Together with the reported interaction of PITPβ and p53[33], the role of PITPs in regulating
139 nuclear PIP_n levels suggests PITPs may play a functional role in generating nuclear p53-
140 PIP_n complexes. To explore this, we investigated the interaction of p53 with all five PITPs
141 using multiple approaches. Proximity ligation assay (PLA) is an established approach to
142 detect posttranslational modifications (PTMs) on proteins and molecules in close
143 proximity *in situ*, although the technical limitations of this approach do not certify a direct
144 interaction alone[35, 38]. PLA demonstrated class I PITPs (PITPα and PITPβ), but not class
145 II PITPs (PITPNCI, PITPNM1 and PITPNM2), associated with mutant p53 ($p53^{mt}$) and
146 wild-type p53 ($p53^{wt}$) in the nucleus as indicated by PLA foci, and that their association

147 was enhanced by cisplatin (Fig. 2a,b and Extended Data Fig. 6a-c). Notably, the
148 association of PITPα/β with $p53^{wt}$ was minimal under basal conditions and dramatically
149 increased by stress, while PITPα/β associated constitutively with $p53^{mt}$ with a modest
150 increase in response to stress. Like the nuclear localization of PITPs (Fig. 1d, Extended
151 Data Fig. 2a-d and Extended Data Fig. 4d,e), the PITPα/β-p53 PLA complexes were
152 present in the nucleoplasm in regions distinct from the nuclear envelope (Fig. 2c,
153 Extended Data Fig. 6d-f, and Supplementary Video 1-2).

154 The PITPα/β-p53 complex was next examined by immunoprecipitation (IP). Consistent
155 with the PLA data, class I, but not class II PITPs, bound $p53^{wt}$ and $p53^{mt}$, and these
156 interactions were increased by stress in all cell lines examined (Fig. 2d-f, h-i and Extended
157 Data Fig. 7a,b,e-n). Although nuclear levels of PITPα/β and PITPNC1 increased in
158 response to stress (Fig.1b,c and Extended Data Fig. 1a), the interaction with p53 was
159 specific for the class I PITPs, indicating specificity within the family. Moreover, the small
160 heat shock proteins (sHSPs) Hsp27 and αB-crystallin, which stabilize the p53-PIP_n
161 complex[18], were also detected as stress-regulated components of the PITPα/β-p53
162 complex (Fig. 2d,g,h,j,k and Extended Data Fig. 7a,c,d). Additionally, *in vitro* binding
163 studies with recombinant PITPα/β proteins and p53 demonstrated a high-affinity,
164 saturable binding of class I PITPs to p53 (Fig. 2l-o). Consistent with these results, PITPα
165 and PITPβ, but not PITPNC1, bound p53 with high affinity as determined by microscale
166 thermophoresis (MST) and these interactions were regulated by PI (Table 1). Collectively,
167 these data show that PITPα/β form a nuclear complex with p53 in response to stress and
168 that PI loading of PITPs regulates these interactions (Fig. 2p).

169 **PITPα/β control the PIP_n linkage to p53 and other proteins**

170 As PITPα/β regulate nuclear PIP_n levels and bind to p53 in the nucleus, we examined the
171 potential role of PITPα/β in regulating the PIP_n interactions with p53, which stabilize p53[18].
172 The p53-PIP_n complexes[17, 18] were first analyzed by PLA. Single or combined KD of
173 PITPα/β, but not PITPNC1, reduced or largely eliminated, respectively, $p53^{mt}$-PI4,5P_2 and
174 $p53^{mt}$-PI3,4,5P_3 complexes detected by PLA; combined KD of PITPα/β disrupted $p53^{mt}$-
175 PIP_n complexes to a similar degree as p53 KD (Fig. 3a-c and Extended Data Fig. 8a,b).
176 Similar results were observed in $p53^{wt}$ cells: individual or combined PITPα/β KD inhibited
177 $p53^{wt}$-PI4,5P_2 and $p53^{wt}$-PI3,4,5P_3 complexes (Fig. 3d-f and Extended Data Fig. 8c). We
178 next quantified the cisplatin-induced PIP_n isoforms linked to p53 by p53-IP followed by
179 simultaneous Western blotting (WB) with antibodies (Abs) against specific PIP_n isoforms
180 detected with fluorescently labeled secondary Abs (IP fluorescent-WB) (Fig. 3g and
181 Extended Data Fig. 8d). KD of PITPα or PITPβ markedly reduced the PI4P, PI4,5P_2 and
182 PI3,4,5P_3 that co-IPed with $p53^{mt}$ in response to genotoxic stress, while the combined KD
183 largely eliminated all PIP_ns associated with $p53^{mt}$ (Fig. 3h-k). To further define the p53-
184 PIP_n linkage, cells with $p53^{mt}$ were metabolically labeled with [^{3}H]*myo*-inositol, a standard
185 approach to specifically label phosphoinositides and their downstream metabolites in
186 cells[39-41]. p53 was IPed in labeled cells, and lysates were analyzed by WB after SDS-
187 PAGE, which revealed [^{3}H]*myo*-inositol incorporated into p53 that corresponded to the
188 cisplatin-induced PI4,5P_2 detected by WB (Fig. 3l,m). Similar observations were made in
189 cells with $p53^{wt}$: single or combined PITPα/β KD also inhibited cisplatin-stimulated $p53^{wt}$-
190 PI4,5P_2 complex formation (Fig. 3n,o). These findings indicate that class I PITPα and

191 PITPβ play a key role in the stress-responsive coupling of PIP_ns to $p53^{wt}$ and $p53^{mt}$
192 proteins, which are resistant to denaturation and SDS-PAGE analysis.

193 Consistent with the reported role of PIP_ns in stabilizing p53[18], KD of PITPα or PITPβ, but
194 not PITPNC1, modestly reduced $p53^{mt}$ levels in cells treated with cisplatin, while the
195 combined KD of PITPα and PITPβ robustly suppressed $p53^{mt}$ levels under basal and
196 stress conditions (Fig. 4a). The reduction in $p53^{mt}$ levels induced by combined KD of
197 PITPα and PITPβ was not rescued by the MDM2 inhibitor Nutlin3 (Extended Data Fig.
198 8e), indicating a MDM2-independent mechanism. The induction of $p53^{wt}$ by cisplatin was
199 dramatic and was markedly inhibited by individual PITPα/β KD and abrogated by
200 combined PITPα/β KD (Fig. 4b). Remarkably, WBs of whole cell lysates with antibodies
201 specific for PI4P, $PI4,5P_2$ or $PI3,4,5P_3$ detected multiple protein bands, including some
202 that were enhanced by genotoxic stress after 24 hours (Fig. 4b-f and Extended Data Fig.
203 8f), indicating that PIP_ns are linked to additional proteins. Individual and combined KD of
204 PITPα/β robustly reduced the protein-coupled $PI4,5P_2$ levels and $PI4,5P_2$ bound to $p53^{mt}$
205 in response to stress (Fig. 4c,d). This phenotype was recapitulated using a lenti-CRISPR
206 knock out (KO) system. MDA-MB-231 Cas9 expressing cells (MDA-MB-231^{Cas9}) were
207 transfected with PITPβ gRNA or non-targeting gRNA to generate PITPβ KO and control
208 KO cells, respectively. Furthermore, single targeting of PITPα/β (KD or KO), but not
209 PITPNC1, reduced levels of multiple protein-bound PIP_ns (PI4P, $PI4,5P_2$, $PI3,4,5P_3$) and
210 many protein bands detected by PIP_n-specific antibodies in whole cell lysates, while
211 combined PITPα/β targeting had a more dramatic effect (Fig. 4b-f and Extended Data Fig.
212 8g). Combined KD of PITPα/β also reduced [^{3}H]*myo*-inositol labelling of total cellular
213 proteins isolated by two complementary approaches, chloroform/methanol extraction

214 followed by acetone precipitation and extraction of proteins from SDS-PAGE gels (Fig.
215 4g and Extended Data Fig. 9a,b). Overall, our findings point to a much broader signaling
216 pathway whereby PITPα/β regulate PIP_n linkage to multiple cellular proteins. Moreover,
217 the detection of PIP_n-p53 complexes by WB in which the linked PIP_n, is modified by PIP
218 kinases and phosphatases and by metabolic labeling with [^{3}H]*myo*-inositol after
219 denaturing/solvent extraction indicate a highly stable interaction where the inositol
220 headgroup is available for enzymatic modification and recognition by antibodies.

221 To further define these interactions, we utilized a p53 C-terminal domain (CTD) polybasic
222 domain mutant ($p53^{6Q}$), which disrupts PI4,5P_2 binding[17, 18]. Strikingly, the $p53^{6Q}$ mutant
223 in both $p53^{wt}$ and $p53^{mt}$ backgrounds formed more abundant $p53^{6Q}$-PI4P complexes
224 compared to the corresponding wild-type CTD domain p53 proteins (Extended Data Fig.
225 9c-f), highlighting the important distinction between PIP_n binding and linkage. However,
226 the $p53^{6Q}$-PI4P complexes were not phosphorylated further to $p53^{6Q}$-PI3,4,5P_3
227 complexes, likely by disrupting binding of PIPKIα and/or IPMK, which interact with the
228 p53 C-terminus[17, 18].

229 **PI4KIIα interacts with p53 and cooperates with PITPα/β to synthesize p53-PI4P**

230 As PITPα/β have been reported to cooperate with PI 4-kinases (PI4Ks) to synthesize
231 PI4P[34, 42, 43], we postulated that one or more PI4Ks acted in concert with PITPα/β to
232 generate p53-PI4P. To investigate this possibility, each of the four human PI4Ks[44] was
233 individually knocked down, and the effects on p53-PI4P complexes were determined by
234 PLA. Only individual KD of PI4KIIα suppressed basal and cisplatin-stimulated p53-PI4P
235 levels, while combined KD of PI4KIIα and PI4KIIIα reduced p53-PI4P levels to a

236 comparable degree as PI4KIIα KD alone (Fig. 5a,b and Extended Data Fig. 10a). p53-
237 PI4P synthesis requires the catalytic activity of PI4KIIα as the PI4KIIα inhibitors (PI-273
238 and NC03)[45, 46] prevented p53-PI4P and p53-PI4,5P_2 generation (Extended Data Fig.
239 10b-e). p53-PI4P is the substrate for PIPKIα to synthesize p53-PI4,5P_2, which stabilizes
240 p53[18]. Consistent with its role in generating p53-PI4P, PI4KIIα KD, but not KD of other
241 PI4Ks, inhibited cisplatin-stimulated p53 levels (Fig. 5c). Moreover, KD of PI4KIIα
242 mimicked the effects of PIPKIα KD in suppressing p53 induction by cisplatin, and
243 combined KD of PI4KIIα and PIPKIα was equivalent to either individual KD with regard to
244 p53 levels (Fig. 5d). In contrast to PI4KIIα KD which reduced p53-PI4P levels, KD of
245 PIPKIα enhanced p53-PI4P levels (Fig. 5e,f and Extended Data Fig. 10f). Functionally,
246 PI4KIIα co-IPed with $p53^{mt}$ and $p53^{wt}$, and these interactions were enhanced by genotoxic
247 stress (Fig. 5g). PI4KIIIα also co-IPed with $p53^{mt}$ and $p53^{wt}$, but PI4KIIIα KD did not affect
248 p53 or p53-PI4P levels or enhance the effects of PI4KIIα KD (Fig. 5a-c). Recombinant
249 PI4KIIα bound to p53 and was saturable with 8+/-2 nM affinity (Extended Data Fig. 11a
250 and Table 1) consistent with a specific and direct interaction. These findings indicate that
251 PI4KIIα binds to p53 with high affinity and is the PI 4-kinase that specifically synthesizes
252 p53-PI4P and contributes to p53 stabilization by generating the precursor for p53-PI4,5P_2.

253 PI4KIIα also directly bound to PITPα and PITPβ with high affinity, and these interactions
254 were enhanced by PI (Extended Data Fig. 11b,c and Table 1). Furthermore, KD of PI4KIIα
255 phenocopied the effects of combined KD of PITPα/β in inhibiting protein-PIP_n complex
256 formation detected by WB with PIP_n antibodies (Extended Data Fig. 11d). Similarly, KD
257 of PITPα or PI4KIIα in MDA-MB-231 cells with PITPβ KO further reduced the protein-PIP_n
258 signals by WB (Fig. 5h and Extended Data Fig. 11e). PI4KIIα KD also reduced nuclear

259 PI4,5P_2 content determined by IF (Fig. 5i and Extended Data Fig. 11f,g), indicating that
260 PI4KIIα, like PITPα/β, plays a key functional role in generating the nuclear PIP_n pools.
261 These data indicate that PITPα/β and PI4KIIα act in concert to initiate nuclear PIP_n
262 signaling on p53 and other cellular proteins (Fig. 5j).

263 **PITPα/β regulate p53-PIP_n signalosome formation and nuclear Akt activation to**
264 **inhibit stress-induced apoptosis**

265 The p53-PIP_n signalosome is regulated by cellular stress, leading to the formation of p53-
266 PI3,4,5P_3 complexes that recruit and activate Akt in the nucleus and protect cells from
267 stress-induced apoptosis[17]. The identification of class I PITPs as upstream regulators of
268 p53-PIP_n complex assembly implicates these lipid transfer proteins in nuclear Akt
269 activation. Consistent with this concept, individual KD of PITPα or PITPβ, but not
270 PITPNC1, suppressed stress-induced nuclear Akt activation quantified by nuclear
271 $pAkt^{S473}$ IF, an established approach[17], and the combined PITPα/β KD resulted in a more
272 robust loss of $pAkt^{S473}$ (Fig. 6a,b). These results were confirmed by WB (Extended Data
273 Fig. 11h). Similar results were obtained with multiple human cancer cell lines expressing
274 $p53^{mt}$ (Fig. 6c-e and Extended Data Fig. 5c). KD of $p53^{mt}$, PITPα or PITPβ, but not
275 PITPNC1, moderately reduced cell viability under basal conditions and sensitized MDA-
276 MB-231 cells to cisplatin treatment as did KO of PITPβ, while KD of PITPα in MDA-MB-
277 231 cells with PITPβ KO or combined PITPα/β KD in parental cells further decreased cell
278 viability (Fig. 6f-h, Extended Data Fig. 11i, and Extended Data Fig. 12a-g). The
279 cytotoxicity of $p53^{mt}$ KD and individual or combined PITPα/β KD was associated with a
280 corresponding increase in caspase 3 activity (Fig. 6i and Extended Data Fig. 12e-j),

281 indicating that PITPα/β KD triggers apoptosis and sensitizes cells to genotoxic stress.
282 These findings underscore the regulation of nuclear Akt activation by PITPα/β, which
283 confers resistance to genotoxic stress-induced apoptosis.

284 As PITPα/β exchange PI for PC, we investigated whether the PI transfer activity of these
285 PITPs was required to regulate nuclear PIP_n pools and nuclear Akt activation. For this,
286 we utilized the PITPα/β^{T59D} mutant that specifically disrupts PI binding[47-49]. Ectopically
287 expressed HA-tagged PITPα/β^{wt} interacted with $p53^{wt}$ and mutant $p53^{R175H}$, while the
288 corresponding PITPα/β^{T59D} mutants exhibited impaired interaction with p53 (Fig. 7a and
289 Extended Data Fig. 12k-m). Moreover, the reduction in the stress-induced nuclear
290 $PI4,5P_2$ pool, p53 stability, and nuclear $pAkt^{S473}$ levels by combined PITPα and PITPβ KD
291 using distinct siRNAs targeting their 3'-UTR was rescued by expression of $PITP\alpha^{wt}$, but
292 not mutant $PITP\alpha^{T59D}$ (Fig. 7b-e). Notably, the nuclear $PI4,5P_2$ and $pAkt^{S473}$ levels
293 correlated with the content of re-expressed $PITP\alpha^{wt}$, but not mutant $PITP\alpha^{T59D}$ (Fig. 7f-i),
294 indicating that these phenotypes are dose-dependent.

295 The cytotoxicity and sensitization to cisplatin-induced apoptosis by combined PITPα/β KD
296 using the 3'-UTR targeting siRNAs were partly rescued by re-expressing $PITP\alpha^{wt}$ but not
297 the PITPα/β^{T59D} mutant (Fig. 7j,k and Extended Data Fig. 12n). These results
298 demonstrate that the PI transfer activity of class I PITPs regulates their interaction with
299 p53 and subsequent nuclear Akt activation. Combined PITPα/β KD also inhibited EGF-
300 stimulated cell invasion and these effects were partly restored by re-expressing $PITP\alpha^{wt}$
301 but not the $PITP\alpha^{T59D}$ mutant (Fig. 7l,m) consistent with reports that PITPs contribute to
302 EGF signaling[50]. The data also suggest a broader role for PITPα/β in regulating PIP_n

303 linkage to additional proteins beyond p53 that may contribute to cell growth, invasion and
304 protection against genotoxic stress (Fig. 7n).

305 **Discussion**

306 Here we reveal an unexpected role for class I PITPα/β in generating nuclear PIP_n pools
307 that initiate PIP_n signaling. Although the existence of nuclear PIP_ns and their role in the
308 cell cycle[51], oxidative stress[16, 52-57] and the DNA damage response[17, 58-60] is supported by
309 growing evidence[16], the molecular origin of nuclear PIP_ns in regions devoid of membranes
310 has been enigmatic[61]. PITPs have a well-established role in transporting PI from the
311 endoplasmic reticulum to membranes to enable membrane-localized PIP_n signaling via
312 PIP kinases, phosphatases, and phospholipase-C[25-28, 34, 62]. The findings presented here
313 demonstrate that PITPs accumulate in the non-membranous nucleoplasm in response to
314 diverse cellular stressors to regulate the membrane-free nuclear PIP_n pools. As such,
315 these data expand the roles of the PITP lipid transport activities that were thought to act
316 largely in the cytosol and establish their mechanistic roles in generating nuclear PIP_n
317 pools.

318 In addition, PITPα/β, but not other PITP family members, bind directly to $p53^{wt}$ and $p53^{mt}$
319 and these interactions are stimulated by cell stress. This complex also includes the small
320 heat shock proteins (Hsp27 and αB-crystallin), which stabilize p53[18]. PITPα/β binding to
321 p53 is necessary for the linkage of PIP_ns with p53 (p53-PIP_n signalosome). Once the p53-
322 PIP_n linkage is formed it is stable and detected by PIP_n isomer antibodies and acted on
323 by multiple PIP kinases and phosphatases, indicating that the myo-inositol head group is
324 accessible and can be utilized as a substrate for these enzymes[17, 18, 35]. The p53-PIP_n

325 pathway culminates in the formation of p53-PI3,4,5P_3 complexes that in turn, recruit and
326 activate Akt in the nucleus, conferring resistance to stress-induced apoptosis[17]. However,
327 PITPs also contribute to the canonical PI3K/Akt pathway[63] so the observed differences in
328 cellular phenotypes by PITPα/β KD likely reflects some contribution of the canonical
329 pathway as well as the nuclear PI3K/Akt pathway. These PITPα/β activities require PI
330 binding, underscoring the critical functional role of lipid transport in nuclear PIP_n signaling.
331 Indeed, the ability of wild-type PITPα, but not the PI binding-defective mutant, to rescue
332 the phenotype of combined PITPα/β KD suggests a functional redundancy of PITPα and
333 PITPβ for nuclear phosphoinositide signaling. This is consistent with previous reports that
334 either PITPα or PITPβ is sufficient to rescue the phenotype of double PITPα/β knockout
335 in a PI-binding dependent manner[47, 64]. PITPα/β bind the PI 4-kinase PI4KIIα, and both
336 also interact with p53. Indeed, both PITPα/β and PI4KIIα are required to generate the
337 p53-PI4P complex, pointing to a functional collaboration between PITPα/β and PI4KIIα in
338 initiating nuclear PIP_n signaling that is highly reminiscent of their roles in generating PI4P
339 in the membrane-localized pathway[42, 43].

340 Remarkably, PITPα/β and PI4KIIα regulate the coupling of PIP_ns to a suite of cellular
341 proteins that are detected by WB with PIP_n isomers antibodies and by metabolic labelling
342 cells with [^{3}H]*myo*-inositol. These data indicate that the nuclear IF staining of PIP_ns is a
343 composite of PIP_n-linked proteins. Furthermore, our observation that the p53-PIP_n and
344 protein-PIP_n linkages can be detected by metabolic labelling with [^{3}H]*myo*-inositol and are
345 resistant to denaturation and solvent extraction indicates a tight coupling consistent with
346 a putative posttranslational modification. Indeed, our data indicate PIP_n second
347 messengers are linked to p53 and other proteins by the combined activities of PITPα/β

348 and PI4KIIα. The resulting p53-PI4P is acted on by PIP kinases and phosphatases such
349 that the PI3,4,5P_3 linked to p53 acts as a messenger to recruit PDK1, mTORC2, and Akt,
350 culminating in nuclear Akt activation and stress-resistance[17]. These findings suggest a
351 "third messenger" pathway[17] with p53 as the founding member whereby PIP_n second
352 messengers are linked to cellular proteins in membrane-free regions and modified by PIP
353 kinases/phosphatases to regulate their function (Fig. 7n). The assembly of distinct PIP_n
354 isomer-protein complexes with unique binding partners has the potential to enable
355 exquisite spatial and temporal regulation of signaling cascades anchored on cellular
356 proteins instead of membranes. Although the focus here is on the nuclear pathway, there
357 is nothing *per se* that limits PIP_n-linked proteins to the nucleus and p53-PI4P detected by
358 PLA is both nuclear and cytosolic. Given the critical role of class I PITPs in initiating
359 nuclear phosphoinositide signaling, which attenuates cellular stress and apoptosis, these
360 findings also point to these PITPs and PI4KIIα as potential therapeutic targets in a variety
361 of diseases including cancer.

362 **ACKNOWLEDGMENTS**

363 We thank Dr. Adrea Galmozzi for discussions and comments, and Lance Rodenkirch for
364 technical support. N.D.C. is supported by a National Institutes of Health T32 Training
365 Grant 5T32ES007015-43 to the Molecular and Environmental Toxicology graduate
366 training program at UW-Madison. M.C. is currently supported by grant D2301007 from
367 the Shenzhen Medical Research Fund. This work was supported in part by a National
368 Institutes of Health grant R35GM134955 (R.A.A.), R01CA286492 (R.A.A. & V.L.C.),
369 Department of Defense Breast Cancer Research Program grants W81XWH-17-1-0258

370 (R.A.A.), W81XWH-17-1-0259 (V.L.C.), W81XWH-21-1-0129 (V.L.C.), HT9425-23-1-
371 0553 (V.L.C.), and HT9425-23-1-0554 (R.A.A.), and a grant from the Breast Cancer
372 Research Foundation (V.L.C.).

373 **AUTHOR CONTRIBUTIONS**

374 M.C., N.D.C, T.W., V.L.C., and R.A.A. designed the experiments. N.D.C., M.C., T.W.,
375 P.A., T.J.W., and C.S. performed the experiments. N.D.C., M.C., T.W., V.L.C., and R.A.A.
376 wrote the manuscript.

377 **DECLARATION OF INTERESTS**

378 Authors declare that they have no competing interests.

379 **METHODS**

380 **Cell culture and constructs**

381 A549, BT-549, Cal33, HCT116, HS578T, MDA-MB-231, SUM159, SUM1315, HEK293FT,
382 and MCF-10A cells were purchased from ATCC. MCF10A cells were cultured in
383 DMEM/F12 (#11330-032, Invitrogen) supplemented with 10% fetal bovine serum
384 (#SH30910.03, Hyclone), 1% penicillin/streptomycin (#15140-122, Gibco), 20 ng/mL EGF
385 (#CC-4107, Lonza), 0.5 mg/mL Hydrocortisone (#H4001, Sigma), 100 ng/mL Cholera
386 toxin (#C-8052, Sigma), and 10 μg/mL Insulin (#I-1882, Sigma). The other cells were
387 maintained in DMEM (#10-013-CV, Corning) supplemented with 10% fetal bovine serum
388 (#SH30910.03, Hyclone) and 1% penicillin/streptomycin (#15140-122, Gibco). The cell
389 lines used in this study were routinely tested for mycoplasma contamination using

390 MycoAlert Mycoplasma Detection Kit (#LT07-318, Lonza), and mycoplasma-negative
391 cells were used. None of the cell lines used in this study are listed in the database of
392 commonly misidentified cell lines maintained by ICLAC. The Flag-tagged p53 constructs
393 and corresponding PIP_n-binding-defective 6Q mutants in this work have been described
394 previously[18]. The HA-tagged wild-type PITPα/β constructs and PI-binding deficient
395 mutants T59D[47] were purchased from Genscript. Plasmids were transfected into
396 mammalian cells using Lipofectamine™3000, (#L3000015, Thermo Fisher Scientific)
397 according to the manufacturer's instructions. Typically, 2-5 µg of DNA and 6-10 µl of lipid
398 were used for transfecting cells in 6-well plates. Cells with at least 80% transfection
399 efficiency were used for further analysis.

400 **Antibodies and reagents**

401 Monoclonal antibodies against p53 (clone DO-1, #SC-126, Santa Cruz Biotechnology),
402 p53 (clone 7F5, #2527, Cell Signaling), $pAkt^{S473}$ (clone 193H12, #4058, Cell Signaling),
403 HA-tag (clone C29F4, #3724, Cell Signaling), Flag-tag (clone D6W5B, #14793, Cell
404 Signaling), GAPDH (clone 0411, #sc-47724, Santa Cruz Biotechnology), Lamin B2 (clone
405 D8P3U, #12255, Cell Signaling), EGFR (clone D6B6, #2085, Cell Signaling), HSP27
406 (clone D6W5V, #95357, Cell Signaling), and polyclonal antibodies against PITPα
407 (#16613-1-AP, ThermoFisher), PITPβ (#ab127563, abcam), PITPNC1 (IF, #ab222078,
408 abcam), PITPNC1 (WB, #NBP2-19842, Novus), PITPNM1 (#26983-1-AP, Proteintech),
409 PITPNM2 (#PA5-48616, Invitrogen), PI4KIIα (#NBP2-44158, Novus), PI4KIIIα (#4902S,
410 CST), PI4KIIβ (#PA5-82133, Thermo), PI4KIIIβ (#ab134756, abcam), and αB-Crystallin
411 (#ADI-SPA-223-F, Enzo) were used in this study. For conventional immunostaining and

412 PLA analysis of phosphoinositides, anti-PI4P (#Z-P004), PI4,5P_2 (#Z-P045) and PI3,4,5P_3
413 (#Z-P345) antibodies were purchased from Echelon Biosciences. For immunoblotting
414 analyses, antibodies were diluted at a 1:1000 ratio except for p53 (clone DO-1, 1:5000)
415 and GAPDH (clone 0411, 1:5000). For immunoprecipitation, antibody-conjugated
416 agarose was purchased from Santa Cruz Biotechnology, including agarose-conjugated
417 antibodies against p53 (#sc-126AC), PITPα/β (#sc-398050AC), HA-tag (#sc-7392AC),
418 and Flag-tag (#sc-166355AC). For immunostaining analyses and proximity ligation assay
419 (PLA), antibodies were diluted at a 1:100 ratio. Nuclear envelope marker (Alexa
420 Fluor®488 Lamin A/C, clone 4C11, #8617, Cell Signaling, 1:200) was used to examine
421 subnuclear regions. For the knockdown (KD) experiments, the ON-TARGETplus siRNA
422 SMARTpool with 4 siRNAs in combination against human p53 (#L-003329-00), PITPα
423 (#L-018010-00), PITPβ (#L-006459-01), and PITPNC1 (#L-012476-02) were purchased
424 from Dharmacon. Non-targeting siRNA (#D-001810-01, Dharmacon) was used as a
425 control. For the KD and rescue experiments, pooled-siRNAs targeting the 3'UTR of PITPα
426 (sense 5'-AGGCAACUUUCGAUUCCUUACUGUA-3' and antisense 5'-
427 UACAGUAAGGAAUCGAAAGUUGCCU-3'; sense 5'-
428 CCGUCUCUCUCCAUUGUGUUCCGAU-3' and antisense 5'-
429 AUCGGAACACAAUGGAGAGAGACGG-3') and pooled-siRNAs targeting the 3'UTR of
430 PITPβ (sense 5'- GAGUGAACAACAAUCUGACCAGUAU-3' and antisense 5'-
431 AUACUGGUCAGAUUGUUGUUCACUC-3'; sense 5'- CUACAAAGCUGAUGAAGAC-3'
432 and antisense 5'-GUCUUCAUCAGCUUUGUAG-3') were purchased from Thermo Fisher
433 Scientific. The siRNAs were delivered to cells by RNAiMAX reagent (#13778150, Thermo
434 Fisher Scientific), and KD efficiency was determined by immunoblotting. KD efficiency

435 greater than 80% was required to observe phenotypic changes in the study. Cisplatin,
436 (#NC1706394, Fisher Scientific), etoposide (#S1225, Sellekchem), Erastin (#S7242,
437 Selleckchem), tert-Butylhydroquinone (tBHQ, #SPCM-T1540-06, Spectrum), and
438 hydroxyurea (HU, #1332000, Millipore Sigma) were used as cellular stressors. Nutlin 3a
439 (#S8059, Sellekchem), PI-273 (#AOB37765, aobious), and NC03 (#AOB17420, aobious)
440 were also used.

441 **Immunoprecipitation and immunoblotting**

442 Cells were removed from the medium after the indicated treatment, washed three times
443 with ice-cold PBS, and lysed in an ice-cold RIPA lysis buffer system (#sc-24948, Santa
444 Cruz Biotechnology) with 1 mM Na_3VO_4, 5 mM NaF, and 1x protease inhibitor cocktail
445 (#11836153001, Roche). The cell lysates were then sonicated at 15% amplitude for 15 s.
446 After sonication, the cell lysates were incubated at 4°C with continuous rotation for 1 h
447 and subsequently centrifuged at maximum speed for 10 min to collect the supernatant.
448 The protein concentration in the supernatant was measured by the Bradford protein assay
449 (#5000201, BIO-RAD) according to the manufacturer's instructions. Equal amounts of
450 protein were used for further analysis. All antibodies were diluted at a 1:1000 ratio for
451 immunoblotting unless otherwise indicated. For immunoprecipitation, 0.5-1 mg of protein
452 was incubated with 20 µl of antibody-conjugated agarose (Santa Cruz Biotechnology) at
453 4°C for 24 h. After washing three times with PBST (PBS with 0.1% Tween 20), the protein
454 complex was eluted with SDS sample buffer and boiled at 95°C for 10 min. For
455 immunoblotting, 5-20 µg of protein were loaded. For immunoblotting of
456 immunoprecipitated complexes, horseradish peroxidase (HRP)-conjugated antibodies

457 were used to avoid non-specific detection of immunoglobulin in the immunoprecipitated
458 samples. HRP-conjugated p53 (#sc-126HRP), PITPα (#sc-13569HRP), PITPβ (#sc-
459 390500HRP) antibodies were purchased from Santa Cruz Biotechnology. Immunoblots
460 were developed by Odyssey Imaging System (LI-COR Biosciences) and the intensity of
461 protein bands was quantified using ImageJ. The unsaturated exposure of immunoblot
462 images was used for quantification with the appropriate loading controls as standards.
463 Statistical data analysis was performed with Microsoft Excel, using data from at least
464 three independent experiments.

465 **Fluorescent IP-WB**

466 Cells were lysed in a RIPA lysis buffer system[17] after the indicated treatment and
467 quantified for protein concentration as described above. For endogenous p53 or FLAG-
468 tagged p53 immunoprecipitation, 0.5-1 mg of cell lysates were incubated with 20 μl anti-
469 p53 (#sc-126 AC, Santa Cruz Biotechnology) or anti-FLAG (#sc-166355AC, Santa Cruz
470 Biotechnology) mouse monoclonal IgG antibody-conjugated agarose at 4°C for 24 h.
471 Normal immunoglobulin (IgG)-conjugated agarose was used as a negative control (#sc-
472 2343, Santa Cruz Biotechnology). After washing three times with PBST, the protein
473 complex was eluted with SDS sample buffer. The sample was then boiled at 95°C for 10
474 min. For immunoblotting, 5-20 μg of protein were loaded. The protein complexes
475 associated with p53 were resolved by SDS-PAGE and transferred onto a PVDF
476 membrane (#IPVH00010, MilliporeSigma). The membrane was blocked with 1% BSA in
477 TBS for 1 h at room temperature. For double fluorescent IP-WB detecting p53-
478 PI4P/PI4,5P_2/PI3,4,5P_3 complexes, anti-p53 rabbit monoclonal IgG antibody (clone 7F5,

479 #2527, Cell Signaling) at 1:2000 dilution and anti-PI4P mouse monoclonal IgM antibody
480 (#Z-P004, Echelon Biosciences), PI4,5P_2 mouse monoclonal IgM antibody (#Z-P045,
481 Echelon Biosciences), or PI3,4,5P_3 mouse monoclonal IgM antibody (#Z-P345, Echelon
482 Biosciences) at 1:1000 dilution were mixed together in blocking buffer with 0.02 % Sodium
483 Azide and incubated with the membrane at 4°C overnight. The next day, the membrane
484 was washed three times with TBST for 10 min each time. For the secondary antibody
485 incubation, goat anti-rabbit IgG antibody conjugated with IRDye 800CW fluorophore
486 (#926-32211, LI-COR) detectable on the 800 nm wavelength channel of the Odyssey Fc
487 Imaging System (LI-COR Biosciences) and goat anti-mouse IgM antibody conjugated
488 with IRDye 680RD fluorophore (#926-68180, LI-COR) detectable on the 700 nm
489 wavelength channel at 1:10000 dilution were mixed in blocking buffer with 0.01 % SDS
490 and 0.1% Tween 20 and incubated with the membrane at room temperature for 2 h. The
491 membrane was then washed three times with TBST for 10 min each time. The images
492 were subsequently acquired simultaneously using the 700 and 800 nm wavelength
493 channels on the Odyssey Fc Imaging System (LI-COR Biosciences). The p53-associated
494 PI4P/PI4,5P_2/PI3,4,5P_3 complex was visualized by overlapping the 700 and 800 nm
495 channels. Statistical data analysis was performed with Microsoft Excel, using data from
496 at least three independent experiments.

497 ***In vitro* binding assay**

498 The recombinant proteins p53 (#81091, Active Motif), PITPα (#ab101666, Abcam), PITPβ
499 (#ab101091, Abcam), and PI4KIIα (lab made) were used for *In Vitro* binding assays. The
500 binding assay was performed in PBS by incubating a constant amount of p53 with an

501 increasing amount of PITPα/β or PI4KIIα in the presence of 20 µl anti-p53 antibody-
502 conjugated agarose (#sc-126AC, Santa Cruz). After incubating overnight at 4°C, unbound
503 proteins were removed by washing three times with PBST, and the protein complex was
504 analyzed by immunoblotting.

505 **Immunofluorescence (IF) and Confocal Microscopy**

506 For immunofluorescence studies, cells were grown on coverslips coated with 0.2 %
507 gelatin (#G9391, MilliporeSigma). Cells were fixed with 4% paraformaldehyde (PFA) (#sc-
508 281692, Santa Cruz Biotechnology) for 20 min at room temperature followed by washing
509 three times with PBS. Next, the cells were permeabilized with 0.3% Triton-X100 for 30
510 min to thoroughly permeate the nuclear envelope and rewashed three times with PBS.
511 The cells were then blocked with 1% BSA in PBS for one hour at room temperature. After
512 blocking, cells were incubated with primary antibodies overnight at 4ºC. The cells were
513 then washed three times with PBS and incubated with fluorescent-conjugated secondary
514 antibodies (Molecular Probes) for 1 hour at room temperature. After secondary antibody
515 incubation, the cells were washed three times. Then the coverslips were taken out from
516 the dishes, air-dried for 10 min at room temperature and mounted in Prolong™ Glass
517 Antifade Mountant with NucBlue™ Stain (#P36985, Thermo Fisher Scientific). The
518 images were taken by Leica SP8 3xSTED Super-Resolution Microscope, which is both a
519 point scanning confocal and 3xSTED super-resolution microscope. The Leica SP8
520 3xSTED microscope was controlled by LASX software (Leica Microsystems). All images
521 were acquired using the 100X objective lens (N.A. 1.4 oil). The z-stack images were taken
522 with each frame of 0.2 µm thickness. For quantification, the mean fluorescent intensity of

523 channels in each cell was measured by LASX. GraphPad Prism Version 9.4.1 generated
524 quantitative graphs. The images were processed using ImageJ. The correlation of double
525 staining channels was quantified by GraphPad Prism using Pearson's correlation
526 coefficient (Pearson's r), ranging between 1 and −1. A value of 1 represents perfect
527 correlation, 0 means no correlation, and -1 means perfect negative correlation[65].
528 Pearson's r greater than 0.7 suggests a strong correlation[66].

529 **Proximity Ligation Assay (PLA)**

530 PLA was utilized to detect *in situ* protein-protein/PIP_n interaction or close proximity as
531 previously described[17, 18, 35]. After fixation and permeabilization, cells were blocked before
532 incubation with primary antibodies as in routine IF staining. The cells were then processed
533 for PLA (#DUO92101, MilliporeSigma) according to the manufacturer's instruction and
534 previous publications[17, 18, 35]. Post-PLA slides were further processed for
535 immunofluorescent staining against the nuclear membrane marker (Lamin A/C, #8617,
536 Cell Signaling). After washing three times with PBST, the slides were mounted with
537 Prolong™ Glass Antifade Mountant with NucBlue™ Stain (#P36985, Thermo Fisher
538 Scientific). The Leica SP8 confocal microscope detected PLA signals as discrete punctate
539 foci and provided the intracellular localization of the complex. ImageJ was used to
540 quantify the nuclear PLA foci.

541 **Crystal Violet Cell Viability assay**

542 In 96-well plates, 5×10^4 cells/well of MDA-MB-231, MDA-MB-231^{Cas9}, BT549, SUM159,
543 or SUM1315 cells were transfected with control siRNAs or siRNAs targeting p53, PITPα,
544 PITPβ, PITPNC1, or the combination of PITPα and PITPβ as indicated for 48 h. For the

545 KD rescue experiments, MDA-MB-231 cells were transfected with control siRNAs or
546 siRNAs targeting 3'UTR of PITPα and PITPβ for 24 h. Next, the cells were transfected
547 with either HA-tagged wild-type PITPα or its PI-binding deficient T59D mutant PITPα for
548 another 24 h. The cells were then treated with the control vehicle or 30 μM cisplatin for
549 24 h, and the cells were subsequently fixed with 4% PFA and stained with 0.2% Crystal
550 Violet. After washing the cells 3 times with PBS, the plates were air-dried at room
551 temperature and imaged using EVOS M5000 Imaging System (ThermoFisher Scientific).
552 After imaging, the dye was extracted from the cells with 10% acetic acid and quantified
553 by measuring the absorbance at 570 nm using a Synergy HTX Multi-Mode Microplate
554 reader.

555 **Caspase 3 Activity Assay**

556 In 6-well plates, 1×10^6 cells/well of MDA-MB-231, BT549, SUM159, or SUM1315 were
557 transfected with control siRNAs or siRNAs targeting p53, PITPα, PITPβ, PITPNC1, or the
558 combination of PITPα and PITPβ as indicated for 48 h. For the KD rescue experiments,
559 MDA-MB-231 cells were transfected with control siRNAs or siRNAs targeting 3'UTR of
560 PITPα and PITPβ for 24 h. Then the cells were transfected with either HA-tagged wild-
561 type PITPα or its PI-binding deficient T59D mutant PITPα for another 24 h, followed by
562 treatment with control vehicle or 30 μM cisplatin for 24 h. Next, the cells were lysed and
563 processed for Caspase 3 activity assay by following the manufacturer's instructions (#E-
564 13183, Thermo Fisher Scientific). At the end of the assay, the fluorescence was read at
565 excitation/emission 342/441 nm using a Synergy HTX Multi-Mode Microplate reader.

566 **Transwell Invasion Assay**

567 The bottom polycarbonate filter surface of a 6.5 mm diameter insert with 8 μm pores in a
568 24-well plate (#3422, Corning) was coated with 10 μg/ml of Laminin (#CC095,
569 MilliporeSigma) diluted in PBS for 3 h at 37°C. MDA-MB-231 cells were transiently
570 transfected with control siRNAs or siRNAs targeting the 3'UTR of both PITPα and PITPβ
571 for 24 h. Then the cells were transfected with either HA-tagged wild-type PITPα or its PI-
572 binding deficient T59D mutant PITPα. After 24 h, cells were serum starved for an
573 additional 24 h. Next, $5x10^4$ transfected cells were suspended in 200 μl serum-free
574 medium containing 0.5% BSA and then were plated in the upper insert chamber in 500
575 μl serum-free medium with 0.5% BSA. 10 ng/ml EGF was added to the lower chamber.
576 Cells were allowed to invade for 16 h at 37°C. Cells on the bottom of the filter were then
577 fixed with 4% PFA and stained with 0.2% Crystal Violet. The stained cells were imaged
578 using EVOS M5000 Imaging System (ThermoFisher Scientific). At the end of the assay,
579 the dye was extracted by 10% acetic acid from the cells and quantified by measuring the
580 optical density at 570 nm using a Synergy HTX Multi-Mode Microplate reader.

581 **Microscale Thermophoresis (MST) Assay**

582 The microscale thermophoresis (MST) assay was used to calculate the binding affinities
583 of purified recombinant proteins (p53 (#81091, Active Motif), PITPα (#ab101666, Abcam),
584 PITPβ (#LS-C794864, LSBio), PITPNC1 (#LS-G33119-10, LSBio) PI4KIIα (lab made))
585 and other contributing factors *in vitro* as previously described[67]. The target protein was
586 fluorescently labeled using a Monolith Protein Labeling kit (RED-NHS 2nd Generation
587 MO-L011, Nano Temper) following the manufacturer's instruction. Then, sequential
588 titration of unlabeled ligand proteins or PI (#840042P, Avanti), was made in a Tris-based

589 MST buffer containing 50 mM Tris-HCl, pH 8.0, 50 mM NaCl, 80 mM KCl and 0.05%
590 Tween 20 and mixed with an equal volume of fluorescently labelled target protein
591 prepared at 10 nM concentration in the same MST buffer, making the final target protein
592 at a constant concentration of 5 nM and the ligand protein or lipid as the gradient. For PI
593 cofactor analysis, target proteins were mixed with 1 μM PI prior to ligand proteins and PI
594 concentration remained constant across the gradient of ligand protein. The target–ligand
595 mixtures were loaded into Monolith NT.115 series capillaries (MO-K022, Nano Temper),
596 and the MST traces were measured using Monolith NT.115 pico. The binding affinity was
597 autogenerated using MO Control v.1.6 software.

598 **[^{3}H]*myo*-inositol Metabolic Labeling**

599 Cells were split and cultured in low serum Opti-MEM (#31985070, Thermo) supplemented
600 with 10% dialyzed FBS with a 10,000 mw cut-off (#F0392, Sigma) and 1% Pen/strep
601 (#15140-122, Gibco) to minimize inositol in the culture media. In 10 cm dishes, 0.5×10^6
602 MDA-MB-231 cells were seeded to achieve ~5% confluency the following day. 24 h after
603 plating, cells were treated with either 1.322 μM (25 μCi/mL) of [^{3}H]*myo*-inositol
604 (#NET1156005MC, PerkinElmer) or unlabeled *myo*-inositol (#J60828.22, Thermo) and
605 allowed to uptake the metabolic label for 48 h. For KD experiments, PITPα/β siRNAs were
606 added and recovered as normal and fresh [^{3}H]*myo*-inositol supplemented media was
607 used to replace the transfection media. 24 h after siRNA transfection (72 h after original
608 plating), cells were treated with control vehicle or 30 μM cisplatin for another 24 h. Labeled
609 and unlabeled cells were then lysed and p53 was immunoprecipitated as described in
610 *immunoprecipitation and* immunoblotting, before performing SDS-PAGE or $CHCl_3$/MeOH

611 extraction as indicated. For extraction, MeOH:$CHCl_3$ (2:1) was added to RIPA cell
612 lysates to form the protein precipitate. Soluble phases in MeOH and $CHCl_3$ were
613 aspirated out and the protein flake was dried using a speed vacuum. Protein samples
614 were then resuspended and solubilized in PBS with sonication. SDS-PAGE samples
615 were excised from the gel and each lane was either further sectioned or treated as a
616 whole and dissolved in 30% H_2O_2 before liquid scintillation counting (LSC). Dissolved gel
617 samples or resuspended protein samples from the $CHCl_3$/MeOH extraction were added
618 to LSC vials with LSC cocktail (#6013319, PerkinElmer) before being processed by
619 PerkinElmer Tri-Carb 4910 TR liquid scintillation analyzer. Analysis and DPM calculation
620 were automated using QuantaSmart software.

621 **Lenti-CRISPR Gene Editing**

622 CRISPR-Cas9 genome-editing was used to knockout the gene encoding PITPβ in MDA-
623 MB-231 cells. First a Cas9 expressing stable cell line was generated by transducing cells
624 with viral particles (#LVCAS9BST, Sigma Aldrich) at the multiplicity of infection (MOI) of
625 0.5. Transduction was performed in complete media containing 8μg/mL polybrene. After
626 24 h incubation, Cas9-expressing cells were selected with 10μg/mL blasticidin
627 (#DSB12150; Dot Scientific) for 1 week and expression was confirmed. To generate
628 PITPβ KO cells, viral particles containing the guide RNA sequence for PITPβ (5'-
629 CAATCATCCTCACGAATGC-3') and negative control (5'-
630 CGCGATAGCGCGAATATATT-3') were purchased from Sigma Aldrich. Sequences were
631 cloned into LV21 lentiviral vectors (Sigma Aldrich). Cas9-expressing cells were then
632 transduced with viral particles at a MOI of 0.5 and incubated for 24 h. Transduction was
633 performed in the presence of 8μg/mL polybrene in complete media. Media was removed

634 24 h after viral transduction and 1500 µg/mL geneticin (#10131035; Sigma Aldrich) was
635 added for selection. After 1 week of selection in antibiotics, single cells were isolated in
636 the 96-well tissue culture dish by BD FACS AriaII. Cells were expanded and positive
637 colonies were selected by immunoblotting.

638 **Nuclear Fractionation**

639 Nuclear fractionation was used to analyze compartmentalized protein expression. MDA-
640 MB-231 cells were processed using the NE-PER nuclear and cytoplasmic extraction
641 reagents (#78833, Thermo) according to manufacturers instructions. Cells were manually
642 removed from their culture dishes into suspension and the cytosolic extraction reagent
643 was used to isolate cytosolic fractions. Then, the nuclear extraction reagent was used to
644 produce the nuclear fraction. Samples were then further processed by WB.

645 **Statistics and Reproducibility**

646 Two-tailed unpaired *t*-tests were used for pair-wise significance and one-way ANOVA
647 was used for group significance with Bonferroni's multiple comparisons test used for
648 significance within grouped samples. We note that no power calculations were used.
649 Sample sizes were determined based on previously published experiments where
650 significant differences were observed[17, 18]. Each experiment was repeated at least three
651 times independently, and the number of repeats is defined in each figure legend. We used
652 at least three independent experiments or biologically independent samples for statistical
653 analysis.

654 **Resource and Data Availability**

All data supporting the findings of this study are available from the corresponding authors on reasonable request.

671 **References**

672 1. Hammond, G.R.V. & Burke, J.E. Novel roles of phosphoinositides in signaling, lipid
673 transport, and disease. *Curr Opin Cell Biol* **63**, 57-67 (2020).
674 2. Fruman, D.A. *et al.* The PI3K Pathway in Human Disease. *Cell* **170**, 605-635 (2017).
675 3. Hoxhaj, G. & Manning, B.D. The PI3K-AKT network at the interface of oncogenic
676 signalling and cancer metabolism. *Nat Rev Cancer* **20**, 74-88 (2020).
677 4. Manning, B.D. & Toker, A. AKT/PKB Signaling: Navigating the Network. *Cell* **169**,
678 381-405 (2017).
679 5. Burke, J.E., Triscott, J., Emerling, B.M. & Hammond, G.R.V. Beyond PI3Ks: targeting
680 phosphoinositide kinases in disease. *Nat Rev Drug Discov*, 1-30 (2022).
681 6. Currie, R.A. *et al.* Role of phosphatidylinositol 3,4,5-trisphosphate in regulating the
682 activity and localization of 3-phosphoinositide-dependent protein kinase-1. *Biochem J*
683 **337 (Pt 3)**, 575-583 (1999).
684 7. Liu, P. *et al.* PtdIns(3,4,5)P3-Dependent Activation of the mTORC2 Kinase Complex.
685 *Cancer Discov* **5**, 1194-1209 (2015).
686 8. Calleja, V. *et al.* Intramolecular and intermolecular interactions of protein kinase B
687 define its activation in vivo. *PLoS Biol* **5**, e95 (2007).
688 9. Altomare, D.A. & Testa, J.R. Perturbations of the AKT signaling pathway in human
689 cancer. *Oncogene* **24**, 7455-7464 (2005).
690 10. Kondapaka, S.B., Singh, S.S., Dasmahapatra, G.P., Sausville, E.A. & Roy, K.K.
691 Perifosine, a novel alkylphospholipid, inhibits protein kinase B activation. *Mol Cancer*
692 *Ther* **2**, 1093-1103 (2003).
693 11. Kikani, C.K. *et al.* Proliferative and antiapoptotic signaling stimulated by nuclear-
694 localized PDK1 results in oncogenesis. *Science signaling* **5**, ra80 (2012).
695 12. Shiraishi, I. *et al.* Nuclear targeting of Akt enhances kinase activity and survival of
696 cardiomyocytes. *Circ Res* **94**, 884-891 (2004).
697 13. Fu, W. & Hall, M.N. Regulation of mTORC2 Signaling. *Genes (Basel)* **11** (2020).
698 14. Martelli, A.M. *et al.* The emerging multiple roles of nuclear Akt. *Biochim Biophys Acta*
699 **1823**, 2168-2178 (2012).
700 15. Liu, L. *et al.* DNA-PK promotes activation of the survival kinase AKT in response to
701 DNA damage through an mTORC2-ECT2 pathway. *Science signaling* **15**, eabh2290
702 (2022).
703 16. Chen, M. *et al.* The nuclear phosphoinositide response to stress. *Cell Cycle* **19**, 268-289
704 (2020).
705 17. Chen, M. *et al.* A p53-phosphoinositide signalosome regulates nuclear AKT activation.
706 *Nat Cell Biol* **24**, 1099-1113 (2022).
707 18. Choi, S., Chen, M., Cryns, V.L. & Anderson, R.A. A nuclear phosphoinositide kinase
708 complex regulates p53. *Nat Cell Biol* **21**, 462-475 (2019).
709 19. Muller, P.A. & Vousden, K.H. p53 mutations in cancer. *Nat Cell Biol* **15**, 2-8 (2013).
710 20. Hassin, O. & Oren, M. Drugging p53 in cancer: one protein, many targets. *Nat Rev Drug*
711 *Discov* **22**, 127-144 (2023).
712 21. Emerling, B.M. *et al.* Depletion of a putatively druggable class of phosphatidylinositol
713 kinases inhibits growth of p53-null tumors. *Cell* **155**, 844-857 (2013).

714 22. Cocco, L. *et al.* Synthesis of polyphosphoinositides in nuclei of Friend cells. Evidence for
715 polyphosphoinositide metabolism inside the nucleus which changes with cell
716 differentiation. *Biochem J* **248**, 765-770 (1987).
717 23. Boronenkov, I.V., Loijens, J.C., Umeda, M. & Anderson, R.A. Phosphoinositide
718 signaling pathways in nuclei are associated with nuclear speckles containing pre-mRNA
719 processing factors. *Mol Biol Cell* **9**, 3547-3560 (1998).
720 24. Blind, R.D. *et al.* The signaling phospholipid PIP3 creates a new interaction surface on
721 the nuclear receptor SF-1. *Proc Natl Acad Sci U S A* **111**, 15054-15059 (2014).
722 25. Hunt, A.N., Clark, G.T., Attard, G.S. & Postle, A.D. Highly saturated endonuclear
723 phosphatidylcholine is synthesized in situ and colocated with CDP-choline pathway
724 enzymes. *J Biol Chem* **276**, 8492-8499 (2001).
725 26. Wang, Y., Sweitzer, T.D., Weinhold, P.A. & Kent, C. Nuclear localization of soluble
726 CTP:phosphocholine cytidylyltransferase. *J Biol Chem* **268**, 5899-5904 (1993).
727 27. Tribble, E.K. *et al.* Quantitative profiling of the endonuclear glycerophospholipidome of
728 murine embryonic fibroblasts. *J Lipid Res* **57**, 1492-1506 (2016).
729 28. Blunsom, N.J. & Cockcroft, S. Phosphatidylinositol synthesis at the endoplasmic
730 reticulum. *Biochim Biophys Acta Mol Cell Biol Lipids* **1865**, 158471 (2020).
731 29. Bahmanyar, S. Spatial regulation of phospholipid synthesis within the nuclear envelope
732 domain of the endoplasmic reticulum. *Nucleus-Phila* **6**, 102-106 (2015).
733 30. Shadan, S. *et al.* Dynamics of lipid transfer by phosphatidylinositol transfer proteins in
734 cells. *Traffic* **9**, 1743-1756 (2008).
735 31. Morgan, C.P. *et al.* Differential expression of a C-terminal splice variant of
736 phosphatidylinositol transfer protein beta lacking the constitutive-phosphorylated Ser262
737 that localizes to the Golgi compartment. *Biochem J* **398**, 411-421 (2006).
738 32. van Tiel, C.M. *et al.* The Golgi localization of phosphatidylinositol transfer protein beta
739 requires the protein kinase C-dependent phosphorylation of serine 262 and is essential for
740 maintaining plasma membrane sphingomyelin levels. *J Biol Chem* **277**, 22447-22452
741 (2002).
742 33. Huang, Y. *et al.* Global tumor protein p53/p63 interactome: making a case for cisplatin
743 chemoresistance. *Cell Cycle* **11**, 2367-2379 (2012).
744 34. Ashlin, T.G., Blunsom, N.J. & Cockcroft, S. Courier service for phosphatidylinositol:
745 PITPs deliver on demand. *Biochim Biophys Acta Mol Cell Biol Lipids* **1866**, 158985
746 (2021).
747 35. Chen, M., Horn, H.T., Wen, T., Cryns, V.L. & Anderson, R.A. Assessing In Situ
748 Phosphoinositide-Protein Interactions Through Fluorescence Proximity Ligation Assay in
749 Cultured Cells. *Methods Mol Biol* **2251**, 133-142 (2021).
750 36. Kalasova, I. *et al.* Tools for visualization of phosphoinositides in the cell nucleus.
751 *Histochem Cell Biol* **145**, 485-496 (2016).
752 37. Balla, T. Phosphoinositides: tiny lipids with giant impact on cell regulation.
753 *Physiological reviews* **93**, 1019-1137 (2013).
754 38. Oliveira, F.M.S. *et al.* Detection of post-translational modifications using solid-phase
755 proximity ligation assay. *N Biotechnol* **45**, 51-59 (2018).
756 39. Wilson, M.S.C. & Saiardi, A. Importance of Radioactive Labelling to Elucidate Inositol
757 Polyphosphate Signalling. *Top Curr Chem (Cham)* **375**, 14 (2017).

758 40. Hale, A.T., Clarke, B.P. & York, J.D. Metabolic Labeling of Inositol Phosphates and
759 Phosphatidylinositols in Yeast and Mammalian Cells. *Methods Mol Biol* **2091**, 83-92
760 (2020).
761 41. Steinfeld, N., Giridharan, S.S.P., Kauffman, E.J. & Weisman, L.S. Simultaneous
762 Detection of Phosphoinositide Lipids by Radioactive Metabolic Labeling. *Methods Mol*
763 *Biol* **2251**, 1-17 (2021).
764 42. Lete, M.G., Tripathi, A., Chandran, V., Bankaitis, V.A. & McDermott, M.I. Lipid
765 transfer proteins and instructive regulation of lipid kinase activities: Implications for
766 inositol lipid signaling and disease. *Adv Biol Regul* **78**, 100740 (2020).
767 43. Grabon, A., Bankaitis, V.A. & McDermott, M.I. The interface between
768 phosphatidylinositol transfer protein function and phosphoinositide signaling in higher
769 eukaryotes. *J Lipid Res* **60**, 242-268 (2019).
770 44. Boura, E. & Nencka, R. Phosphatidylinositol 4-kinases: Function, structure, and
771 inhibition. *Experimental cell research* **337**, 136-145 (2015).
772 45. Li, J. *et al.* PI-273, a Substrate-Competitive, Specific Small-Molecule Inhibitor of
773 PI4KIIalpha, Inhibits the Growth of Breast Cancer Cells. *Cancer Res* **77**, 6253-6266
774 (2017).
775 46. Sengupta, N. *et al.* A large scale high-throughput screen identifies chemical inhibitors of
776 phosphatidylinositol 4-kinase type II alpha. *J Lipid Res* **60**, 683-693 (2019).
777 47. Xie, Z., Hur, S.K., Zhao, L., Abrams, C.S. & Bankaitis, V.A. A Golgi Lipid Signaling
778 Pathway Controls Apical Golgi Distribution and Cell Polarity during Neurogenesis. *Dev*
779 *Cell* **44**, 725-740 e724 (2018).
780 48. Tilley, S.J. *et al.* Structure-function analysis of human [corrected] phosphatidylinositol
781 transfer protein alpha bound to phosphatidylinositol. *Structure* **12**, 317-326 (2004).
782 49. Alb, J.G., Jr., Gedvilaite, A., Cartee, R.T., Skinner, H.B. & Bankaitis, V.A. Mutant rat
783 phosphatidylinositol/phosphatidylcholine transfer proteins specifically defective in
784 phosphatidylinositol transfer: implications for the regulation of phospholipid transfer
785 activity. *Proc Natl Acad Sci U S A* **92**, 8826-8830 (1995).
786 50. Kauffmann-Zeh, A. *et al.* Requirement for phosphatidylinositol transfer protein in
787 epidermal growth factor signaling. *Science* **268**, 1188-1190 (1995).
788 51. Stallings, J.D., Tall, E.G., Pentyala, S. & Rebecchi, M.J. Nuclear translocation of
789 phospholipase C-delta1 is linked to the cell cycle and nuclear phosphatidylinositol 4,5-
790 bisphosphate. *J Biol Chem* **280**, 22060-22069 (2005).
791 52. Jones, D.R. *et al.* Nuclear PtdIns5P as a transducer of stress signaling: an in vivo role for
792 PIP4Kbeta. *Mol Cell* **23**, 685-695 (2006).
793 53. Bua, D.J., Martin, G.M., Binda, O. & Gozani, O. Nuclear phosphatidylinositol-5-
794 phosphate regulates ING2 stability at discrete chromatin targets in response to DNA
795 damage. *Sci Rep* **3**, 2137 (2013).
796 54. Yokogawa, T. *et al.* Evidence that 3 '-phosphorylated polyphosphoinositides are
797 generated at the nuclear surface: use of immunostaining technique with monoclonal
798 antibodies specific for PI 3,4-P-2. *Febs Lett* **473**, 222-226 (2000).
799 55. Li, W. *et al.* Star-PAP control of BIK expression and apoptosis is regulated by nuclear
800 PIPKIalpha and PKCdelta signaling. *Mol Cell* **45**, 25-37 (2012).
801 56. Mellman, D.L. *et al.* A PtdIns4,5P2-regulated nuclear poly(A) polymerase controls
802 expression of select mRNAs. *Nature* **451**, 1013-1017 (2008).

57. Tanaka, K. *et al.* Evidence that a phosphatidylinositol 3,4,5-trisphosphate-binding protein can function in nucleus. *Journal of Biological Chemistry* **274**, 3919-3922 (1999).
58. Wang, Y.H. *et al.* DNA damage causes rapid accumulation of phosphoinositides for ATR signaling. *Nat Commun* **8**, 2118 (2017).
59. Wang, Y.H. & Sheetz, M.P. When PIP(2) Meets p53: Nuclear Phosphoinositide Signaling in the DNA Damage Response. *Front Cell Dev Biol* **10**, 903994 (2022).
60. Wang, Y.H. & Sheetz, M.P. Transcription-independent functions of p53 in DNA repair pathway selection. *Bioessays* **45**, e2200122 (2023).
61. Barlow, C.A., Laishram, R.S. & Anderson, R.A. Nuclear phosphoinositides: a signaling enigma wrapped in a compartmental conundrum. *Trends Cell Biol* **20**, 25-35 (2010).
62. Cockcroft, S. & Carvou, N. Biochemical and biological functions of class I phosphatidylinositol transfer proteins. *Biochim Biophys Acta* **1771**, 677-691 (2007).
63. Cosker, K.E. *et al.* Regulation of PI3K signalling by the phosphatidylinositol transfer protein PITPalpha during axonal extension in hippocampal neurons. *J Cell Sci* **121**, 796-803 (2008).
64. Li, F.L. *et al.* Hippo pathway regulation by phosphatidylinositol transfer protein and phosphoinositides. *Nat Chem Biol* **18**, 1076-1086 (2022).
65. Costes, S.V. *et al.* Automatic and quantitative measurement of protein-protein colocalization in live cells. *Biophys J* **86**, 3993-4003 (2004).
66. Schober, P., Boer, C. & Schwarte, L.A. Correlation Coefficients: Appropriate Use and Interpretation. *Anesth Analg* **126**, 1763-1768 (2018).
67. Asmari, M., Ratih, R., Alhazmi, H.A. & El Deeb, S. Thermophoresis for characterizing biomolecular interaction. *Methods* **146**, 107-119 (2018).

837 **FIGURE LEGEND**

838 **Figure 1. PITPs are required for the nuclear PIP_n pool**

839 **a**, Domains of PITP class I and II protein family members. PITD, PI transfer domain; FFAT,
840 two phenylalanines in an acidic tract; DDHD, Asp-Asp-His-Asp motif; LNS2,
841 Lipin/Nde1/Smp2 domain.

842 **b-c**, Confocal images of IF staining against PITPα/PITPβ/PITPNC1 and $PI4,5P_2$ in MDA-
843 MB-231 cells treated with vehicle or 30 μM cisplatin for 24 h. The nuclei were
844 counterstained by DAPI. The nuclear levels of PITPs and $PI4,5P_2$ were quantified by
845 ImageJ (**c**). n=3, 15 cells from each independent experiment. *p* value denotes two-sided
846 paired t-test. See expanded images in Extended Data Fig. 1a.

847 **d**, Confocal IF of PITPα or PITPβ overlaid with the nuclear envelope marker Lamin A/C
848 in MDA-MB-231 cells treated with vehicle or 30 μM cisplatin for 24 h. The nuclei were
849 counterstained by DAPI. n=3 independent experiments.

850 **e-f**, MDA-MB-231 cells were transfected with control siRNAs or siRNAs against PITPα,
851 PITPβ, PITPNC1, or both PITPα and PITPβ. After 24 h, cells were treated with 30 μM
852 cisplatin or vehicle for 24 h before being processed for IF staining. The nuclear $PI4,5P_2$
853 level was quantified by ImageJ (**f**). n=3, 15 cells from each independent experiment. *p*
854 value denotes ANOVA with Bonferroni's multiple comparisons test. See KD validation in
855 Fig. 4a and expanded images in Extended Data Fig. 5a.

856 **g**, MDA-MB-231 cells were transfected with control siRNAs or siRNAs against both
857 PITPα and PITPβ. After 24 h, cells were treated with 30 μM cisplatin or vehicle for 24 h
858 before being processed for IF staining against $PI4P/PI3,4,5P_3$ and the shared
859 epitope of PITPα and PITPβ. The nuclei were counterstained by DAPI. The

860 nuclear PI4P and PI3,4,5P3 levels were quantified by ImageJ. n=3, 15 cells from each
861 independent experiment. *p* value denotes two-sided paired t-test. See KD validation in
862 Fig. 4a and expanded images in Extended Data Fig. 5b.
863 **h-i**, A549, BT-549, MCF10A, and SUM1315 cells were transfected with control siRNAs
864 or siRNAs against both PITPα and PITPβ. After 24 h, cells were treated with 30 μM
865 cisplatin or vehicle for 24 h before being processed for IF staining against PI4,5P_2 and
866 the shared epitope of PITPα and PITPβ. The nuclei were counterstained by DAPI. The
867 nuclear PI4,5P_2 levels were quantified by ImageJ (**i**). n=3, 15 cells from each independent
868 experiment. *p* value denotes two-sided paired t-test. See KD validation in Extended Data
869 Fig. 5c and expanded images in Extended Data Fig. 5d.
870 **j**, Models showing stress-induced nuclear translocation of PITPα/β to regulate nuclear
871 PIP_n pools.
872 For all panels, data are represented as mean ± SD. Scale bar, 5 μm.

873 **Figure 2. PITPα/β bind p53 and their interaction is regulated by cellular stress**

874 **a-b,** PLA of p53-PITPα/PITPβ/PITPNC1/PITPNM1/PITPNM2 in MDA-MB-231 cells
875 treated with vehicle or 30 μM cisplatin for 24 h. The nuclear p53-PITP foci were quantified
876 (**b**). n=3, 10 cells from each independent experiment. *p* value denotes two-sided paired
877 t-test. See expanded images in Extended Data Fig. 6a.
878 **c,** PLA of p53-PITPα/PITPβ/PITPNC1 overlaid with the nuclear envelope marker Lamin
879 A/C in MDA-MB-231 cells treated with vehicle or 30 μM cisplatin for 24 h. The nuclei were
880 counterstained by DAPI.
881 **d-g**, Co-IP of PITPα/PITPβ/Hsp27 with p53 from MDA-MB-231 cells treated with vehicle
882 or 30 μM cisplatin for 24 h. PITPα IP-ed by p53 (**e**), PITPβ IP-ed by p53 (**f**), and Hsp27

883 IP-ed by p53 (**g**), as well as PITPNC1/PITPNM1/PITPNM2 were analyzed by WB. n=3
884 independent experiments. *p* value denotes two-sided paired t-test.
885 **h-k**, Co-IP of p53/Hsp27/αB-crystallin (αBC) with the shared epitope of PITPα/β from
886 MDA-MB-231 cells treated with vehicle or 30 μM cisplatin for 24 h. p53 IP-ed by PITPα/β
887 (**i**), Hsp27 IP-ed by PITPα/β (**j**), and αBC IP-ed by PITPα/β (**k**) were analyzed by WB. n=3
888 independent experiments. *p* value denotes two-sided paired t-test.
889 **l-o**, *In vitro* binding of recombinant p53 with PITPα or PITPβ. p53 immobilized on anti-
890 p53 agarose was incubated with PITPα or PITPβ protein. p53 was IP'ed and p53-bound
891 PITPα (**l**,**m**) or PITPβ (**n**,**o**) was analyzed by WB and quantified by ImageJ. n=3
892 independent experiments.
893 **p**, Model showing stress-induced formation of nuclear PITPα/β, p53, and small heat
894 shock protein (sHSP) complexes.
895 For all panels, data are represented as mean ± SD. Scale bar, 5 μm.

896 **Figure 3. PITPα/β regulate PIP_n interactions with p53**

897 **a-c,** MDA-MB-231 cells were transfected with control siRNAs or siRNAs against p53,
898 PITPα, PITPβ, PITPNC1, or both PITPα and PITPβ. After 24 h, cells were treated with 30
899 μM cisplatin or vehicle for 24 h before being processed for PLA to detect p53-PI4,5P_2/-
900 PI3,4,5P_3 complexes (**b,c**). n=3, 10 cells from each independent experiment. *p* value
901 denotes ANOVA with Bonferroni's multiple comparisons test. See KD validation in Fig. 4a
902 and expanded images in Extended Data Fig. 8a,b.
903 **d-f,** A549 cells were transfected with control siRNAs or siRNAs against PITPα, PITPβ, or
904 both PITPα and PITPβ. After 24 h, cells were treated with 30 μM cisplatin or vehicle for

905 24 h before being processed for PLA to detect p53-PI4,5P_2/PI3,4,5P_3 complexes (**e,f**).
906 n=3, 10 cells from each independent experiment. *p* value denotes ANOVA with
907 Bonferroni's multiple comparisons test. See KD validation in Fig. 4b and expanded
908 images in Extended Data Fig. 8c.
909 **g,** MDA-MB-231 cells were treated with 30 μM cisplatin or vehicle for 24 h before being
910 processed for IP against p53. p53-bound PI4P/PI4,5P_2/PI3,4,5P_3 were examined by
911 fluorescent WB. n=3 independent experiments. See quantification in Extended Data Fig.
912 8d.
913 **h-k**, MDA-MB-231 cells were transfected with control siRNAs or siRNAs against PITPα,
914 PITPβ, or both PITPα and PITPβ. After 24 h, cells were treated with 30 μM cisplatin or
915 vehicle for 24 h before being processed for IP against p53. p53-bound
916 PI4P/PI4,5P_2/PI3,4,5P_3 were examined by fluorescent WB and quantified by ImageJ (**i-**
917 **k**)**.** n=3 independent experiments. *p* value denotes ANOVA with
918 Bonferroni's multiple comparisons test. See KD validation in Fig. 4a.
919 **l-m,** MDA-MB-231 cells were cultured from low confluency in media containing [^{3}H]*myo*-
920 inositol or unlabeled *myo*-inositol. After 72 h of growth to confluency, cells were treated
921 with 30 μM cisplatin or vehicle for 24 h before being processed for IP against p53. p53
922 and PI4,5P_2 were confirmed by flourecent WB (**l**) before samples were resolved by SDS-
923 PAGE and the gel lane was excised and sectioned. Gel sections were then dissolved and
924 analyzed by liquid scintillation counting (LSC) (**m**). n=3 independent experiments, error
925 bar denotes SD, t-test, $p<0.01$*, $p<0.001$**
926 **n-o**, A549 cells were transfected with control siRNAs or siRNAs against PITPα, PITPβ,
927 or both PITPα and PITPβ. After 24 h, cells were treated with 30 μM cisplatin or vehicle

928 for 24 h before being processed for IP against p53. The PI4,5P_2 level on IPed p53 was
929 quantified by ImageJ (**o**). n=3 independent experiments. *p* value denotes ANOVA with
930 Bonferroni's multiple comparisons test. See KD validation in Fig. 4b.
931 For all graphs, data are presented as the mean ± SD. Scale bar, 5 μm.

932 **Figure 4. PITPα/β regulate p53 stability and PIP_n linkage to protein targets**

933 **a**, MDA-MB-231 cells were transfected with control siRNAs or siRNAs against p53,
934 PITPα, PITPβ, PITPNC1, or both PITPα and PITPβ. After 24 h, cells were treated with
935 30 μM cisplatin or vehicle for 24 h before being processed for WB to validate the KD.
936 The p53 level was quantified by ImageJ. n=3 independent experiments. *p* value denotes
937 ANOVA with Bonferroni's multiple comparisons test.
938 **b**, A549 cells were transfected with control siRNAs or siRNAs against PITPα, PITPβ, or
939 both PITPα and PITPβ. After 24 h, cells were treated with 30 μM cisplatin or vehicle for
940 24 h before being processed for WB. The p53 level and protein-bound PI4,5P_2 level were
941 quantified by ImageJ. n=3 independent experiments. *p* value denotes ANOVA with
942 Bonferroni's multiple comparisons test.
943 **c-d,** MDA-MB-231 cells were transfected with control siRNAs or siRNAs against p53,
944 PITPα, PITPβ, PITPNC1, or both PITPα and PITPβ. After 24 h, cells were treated with 30
945 μM cisplatin or vehicle for 24 h before being processed for triple fluorescent WB for
946 detecting p53 (Red), GAPDH (Blue), and protein-bound PI4,5P_2 (Green) simultaneously.
947 The protein-bound PI4,5P_2 levels were quantified by ImageJ (**d**). n=3 independent
948 experiments. *p* value denotes ANOVA with Bonferroni's multiple comparisons test. See
949 KD validation in Fig. 4a.

950 **e-f,** A549 cells were transfected with control siRNAs or siRNAs against PITPα or PITPβ.
951 After 24 h, cells were treated with 30 μM cisplatin or vehicle for 24 h before being
952 processed for WB. The protein-bound PIP_n levels were quantified by ImageJ (**f**). n=3
953 independent experiments. *p* value denotes two-sided paired t-test.
954 **g**, MDA-MB-231 cells were cultured from low confluency in media containing in [^{3}H]*myo*-
955 inositol or unlabeled *myo*-inositol. After 48 h, cells were transfected with control siRNAs
956 or siRNAs against PITPα and PITPβ. 24 h later, cells were treated with 30 μM cisplatin
957 or vehicle for another 24 h. KD and loading was confirmed by WB before the protein
958 fraction was extracted with $CHCl_3$/MeOH or resolved by SDS-PAGE and the gel lane was
959 excised. Extracted samples and dissolved gel sections were then analyzed by LSC. n=3
960 independent experiments. *p* value denotes two-sided paired t-test. See experimental
961 approach in Extended Data Fig. 10a and expanded images in Extended Data Fig. 10b.
962 For all graphs, data are presented as the mean ± SD.

963 **Figure 5. PI4KIIα and PITPα/β interact and are necessary to generate p53-PIP_n**
964 **complexes**

965 **a-b,** MDA-MB-231 cells were transfected with control siRNAs or siRNAs against PI4KIIIα,
966 PI4KIIIβ, PI4KIIα, PI4KIIβ or both PI4KIIα and PI4KIIIα. After 24 h, cells were treated with
967 30 μM cisplatin or vehicle for 24 h before being processed for PLA to detect p53-PI4P
968 complexes (**b**). n=3, 15 cells from each independent experiment. *p* value denotes ANOVA
969 with Bonferroni's multiple comparisons test. See KD confirmation in Fig. 5c and expanded
970 images in Extended Data Fig. 10c.
971 **c**, MDA-MB-231 cells were transfected with control siRNAs or siRNAs against PI4KIIIα,
972 PI4KIIIβ, PI4KIIα, PI4KIIβ or both PI4KIIα and PI4KIIIα. After 24 h, cells were treated with

973 30 μM cisplatin or vehicle for 24 h before being processed for WB. p53 levels were
974 quantified by ImageJ. n=3 independent experiments. *p* value denotes ANOVA with
975 Bonferroni's multiple comparisons test.
976 **d,** A549 and MDA-MB-231 cells were transfected with control siRNAs or siRNAs against
977 PI4KIIIα, PIPKIα or both PI4KIIα and PIPKIα. After 24 h, cells were treated with 30 μM
978 cisplatin or vehicle for 24 h before being processed for WB. p53 levels were quantified by
979 ImageJ. n=3 independent experiments. *p* value denotes ANOVA with
980 Bonferroni's multiple comparisons test.
981 **e,f,** MDA-MB-231 and A549 cells were transfected with control siRNAs or siRNAs against
982 PI4KIIIα, PIPKIα or both PI4KIIα and PIPKIα. After 24 h, cells were treated with 30 μM
983 cisplatin or vehicle for 24 h before being processed for PLA to detect p53-PI4P complexes.
984 n=3, 15 cells from each independent experiment. *p* value denotes ANOVA with
985 Bonferroni's multiple comparisons test. See KD confirmation in Fig. 5d and expanded
986 images in Extended Data Fig. 10h.
987 **h,** MDA-MB-231^{Cas9} cells with PITPβ KO and control non-targeted KO were transfected
988 with control siRNAs or siRNAs against PI4KIIα, PITPα or both PI4KIIα and PITPα. After
989 24 h, cells were treated with 30 μM cisplatin or vehicle for 24 h before being processed
990 for WB. n=3 independent experiments.
991 **i,** MDA-MB-231 cells were transfected with control siRNAs or siRNAs against PI4KIIα.
992 After 24h, cells were treated with 30 μM cisplatin or vehicle for 24 h before being
993 processed for PI4KIIα and PI4,5P_2 IF staining. n=3, 15 cells from each independent
994 experiment. See expanded images in Extended Data Fig. 11f and quantification in
995 Extended Data Fig. 11g.

996 **j,** Model showing PITPα/β cooperation with PI4KIIα in generating p53-PI4P complexes
997 that participate in further signaling.
998 For all panels, data are represented as mean ± SD. Scale bar, 5 μm.

999 **Figure 6. PITPα/β regulate p53-dependent nuclear Akt activation and cell survival**

1000 **a-b**, MDA-MB-231 cells were transfected with control siRNAs or siRNAs against PITPα,
1001 PITPβ, PITPNC1, or both PITPα and PITPβ. After 24h, cells were treated with 30 μM
1002 cisplatin or vehicle for 24 h before being processed for IF staining against $pAkt^{S473}$. The
1003 nuclear $pAkt^{S473}$ levels were quantified by ImageJ (**b**). n=3, 15 cells from each
1004 independent experiment. *p* value denotes ANOVA with
1005 Bonferroni's multiple comparisons test. Scale bar, 5 μm.
1006 **c-e**, BT-549, SUM159, and SUM1315 cells with the indicated p53 status were transfected
1007 with control siRNAs or siRNAs against both PITPα and PITPβ. After 24 h, cells were
1008 treated with 30 μM cisplatin or vehicle for 24 h before being processed for IF staining
1009 against $pAkt^{S473}$. The nuclei were counterstained by DAPI. The nuclear $pAkt^{S473}$ levels
1010 were quantified (**d**). n=3, 15 cells from each independent experiment. *p* value denotes
1011 two-sided paired t-test. Scale bar, 5 μm. The double KD of PITPα and PITPβ in SUM159
1012 cells was validated by WB (**e**). See KD validation for BT-549 and SUM1315 cells in
1013 Extended Data Fig. 5c.
1014 **f-g**, MDA-MB-231 cells were transfected with control siRNAs or siRNAs against p53,
1015 PITPα, PITPβ, PITPNC1, or both PITPα and PITPβ. After 24 h, cells were treated with 30
1016 μM cisplatin or vehicle for 24 h before being processed for Crystal Violet viability assay.
1017 The cells were imaged by EVOS M5000 microscope (**f**) and quantified based on the

1018 extracted dye using a plate reader (**g**). n=3 independent experiments. *p* value denotes
1019 ANOVA with Bonferroni's multiple comparisons test. Scale bar, 300 μm.
1020 **h,** MDA-MB-231^{Cas9} cells with PITPβ KO and control non-targeted KO were transfected
1021 with control siRNAs or siRNAs against PITPα, PITPβ or both PITPα and PITPβ. After 24
1022 h, cells were treated with 30 μM cisplatin or vehicle for 24 h before being processed for
1023 Crystal Violet viability assay. The cells were imaged by EVOS M5000 microscope. Scale
1024 bar, 300 μm. n=3 independent experiments. See quantification in Extended Data Fig. 11i.
1025 **i**, MDA-MB-231 cells were transfected with control siRNAs or siRNAs against p53, PITPα,
1026 PITPβ, PITPNC1, or both PITPα and PITPβ. After 24h, cells were treated with 30 μM
1027 cisplatin or vehicle for 24 h before being processed for caspase 3 activity assay. n=3
1028 independent experiments. *p* value denotes ANOVA with
1029 Bonferroni's multiple comparisons test. See quantification in Extended Data Fig. 11i.

1030 For all graphs, data are presented as the mean ± SD.

1031 **Figure 7. PITPα/β initiate the p53-PIP$_n$ signalosome by a PI binding-dependent**
1032 **mechanism**

1033 **a**, HEK293FT cells were co-transfected with either HA-tagged wild-type PITPα or PI
1034 binding-defective mutant T59D PITPα together with Flag-tagged p53^{wt}. After 48 h, cells
1035 were processed for IP against Flag-tag and analyzed by WB. n=3 independent
1036 experiments. *p* value denotes two-sided paired t-test.
1037 **b-e**, MDA-MB-231 cells were transfected with control siRNAs or siRNAs against the
1038 3'UTR of both PITPα and PITPβ for 24 h. Then the cells were transfected with either HA-
1039 tagged wild-type PITPα/β or PI binding-defective mutant T59D PITPα/β. After 24 h, cells

1040 were treated with 30 μM cisplatin or vehicle for 24 h before being processed for WB (**b**)
1041 and IF staining against HA-tag with PI4,5P_2 or pAkt^{S473} (**c**). The nuclear PI4,5P_2 and
1042 pAkt^{S473} levels in HA-positive cells were quantified by ImageJ (**d, e**). n=3, 15 cells from
1043 each independent experiment. *p* value denotes two-sided paired t-test. Scale bar, 5 μm.
1044 **f-i**, Pearson's correlation coefficient (Pearson's r) quantified the correlations between
1045 nuclear PI4,5P_2 or pAkt^{S473} with HA-PITPα$^{wt/T59D}$ levels. n=100 cells pooled from 3
1046 independent experiments.
1047 **j-k**, MDA-MB-231 cells were transfected with control siRNAs or siRNAs against the 3'UTR
1048 of both PITPα and PITPβ for 24 h. The cells were then transfected with either HA-tagged
1049 wild-type PITPα or PI binding-defective mutant T59D PITPα. After 24 h, cells were treated
1050 with 30 μM cisplatin or vehicle for 24 h before being processed for Crystal Violet viability
1051 assay. The cells were imaged by EVOS M5000 microscope (**j**) and quantified based on
1052 the extracted dye using a plate reader (**k**). n=3 independent experiments. *p* value denotes
1053 two-sided paired t-test. Scale bar, 300 μm.
1054 **l-m**, MDA-MB-231 cells were transfected with control siRNAs or siRNAs against the
1055 3'UTR of both PITPα and PITPβ for 24 h. The cells were then transfected with either HA-
1056 tagged wild-type PITPα or PI binding-defective mutant T59D PITPα. After 24 h, cells were
1057 serum starved for an additional 24 h and then scored for invasion through Laminin-coated
1058 transwell inserts with 8 μm pores using 10 ng/ml EGF as a chemoattractant for 16 h. The
1059 invading cells at the insert bottom were stained with Crystal Violet, imaged (**l**), and
1060 quantified (**m**) based on the extracted dye using a plate reader. n=3 independent
1061 experiments. *p* value denotes two-sided paired t-test. Scale bar, 300 μm.

1062 **n**, A model of the stress-induced nuclear accumulation of class I PITPs and PITP-
1063 dependent initiation of the p53-PI signalosome which promotes cell proliferation, survival,
1064 and invasion.
1065 For all graphs, data are presented as the mean ± SD.

1066 **SUPPLEMENTAL INFORMATION**

1067 **Extended Data Figure 1. Cisplatin induces the nuclear accumulation of PITPs**

1068 **a**, Confocal images of IF staining against PITPα/PITPβ/PITPNC1 and PI4,5P2 in MDA-
1069 MB-231 cells treated with vehicle or 30 μM cisplatin for 24 h. The nuclei were
1070 counterstained by DAPI. See quantification in Fig. 1c.
1071 **b**, Ratio calculation of IF staining against PITPα/PITPβ in MDA-MB-231 cells treated
1072 with vehicle or 30 μM cisplatin for 24 h to determine % PITP signal in the nucleus. *p*
1073 value denotes two-sided paired t-test. See expanded images in Fig. 1b and Extended
1074 Data Fig. 1a.
1075 **c**, Pearson's correlation coefficient (Pearson's r) quantified the correlations between
1076 nuclear PI4,5P_2 with endogenous PITPβ levels. n=100 cells pooled from 3 independent
1077 experiments.
1078 **d**, MDA-MB-231^{Cas9} cells with PITPβ KO and control non-targeted KO were transfected
1079 with control siRNAs or siRNAs against PITPα and processed for IF staining against PITPα.
1080 n=3 independent experiments.
1081 **e**, MDA-MB-231^{Cas9} cells with PITPβ KO and control non-targeted KO were transfected
1082 with control siRNAs or siRNAs against PITPβ and processed for IF staining against PITPβ.
1083 n=3 independent experiments.

1084 **f,** MDA-MB-231^{Cas9} cells with PITPβ KO and control non-targeted KO were transfected
1085 with control siRNAs or siRNAs against PITPα and processed for WB against PITPα and
1086 PITPβ. n=3 independent experiments.
1087 **g**, MDA-MB-231 cells were treated with vehicle or cisplatin for 24 h. Cells were then
1088 fractionated using a detergent-based extraction to produce lysates from cytosolic and
1089 nuclear fractions and analyzed via WB. n=3 independent experiments.
1090 For all graphs, data are presented as the mean ± SD.

1091 **Extended Data Figure 2. PITPα/β accumulate in the non-membranous**
1092 **nucleoplasm**

1093 **a-b**, 3D sections of IF staining against PITPα in MDA-MB-231 cells treated with vehicle
1094 or 30 μM cisplatin for 24 h. The nuclei were counterstained by DAPI. Each frame of the
1095 3D sections was over a 0.2 μm thickness.
1096 **c-d**, 3D sections of IF staining against PITPβ in MDA-MB-231 cells treated with vehicle
1097 or 30 μM cisplatin for 24 h. The nuclei were counterstained by DAPI. Each frame of the
1098 3D sections was over a 0.2 μm thickness.
1099 For all panels, Scale bar, 5 μm.

1100 **Extended Data Figure 3. Cisplatin induces the nuclear accumulation of PITPs in**
1101 **multiple cell lines**

1102 **a-b**, Confocal images of the IF staining against PITPα/β in wild-type and mutant p53
1103 expressing cells, including MCF10A (WT), A549 (WT), HCT116 (WT), BT-549 (R249S),
1104 Cal33 (R175H), HS578T (V157F), SUM159 (R158InL), and SUM1315 (C135F). The

1105 nuclei were counterstained by DAPI. Nuclear PITPα and PITPβ levels were quantified by
1106 ImageJ (**b**). *p* value denotes two-sided paired t-test. n=3 independent experiments.
1107 For all graphs, data are presented as the mean ± SD. Scale bar, 5 μm.

1108 **Extended Data Figure 4. Cell stress induces the non-membranous nuclear**
1109 **accumulation of PITPs in multiple cell lines**

1110 **a-b**, MDA-MB-231 cells were treated with 30 μM cisplatin, 20 μM erastin, 100 μM tBHQ,
1111 100 μM etoposide, 100 μM hydroxyurea, or vehicle for 24 h. The cells were then
1112 processed for IF staining against PITPα or PITPβ and PI4,5P_2. The nuclei were
1113 counterstained by DAPI. The nuclear levels of PITPs and PI4,5P_2 were quantified by
1114 ImageJ (**b**). *p* value denotes two-sided paired t-test. n=3, 15 cells from each independent
1115 experiment.
1116 **c**, Confocal IF of PITPα or PITPβ overlaid with the nuclear envelope marker Lamin A/C
1117 in A549 and MDA-MB-231 cells treated with vehicle or 30 μM cisplatin for 24 h. The nuclei
1118 were counterstained by DAPI. n=3 independent experiments.
1119 **d-e**, Confocal IF of PITPα or PITPβ overlaid with the nuclear envelope marker Lamin A/C
1120 in MCF10A, A549, SUM1315, BT-549, HCT116, Cal33, HS578T and SUM159 cells
1121 treated with vehicle or 30 μM cisplatin for 24 h. The nuclei were counterstained by DAPI.
1122 n=3 independent experiments.
1123 For all graphs, data are presented as the mean ± SD. Scale bar, 5 μm.

1124 **Extended Data Figure 5. PITPs regulate nuclear PIP_ns**

1125 **a**, MDA-MB-231 cells were transfected with control siRNAs or siRNAs against PITPα or
1126 PITPβ. After 24 h, cells were treated with 30 μM cisplatin or vehicle for 24 h before being
1127 processed for IF staining. See quantification in Fig. 1f. n=3 independent experiments.
1128 **b**, MDA-MB-231 cells were transfected with control siRNAs or siRNAs against both
1129 PITPα and PITPβ. After 24 h, cells were treated with 30 μM cisplatin or vehicle for 24 h
1130 before being processed for IF staining against PI4P/PI3,4,5P_3 and the shared
1131 epitope of PITPα and PITPβ. The nuclei were counterstained by DAPI. n=3, independent
1132 experiments. See quantification in Fig. 1g.
1133 **c**, A549, BT-549, MCF10A, and SUM1315 cells were transfected with control siRNAs or
1134 siRNAs against both PITPα and PITPβ. After 24 h, cells were treated with 30 μM cisplatin
1135 or vehicle for 24 h before being processed for WB. n=3 independent experiments.
1136 **d**, MCF10A, and SUM1315 cells were transfected with control siRNAs or siRNAs against
1137 both PITPα and PITPβ. After 24 h, cells were treated with 30 μM cisplatin or vehicle for
1138 24 h before being processed for IF staining against PI4,5P_2 and the shared epitope of
1139 PITPα and PITPβ. The nuclei were counterstained by DAPI. n=3 independent
1140 experiments. See quantification in Fig. 1i.
1141 Scale bar, 5 μm.

1142 **Extended Data Figure 6. Stress induces PITPα/β association with p53 in the**
1143 **nucleoplasm**

1144 **a,** PLA of p53-PITPNM1/PITPNM2 in MDA-MB-231 cells treated with vehicle or 30 μM
1145 cisplatin for 24 h. See quantification in Fig. 2b.
1146 **b-c,** PLA of p53-PITPα/PITPβ/PITPNC1/PITPNM1/PITPNM2 in A549 cells treated with
1147 vehicle or 30 μM cisplatin for 24 h. The nuclear p53-PITP PLA foci were quantified by

1148 ImageJ (**c**). *p* value denotes two-sided paired t-test. n=3, 10 cells from each independent
1149 experiment.
1150 **d,** PLA of p53-PITPα/PITPβ/PITPNC1/PITPNM1/PITPNM2 overlaid with the nuclear
1151 envelope marker Lamin A/C in A549 cells treated with vehicle or 30 μM cisplatin for 24 h.
1152 The nuclei were counterstained by DAPI.
1153 **e,** PLA of p53-PITPNM1/PITPNM2 overlaid with the nuclear envelope marker Lamin A/C
1154 in MDA-MB-231 treated with vehicle or 30 μM cisplatin for 24 h. The nuclei were
1155 counterstained by DAPI.
1156 **f**, 3D sections of p53-PITPβ PLA foci overlaid with Lamin A/C in MDA-MB-231 treated
1157 with vehicle or 30 μM cisplatin for 24 h. The nuclei were counterstained by DAPI. Each
1158 frame of the 3D sections was over a 0.2 μm thickness.
1159 For all graphs, data are presented as the mean ± SD. Scale bar, 5 μm.

1160 **Extended Data Figure 7. Stress induces PITPα/β association with p53**

1161 **a-d,** Co-IP of p53/Hsp27/αB-crystallin (αBC) with the shared epitope of PITPα/β in
1162 MCF10A cells treated with vehicle or 30 μM cisplatin for 24 h. p53 immunoprecipitated
1163 (IPed) by PITPα/β (**b**), Hsp27 IPed by PITPα/β (**c**), and αBC IPed by PITPα/β (**d**) were
1164 analyzed by WB. n=3 independent experiments.
1165 **e-f,** Co-IP of p53 with the shared epitope of PITPα/β in A549 cells treated with vehicle or
1166 30 μM cisplatin for 24 h. p53 IPed by PITPα/β was analyzed by WB (**f**). n=3 independent
1167 experiments.
1168 **g-h,** Co-IP of p53 with the shared epitope of PITPα/β in HCT116 cells treated with vehicle
1169 or 30 μM cisplatin for 24 h. p53 IPed by PITPα/β was analyzed by WB (**h**). n=3
1170 independent experiments.

1171 **i-n,** Co-IP of PITPα/PITPβ with p53 in BT549, Cal33, HS578T, SUM159, SUM1315 cells
1172 treated with vehicle or 30 μM cisplatin for 24 h. PITPα/PITPβ IPed by p53 (**n**) as well as
1173 PITPNC1/PITPNM1/PITPNM2 were analyzed by WB. n=3 independent experiments.
1174 For all panels, data are represented as mean ± SD, *p* value denotes two-sided paired t-
1175 test.

1176 **Extended Data Figure 8. PITPα/β and PI4KIIα regulate p53-PIP$_n$ signaling in**
1177 **response to stress**

1178 **a-b,** MDA-MB-231 cells were transfected with control siRNAs or siRNAs against p53,
1179 PITPα, PITPβ, PITPNC1, or both PITPα and PITPβ. After 24 h, cells were treated with 30
1180 μM cisplatin or vehicle for 24 h before being processed for PLA to detect p53-PI4,5P$_2$ (**a**)
1181 and p53-PI3,4,5P$_3$ (**b**) complexes. n=3 independent experiments. See KD validation in
1182 Fig. 4a, expanded images in Fig. 3a, and quantification in Fig. 3b,c.
1183 **c,** A549 cells were transfected with control siRNAs or siRNAs against PITPα, PITPβ, or
1184 both PITPα and PITPβ. After 24 h, cells were treated with 30 μM cisplatin or vehicle for
1185 24 h before being processed for PLA to detect p53-PI4,5P$_2$/PI3,4,5P$_3$ complexes. n=3
1186 independent experiments. See KD validation in Fig. 4b, expanded images in Fig. 3d, and
1187 quantification in Fig. 3e,f.
1188 **d,** MDA-MB-231 cells were treated with 30 μM cisplatin or vehicle for 24 h before being
1189 processed for IP against p53. p53-bound PI4P/PI4,5P$_2$/PI3,4,5P$_3$ were examined by
1190 fluorescent WB in Fig. 3g. n=3 independent experiments. *p* value denotes two-sided
1191 paired t-test.
1192 **e**, MDA-MB-231 cells were transfected with control siRNAs or siRNAs against both PITPα
1193 and PITPβ. After 24 h, cells were treated with 10 μM Nutlin 3a or vehicle for 24 h before

1194 being processed for WB and analyzed using ImageJ. *p* value denotes two-sided paired t-
1195 test. n=3 independent experiments.
1196 **f,** MDA-MB-231 cells were treated with 30 μM cisplatin and lysates were made at the
1197 indicated timepoints along a 24 h time course. Whole cell lysates were then processed
1198 for WB. n=3 independent experiments
1199 **g,** MDA-MB-231^{Cas9} cells with PITPβ KO and control non-targeted KO were transfected
1200 with control siRNAs or siRNAs against PITPα, PITPβ or both PITPα and PITPβ. After 24
1201 h, cells were treated with 30 μM cisplatin or vehicle for 24 h before being processed for
1202 WB. PI4,5P_2 lane signal was quantified using ImageJ. *p* value denotes ANOVA with
1203 Bonferroni's multiple comparisons test. n=3 independent experiments.
1204 For all panels, data are represented as mean ± SD. Scale bar, 5 μm.

1205 **Extended Data Figure 9. PI4P is linked to the p53^{6Q} mutant which disrupts PI4,5P_2**
1206 **binding**

1207 **a-b,** MDA-MB-231 cells were cultured from low confluency in media containing [^{3}H]*myo*-
1208 inositol or unlabeled myo-inositol. After 48 h, cells were transfected with control siRNAs
1209 or siRNAs against PITPα and PITPβ. 24 h later, cells were treated with 30 μM cisplatin
1210 or vehicle for another 24 h. KD and loading was confirmed by WB. Dissolved gel sections
1211 were then analyzed by LSC (**a**). n=3 independent experiments. See expanded images
1212 and LSC quantification in Fig. 4g.
1213 **c-d,** H1299 cells transfected with constructs expressing p53 WT, WT6Q, 175H, 175H6Q,
1214 248Q and 248Q6Q were treated with 30 μM cisplatin for 24 h. Then the cells were
1215 processed for PLA to detect p53-PI4P complexes (**d**). Nuclei were counterstained by
1216 DAPI. *p* value denotes two-sided paired t-test. n=3 independent experiments.

1217 **e-f,** H1299 cells transfected with constructs expressing p53 WT, WT6Q, 175H, 175H6Q,
1218 248Q, and 248Q6Q were treated with 30 μM cisplatin for 24 h. Then the cells were
1219 processed for PLA to detect p53-PI3,4,5P_3 complexes (**f**). Nuclei were counterstained by
1220 DAPI. *p* value denotes two-sided paired t-test. n=3 independent experiments.
1221 For all panels, data are represented as mean ± SD. Scale bar, 5 μm.

1222 **Extended Data Figure 10. PITPs and PI4KIIα generate Protein-PIP$_n$ complexes**

1223 **a,** MDA-MB-231 cells were transfected with control siRNAs or siRNAs against PI4KIIIα,
1224 PI4KIIIβ, PI4KIIα, PI4KIIβ or both PI4KIIα and PI4KIIIα. After 24 h, cells were treated with
1225 30 μM cisplatin or vehicle for 24 h before being processed for PLA to detect p53-PI4P
1226 complexes. n=3, 15 cells from each independent experiment. See KD confirmation in Fig.
1227 5c, expanded images in Fig. 5a, and quantification in Fig. 5b.
1228 **b-c**, MDA-MB-231 cells were treated with vehicle or cisplatin in combination with DMSO
1229 as a control, PI-273, or NC03 for 24 h before being processed for PLA to detect p53-PI4P
1230 complexes and analyzed using ImageJ (**c**). *p* value denotes two-sided paired t-test. n=3,
1231 15 cells from each independent experiment.
1232 **d-e**, MDA-MB-231 cells were treated with vehicle or cisplatin in combination with DMSO
1233 as a control, PI-273, or NC03 for 24 h before being processed for PLA to detect p53-
1234 PI3,4,5P_3 complexes and analyzed using ImageJ (**e**). *p* value denotes two-sided paired
1235 t-test. n=3, 15 cells from each independent experiment.
1236 **f**, MDA-MB-231 and A549 cells were transfected with control siRNAs or siRNAs against
1237 PI4KIIIα, PIPKIα or both PI4KIIα and PIPKIα. After 24 h, cells were treated with 30 μM
1238 cisplatin or vehicle for 24 h before being processed for PLA to detect p53-PI4P complexes.

1239 n=3, 15 cells from each independent experiment. See KD confirmation in Fig. 5d,
1240 expanded images in Fig. 5e, and quantification in Fig. 5f.
1241 For all panels, data are represented as mean ± SD. Scale bar, 5 μm.

1242 **Extended Data Figure 11. PI4KIIα interacts with PITPα/β and p53 to promote p53-**
1243 **PIP_n and protein-PIP_n complex formation**

1244 **a-c**, *In vitro* binding of recombinant PI4KIIα and p53 (**a**), PI4KIIα and PITPα (**b**) and
1245 PI4KIIα and PITPβ (**c**). p53, PITPα or PITPβ immobilized on the indicated antibody-
1246 conjugated agarose was incubated with PI4KIIα protein. p53, PITPα or PITPβ was IPed
1247 and p53-bound PI4KIIα (**a**), PITPα-bound PI4KIIα (**b**) and PITPβ-bound PI4KIIα (**c**) was
1248 analyzed by WB and quantified by ImageJ. n=3 independent experiments.
1249 **d,** MDA-MB-231 cells were transfected with control siRNAs or siRNAs against both PITPα
1250 and PITPβ or PI4KIIα. After 24 h, cells were treated with 30 μM cisplatin or vehicle for 24
1251 h before being processed for WB. n=3 independent experiments.
1252 **e,** MDA-MB-231^{Cas9} cells with PITPβ KO and control non-targeted KO were transfected
1253 with control siRNAs or siRNAs against PI4KIIα, PITPα or both PI4KIIα and PITPα. After
1254 24 h, cells were treated with 30 μM cisplatin or vehicle for 24 h before being processed
1255 for WB. n=3 independent experiments.
1256 **f-g,** MDA-MB-231 cells were transfected with control siRNAs or siRNAs against PI4KIIα.
1257 After 24h, cells were treated with 30 μM cisplatin or vehicle for 24 h before being
1258 processed for IF staining. The nuclear PI4,5P_2 level was quantified by ImageJ (**g**). *p* value
1259 denotes two-sided paired t-test. n=3, 15 cells from each independent experiment. See
1260 expanded images in Fig. 5i.

1261 **h**, MDA-MB-231 cells were transfected with control siRNAs or siRNAs against both PITPα
1262 and PITPβ. After 24 h, cells were treated with 30 μM cisplatin or vehicle for 24 h before
1263 being processed for WB. n=3 independent experiments.
1264 **i,** MDA-MB-231^{Cas9} cells with PITPβ KO and control non-targeted KO were transfected
1265 with control siRNAs or siRNAs against PITPα, PITPβ or both PITPα and PITPβ. After 24
1266 h, cells were treated with 30 μM cisplatin or vehicle for 24 h before being processed for
1267 Crystal Violet viability assay. Viability was quantified based on the extracted dye using a
1268 plate reader. *p* value denotes ANOVA with Bonferroni's multiple comparisons test. n=3
1269 independent experiments. See representative images in Fig. 6h.
1270 For all panels, data are represented as mean ± SD. Scale bar, 5 μm.

1271 **Extended Data Figure 12. PITPα/β and mutant p53 inhibit genotoxic stress-induced**
1272 **apoptosis**

1273 **a-g**, BT-549, SUM159, and SUM1315 cells were transfected with control siRNAs or
1274 siRNAs against p53, PITPα, PITPβ, or both PITPα and PITPβ. After 24 h, cells were
1275 treated with 30 μM cisplatin or vehicle for 24 h before being processed for Crystal Violet
1276 viability assay. The cells were imaged by EVOS M5000 microscope (**a**) and quantified
1277 based on the extracted dye using a plate reader (**b-d**). The KD was validated by WB (**e-**
1278 **g**). *p* value denotes ANOVA with Bonferroni's multiple comparisons test. n=3 independent
1279 experiments.
1280 **h-j**, BT-549, SUM159, and SUM1315 cells were transfected with control siRNAs or
1281 siRNAs against p53, PITPα, PITPβ, or both PITPα and PITPβ. After 24 h, cells were
1282 treated with 30 μM cisplatin or vehicle for 24 h before being processed for caspase 3

1283 activity assay. *p* value denotes ANOVA with Bonferroni's multiple comparisons test. n=3
1284 independent experiments.
1285 For all graphs, data are presented as the mean ± SD, and *p* values are from two-sided
1286 paired t-tests. Scale bar, 300 μm.
1287 **k**, HEK293FT cells were co-transfected with either HA-tagged wild-type PITPα or PI
1288 binding-defective mutant T59D PITPα together with Flag-tagged mutant $p53^{R175H}$. After
1289 48 h, cells were processed for IP against Flag-tag and analyzed by WB. *p* value denotes
1290 two-sided paired t-test. n=3 independent experiments.
1291 **l**, HEK293FT cells were co-transfected with either HA-tagged wild-type PITPβ or PI
1292 binding-defective mutant T59D PITPβ together with Flag-tagged $p53^{wt}$. After 48 h, cells
1293 were processed for IP against Flag-tag and analyzed by WB. *p* value denotes two-sided
1294 paired t-test. n=3 independent experiments.
1295 **m**, HEK293FT cells were co-transfected with either HA-tagged wild-type PITPβ or PI
1296 binding-defective mutant T59D PITPβ together with Flag-tagged mutant $p53^{R175H}$. After
1297 48 h, cells were processed for IP against Flag-tag and analyzed by WB. *p* value denotes
1298 two-sided paired t-test. n=3 independent experiments.
1299 **n**, MDA-MB-231 cells were transfected with control siRNAs or siRNAs against the 3'UTR
1300 of both PITPα and PITPβ for 24 h. The cells were then transfected with either HA-tagged
1301 wild-type PITPα or PI binding-defective mutant T59D PITPα. After 24 h, cells were treated
1302 with 30 μM cisplatin or vehicle for 24 h before being processed for caspase 3 activity
1303 assay. *p* value denotes two-sided paired t-test. n=3 independent experiments.
1304 For all graphs, data are presented as the mean ± SD. Scale bar, 300 μm.

1305 **Table 1. Binding affinities of p53-PIP_n signalosome components**

1306 The binding affinity of the protein-PIP_n complex regulators and p53. The interaction of
1307 recombinant fluorescently labelled p53, PI4KIIα, and PITPβ with other components was
1308 quantitated by MST assay. A constant concentration of fluorescently labelled p53, PI4KIIα,
1309 or PITPβ (target, 5 nM) was incubated with increasing concentrations of non-labelled
1310 binding partners or ligands to calculate the binding affinity. The binding affinities
1311 determined by MST are shown as indicated K_d values. MST was performed using a
1312 Monolith NT.115 pico, and the binding affinity was autogenerated by MO. Control v.1.6
1313 software. Data are presented as the mean ± SD; n = 3.

1314 **Supplementary Video 1**

1315 **3D reconstitution of the p53-PITPβ complex in the nucleoplasm of MDA-MB-231**
1316 **cells under basal conditions**

1317 MDA-MB-231 cells were treated with control vehicle for 24 h before being processed for
1318 PLA between p53 and PITPβ (Red). Lamin A/C stained the nuclear envelope (Green),
1319 and the nuclei were counter-stained with DAPI (Blue). The z-stack images were taken
1320 with a Leica SP8 confocal microscope with each frame over a 0.2 μm thickness. The
1321 video of the 3D reconstitution of a representative cell from three independent experiments
1322 was generated by LASX.

1323 **Supplementary Video 2**

1324 **3D reconstitution of the p53-PITPβ complex in the nucleoplasm of MDA-MB-231**
1325 **cells under stress**

1326 MDA-MB-231 cells were treated with 30 μM cisplatin for 24 h before being processed for
1327 PLA between p53 and PITPβ (Red). Lamin A/C stained the nuclear envelope (Green),
1328 and the nuclei were counter-stained with DAPI (Blue). The z-stack images were taken

1329 with a Leica SP8 confocal microscope with each frame over a 0.2 μm thickness. The
1330 video of the 3D reconstitution of a representative cell from three independent experiments
1331 was generated by LASX.

1332
1333

Table 1

	Binding Affinity Kd (nM)		
Target Protein	**p53**	**PI4KIIα**	**PITPβ**
PITPα	1.23 ± 0.05	189 ± 26	-
PITPα + PI (1μM)	15 ± 1	16 ± 2	-
PITPβ	19 ± 2	263 ± 12	-
PITPβ + PI (1μM)	5 ± 1	113 ± 11	-
PITPNC1	NBD	-	-
p53	-	8 ± 1	15 ± 1
PI4KIIα	4 ± 1	-	201 ± 2

"-" denotes values that were not tested

NBD = No Binding Detected

Fig. 1

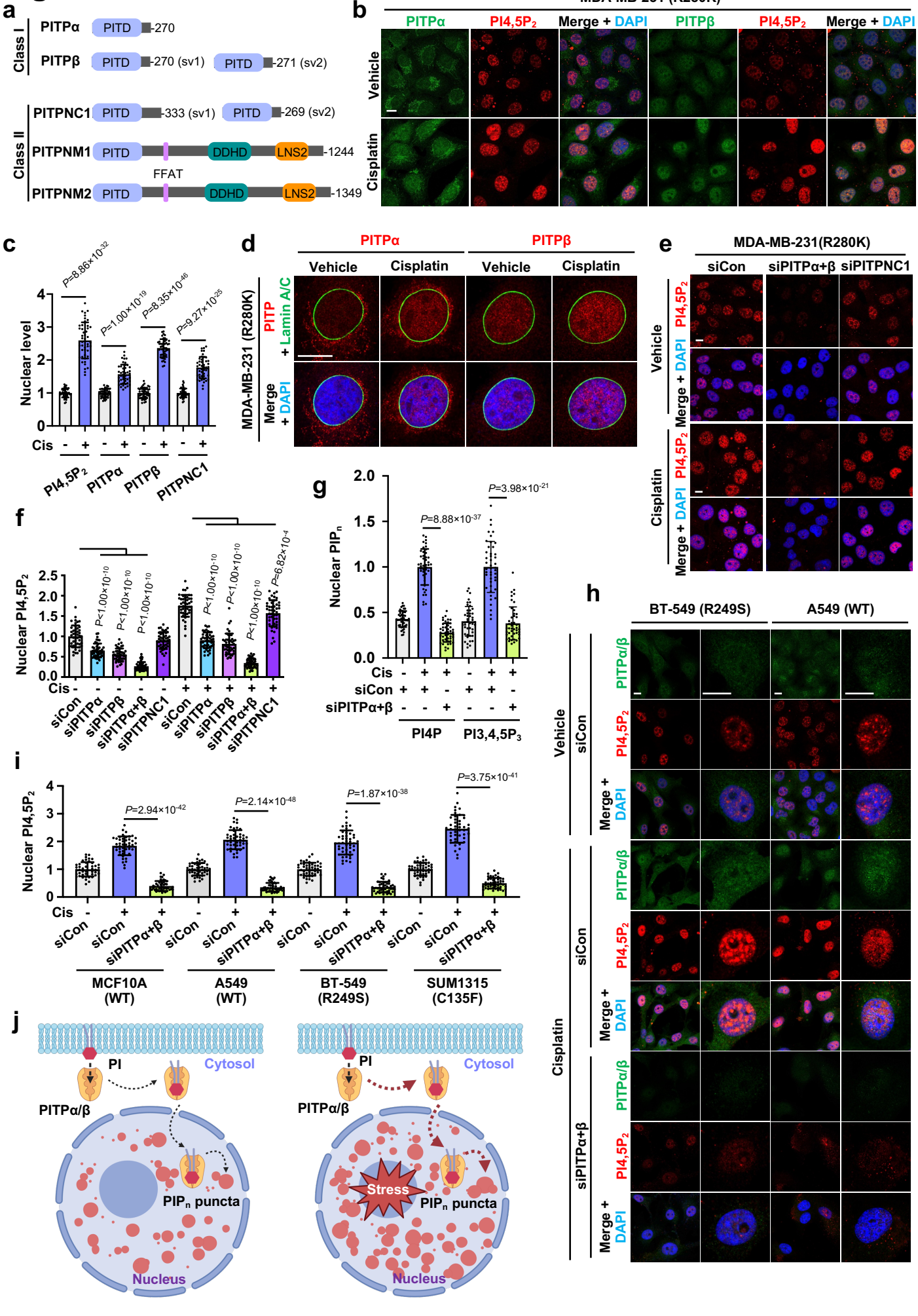
a
Class I
PITPα
PITD
-270
PITPβ
PITD
-270 (sv1)
PITD
-271 (sv2)
Class II
PITPNC1
PITD
-333 (sv1)
PITD
-269 (sv2)
PITPNM1
PITD
DDHD
LNS2
-1244
FFAT
PITPNM2
PITD
DDHD
LNS2
-1349
b
MDA-MB-231 (R280K)
PITPα
PI4,5P2
Merge + DAPI
PITPβ
PI4,5P2
Merge + DAPI
Vehicle
Cisplatin
c
Nuclear level
P=8.86×10-32
P=1.00×10-19
P=8.35×10-46
P=9.27×10-25
Cis
PI4,5P2
PITPα
PITPβ
PITPNC1
d
PITPα
PITPβ
Vehicle
Cisplatin
Vehicle
Cisplatin
MDA-MB-231 (R280K)
PITP + Lamin A/C
Merge + DAPI
e
MDA-MB-231(R280K)
siCon
siPITPα+β
siPITPNC1
Vehicle
Cisplatin
PI4,5P2
Merge + DAPI
f
Nuclear PI4,5P2
P<1.00×10-10
P=6.82×10-4
Cis
siCon
siPITPα
siPITPβ
siPITPα+β
siPITPNC1
g
Nuclear PIPn
P=8.88×10-37
P=3.98×10-21
Cis
siCon
siPITPα+β
PI4P
PI3,4,5P3
h
BT-549 (R249S)
A549 (WT)
Vehicle
Cisplatin
siCon
siPITPα+β
PITPα/β
PI4,5P2
Merge + DAPI
i
Nuclear PI4,5P2
P=2.94×10-42
P=2.14×10-48
P=1.87×10-38
P=3.75×10-41
Cis
siCon
siPITPα+β
MCF10A (WT)
A549 (WT)
BT-549 (R249S)
SUM1315 (C135F)
j
PI
Cytosol
PITPα/β
PIPn puncta
Nucleus
Stress

Fig. 2

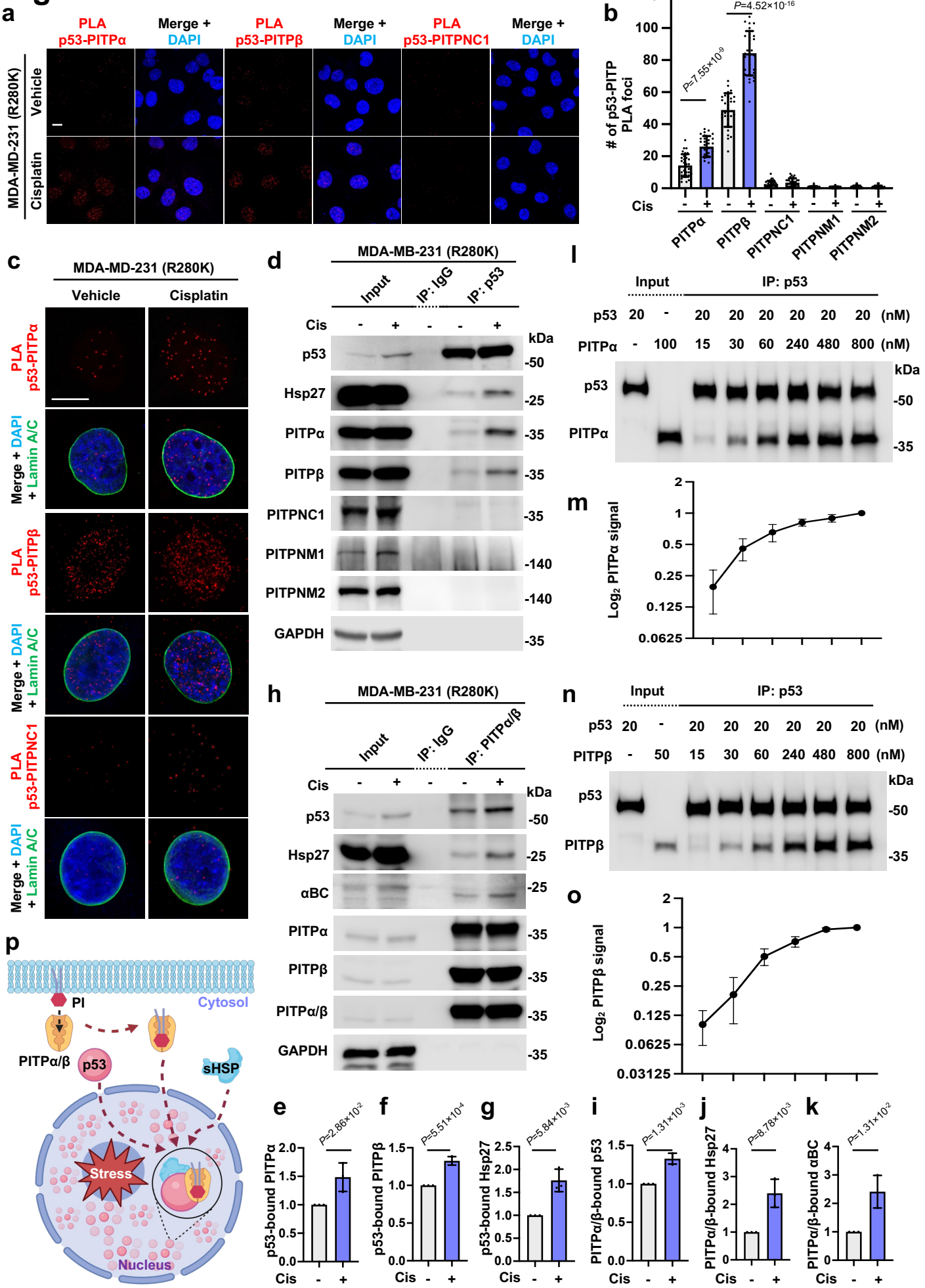
a
PLA p53-PITPα
Merge + DAPI
PLA p53-PITPβ
Merge + DAPI
PLA p53-PITPNC1
Merge + DAPI
MDA-MD-231 (R280K)
Vehicle
Cisplatin
b
P=4.52×10-16
P=7.55×10-9
# of p53-PITP PLA foci
Cis
PITPα
PITPβ
PITPNC1
PITPNM1
PITPNM2
c
MDA-MD-231 (R280K)
Vehicle
Cisplatin
PLA p53-PITPα
Merge + DAPI + Lamin A/C
PLA p53-PITPβ
Merge + DAPI + Lamin A/C
PLA p53-PITPNC1
Merge + DAPI + Lamin A/C
d
MDA-MB-231 (R280K)
Input
IP: IgG
IP: p53
Cis
kDa
p53
Hsp27
PITPα
PITPβ
PITPNC1
PITPNM1
PITPNM2
GAPDH
l
Input
IP: p53
p53 20 - 20 20 20 20 20 20 (nM)
PITPα - 100 15 30 60 240 480 800 (nM)
kDa
p53
PITPα
m
Log2 PITPα signal
h
MDA-MB-231 (R280K)
Input
IP: IgG
IP: PITPα/β
Cis
kDa
p53
Hsp27
αBC
PITPα
PITPβ
PITPα/β
GAPDH
n
Input
IP: p53
p53 20 - 20 20 20 20 20 20 (nM)
PITPβ - 50 15 30 60 240 480 800 (nM)
kDa
p53
PITPβ
o
Log2 PITPβ signal
p
PI
Cytosol
PITPα/β
p53
sHSP
Stress
Nucleus
e
P=2.86×10-2
p53-bound PITPα
f
P=5.51×10-4
p53-bound PITPβ
g
P=5.84×10-3
p53-bound Hsp27
i
P=1.31×10-3
PITPα/β-bound p53
j
P=8.78×10-3
PITPα/β-bound Hsp27
k
P=1.31×10-2
PITPα/β-bound αBC
Cis

Fig. 3

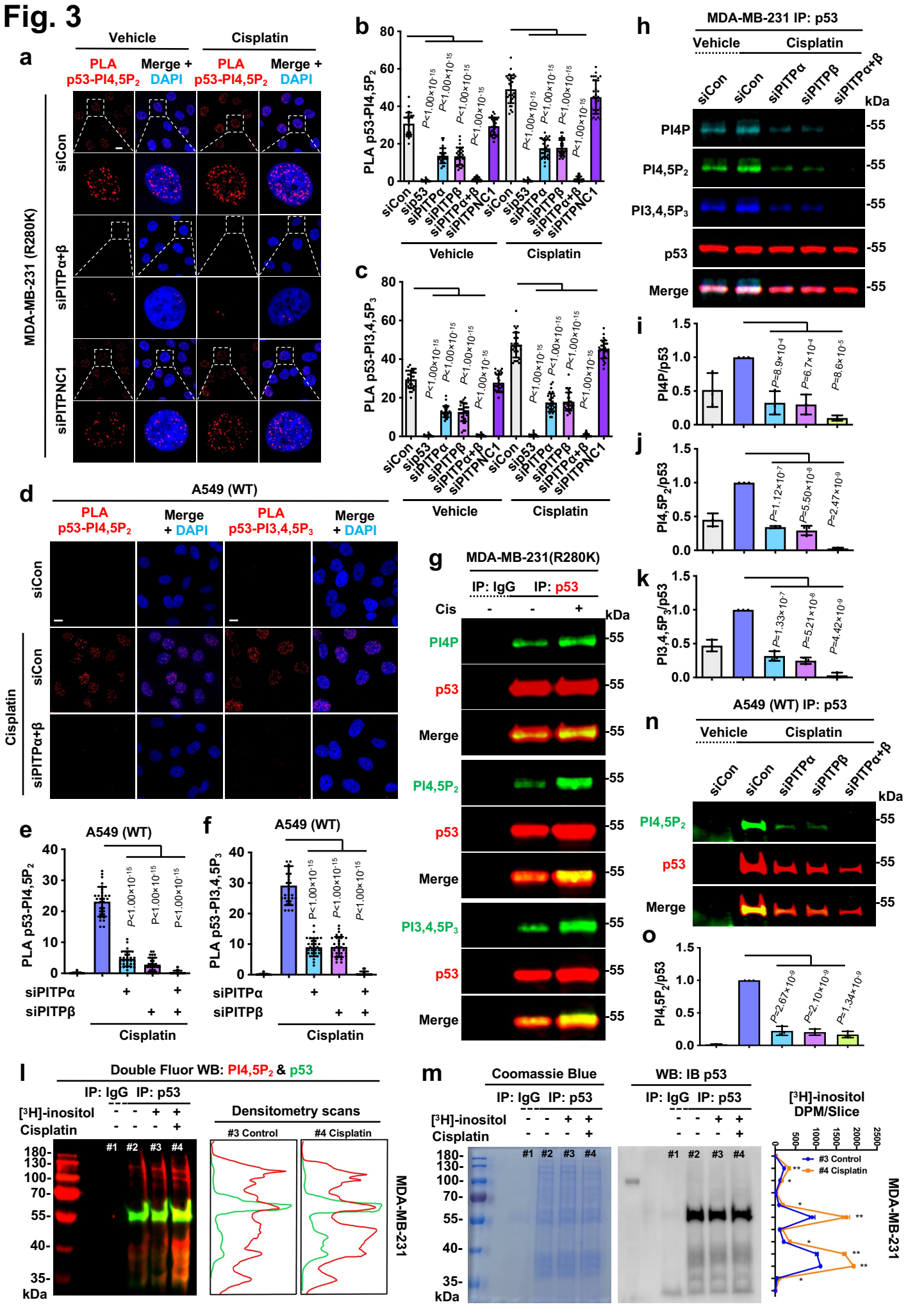
a
Vehicle
Cisplatin
PLA p53-PI4,5P2
Merge + DAPI
MDA-MB-231 (R280K)
siCon
siPITPα+β
siPITPNC1
b
PLA p53-PI4,5P2
siCon
sip53
siPITPα
siPITPβ
siPITPα+β
siPITPNC1
Vehicle
Cisplatin
c
PLA p53-PI3,4,5P3
d
A549 (WT)
PLA p53-PI4,5P2
Merge + DAPI
PLA p53-PI3,4,5P3
Cisplatin
e
A549 (WT)
PLA p53-PI4,5P2
siPITPα
siPITPβ
f
A549 (WT)
PLA p53-PI3,4,5P3
g
MDA-MB-231(R280K)
IP: IgG
IP: p53
Cis
PI4P
p53
Merge
PI4,5P2
PI3,4,5P3
h
MDA-MB-231 IP: p53
Vehicle
Cisplatin
siPITPα+β
kDa
PI4P
PI4,5P2
PI3,4,5P3
p53
Merge
i
PI4P/p53
j
PI4,5P2/p53
k
PI3,4,5P3/p53
n
A549 (WT) IP: p53
o
PI4,5P2/p53
l
Double Fluor WB: PI4,5P2 & p53
[3H]-inositol
Densitometry scans
#3 Control
#4 Cisplatin
MDA-MB-231
m
Coomassie Blue
WB: IB p53
[3H]-inositol DPM/Slice

Fig. 4

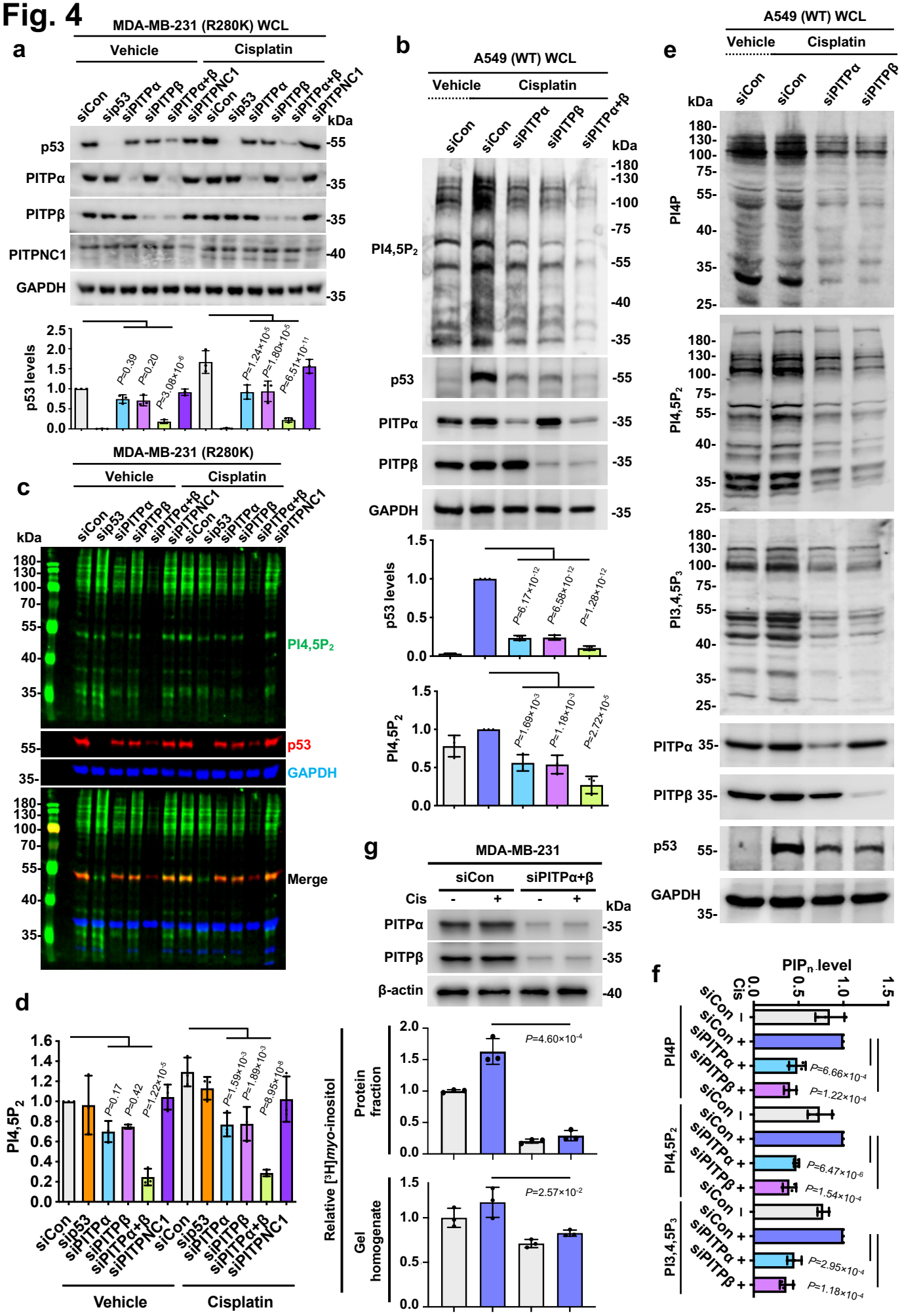
a
MDA-MB-231 (R280K) WCL
Vehicle
Cisplatin
siCon
sip53
siPITPα
siPITPβ
siPITPα+β
siPITPNC1
kDa
p53
PITPα
PITPβ
PITPNC1
GAPDH
p53 levels
P=0.39
P=0.20
P=3.08×10-6
P=1.24×10-5
P=1.80×10-5
P=6.51×10-11
b
A549 (WT) WCL
PI4,5P2
p53 levels
P=6.17×10-12
P=6.58×10-12
P=1.28×10-12
PI4,5P2
P=1.69×10-3
P=1.18×10-3
P=2.72×10-5
c
MDA-MB-231 (R280K)
PI4,5P2
p53
GAPDH
Merge
d
PI4,5P2
P=0.17
P=0.42
P=1.22×10-5
P=1.59×10-3
P=1.89×10-3
P=8.95×10-6
e
A549 (WT) WCL
PI4P
PI4,5P2
PI3,4,5P3
PITPα
PITPβ
p53
GAPDH
f
PIPn level
Cis
PI4P
PI4,5P2
PI3,4,5P3
P=6.66×10-4
P=1.22×10-4
P=6.47×10-6
P=1.54×10-4
P=2.95×10-4
P=1.18×10-4
g
MDA-MB-231
siCon
siPITPα+β
Cis
PITPα
PITPβ
β-actin
Relative [3H]myo-inositol
Protein fraction
Gel homogenate
P=4.60×10-4
P=2.57×10-2

Fig. 5

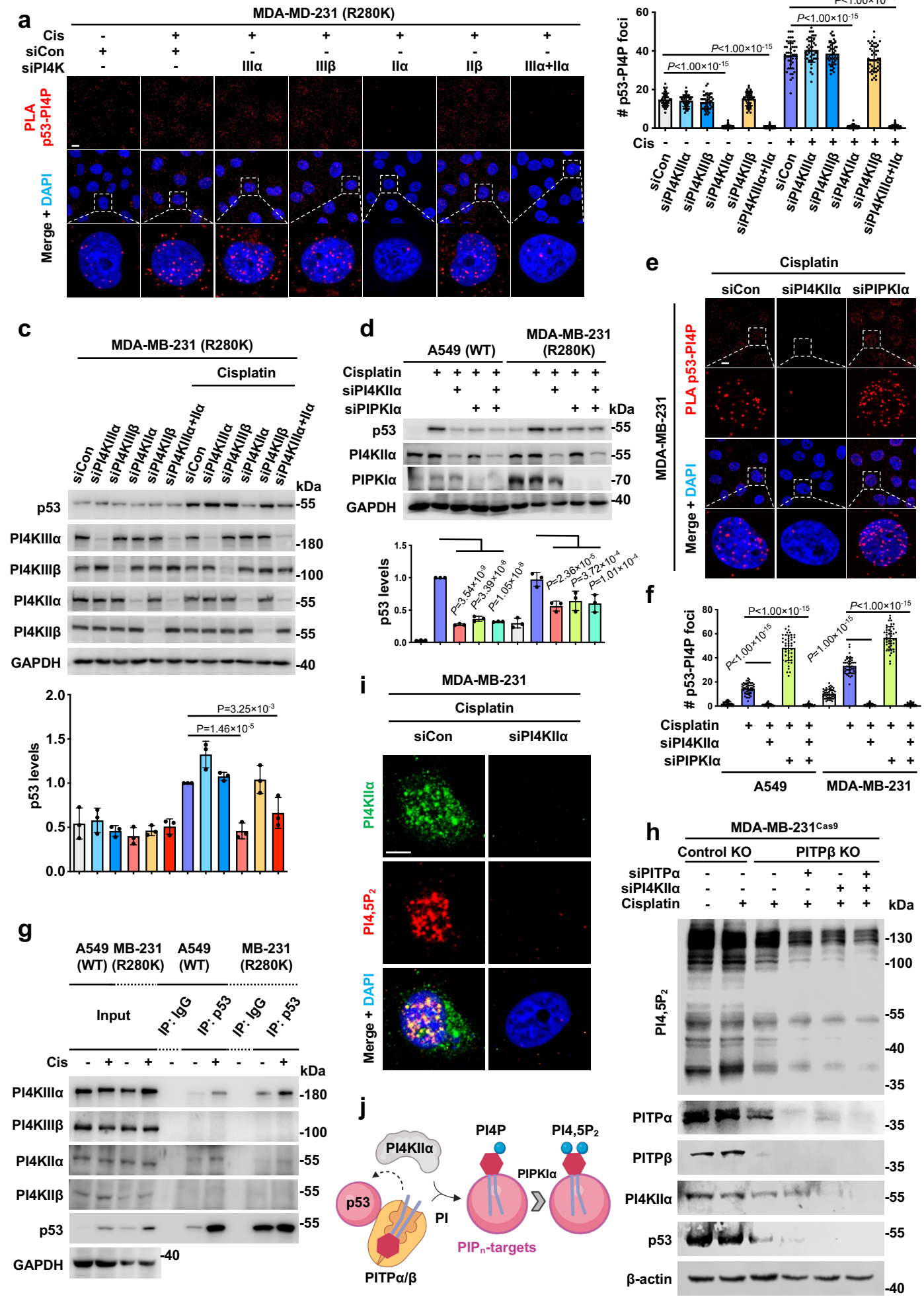
a
MDA-MD-231 (R280K)
Cis
siCon
siPI4K
IIIα
IIIβ
IIα
IIβ
IIIα+IIα
PLA p53-PI4P
Merge + DAPI
b
MDA-MB-231 (R280K)
p53-PI4P foci
P<1.00×10-15
Cis
siCon
siPI4KIIIα
siPI4KIIIβ
siPI4KIIα
siPI4KIIβ
siPI4KIIIα+IIα
c
MDA-MB-231 (R280K)
Cisplatin
kDa
p53
PI4KIIIα
PI4KIIIβ
PI4KIIα
PI4KIIβ
GAPDH
p53 levels
P=3.25×10-3
P=1.46×10-5
d
A549 (WT)
MDA-MB-231 (R280K)
Cisplatin
siPI4KIIα
siPIPKIα
PIPKIα
p53 levels
P=3.54×10-9
P=3.39×10-8
P=1.05×10-8
P=2.36×10-5
P=3.72×10-4
P=1.01×10-4
e
Cisplatin
siCon
siPI4KIIα
siPIPKIα
MDA-MB-231
PLA p53-PI4P
Merge + DAPI
f
p53-PI4P foci
P<1.00×10-15
A549
MDA-MB-231
g
A549 (WT)
MB-231 (R280K)
Input
IP: IgG
IP: p53
Cis
h
MDA-MB-231Cas9
Control KO
PITPβ KO
siPITPα
siPI4KIIα
Cisplatin
PI4,5P2
PITPα
PITPβ
β-actin
i
MDA-MB-231
Cisplatin
siCon
siPI4KIIα
PI4KIIα
PI4,5P2
Merge + DAPI
j
PI4KIIα
p53
PI
PI4P
PI4,5P2
PIPKIα
PIPn-targets
PITPα/β

Fig. 6

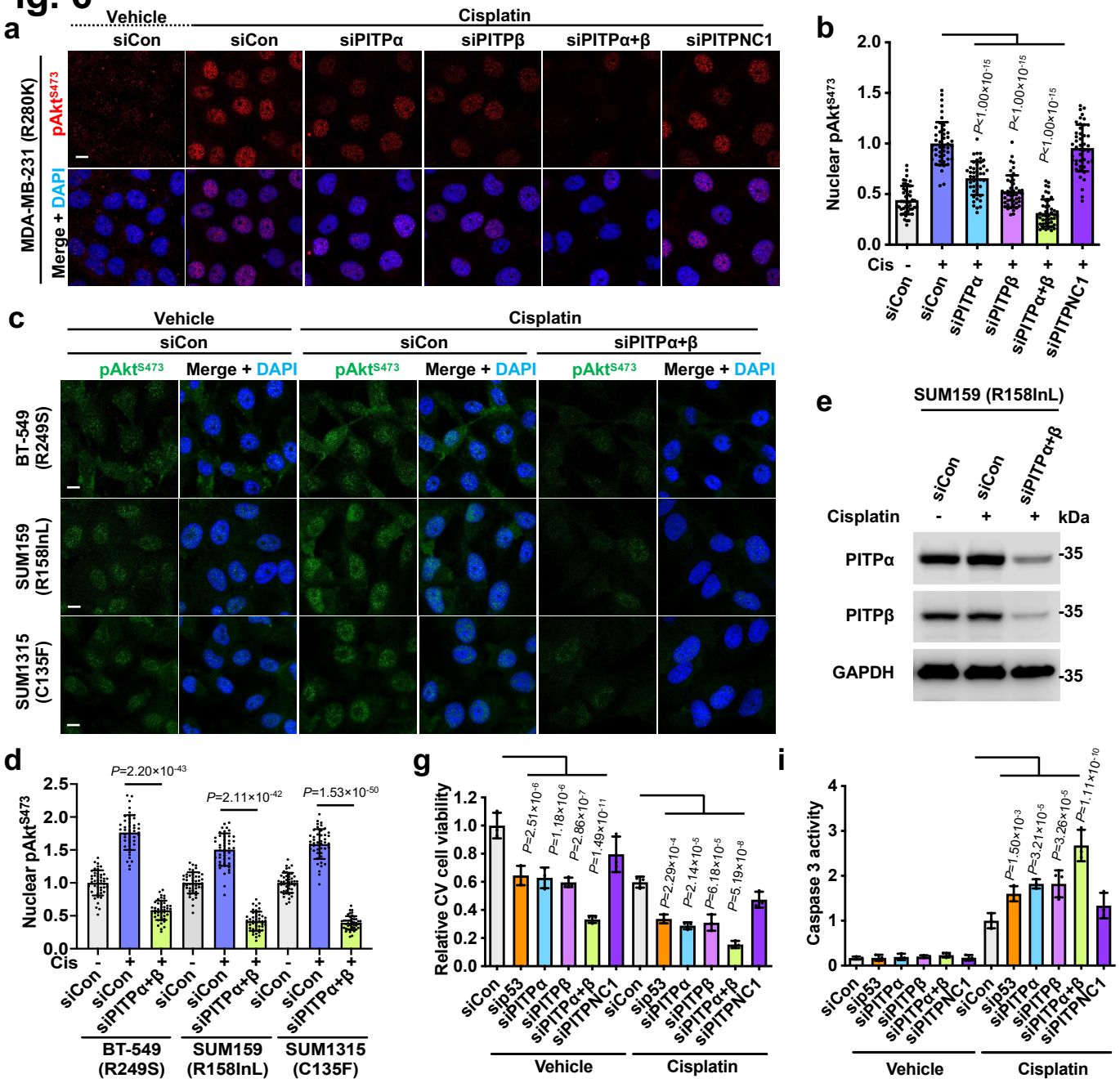
a
Vehicle
Cisplatin
siCon
siCon
siPITPα
siPITPβ
siPITPα+β
siPITPNC1
MDA-MB-231 (R280K)
pAkt^{S473}
Merge + DAPI
b
Nuclear pAkt^{S473}
Cis
siCon
siPITPα
siPITPβ
siPITPα+β
siPITPNC1
P<1.00×10^{-15}
c
Vehicle
Cisplatin
siCon
siPITPα+β
pAkt^{S473}
Merge + DAPI
BT-549 (R249S)
SUM159 (R158InL)
SUM1315 (C135F)
e
SUM159 (R158InL)
siCon
siPITPα+β
Cisplatin
kDa
PITPα
PITPβ
GAPDH
-35
d
Nuclear pAkt^{S473}
P=2.20×10^{-43}
P=2.11×10^{-42}
P=1.53×10^{-50}
Cis
siCon
siPITPα+β
BT-549 (R249S)
SUM159 (R158InL)
SUM1315 (C135F)
g
Relative CV cell viability
P=2.51×10^{-6}
P=1.18×10^{-6}
P=2.86×10^{-7}
P=1.49×10^{-11}
P=2.29×10^{-4}
P=2.14×10^{-5}
P=6.18×10^{-5}
P=5.19×10^{-8}
siCon
sip53
siPITPα
siPITPβ
siPITPα+β
siPITPNC1
Vehicle
Cisplatin
i
Caspase 3 activity
P=1.50×10^{-3}
P=3.21×10^{-5}
P=3.26×10^{-5}
P=1.11×10^{-10}
f
MDA-MB-231 (R280K)
siCon
sip53
siPITPα
siPITPβ
siPITPα+β
siPITPNC1
Vehicle
Cisplatin
h
MDA-MB-231^{Cas9}
Control KO
PITPβ KO
siCon
siPITPα
siPITPα+β
+Cis

Fig. 7

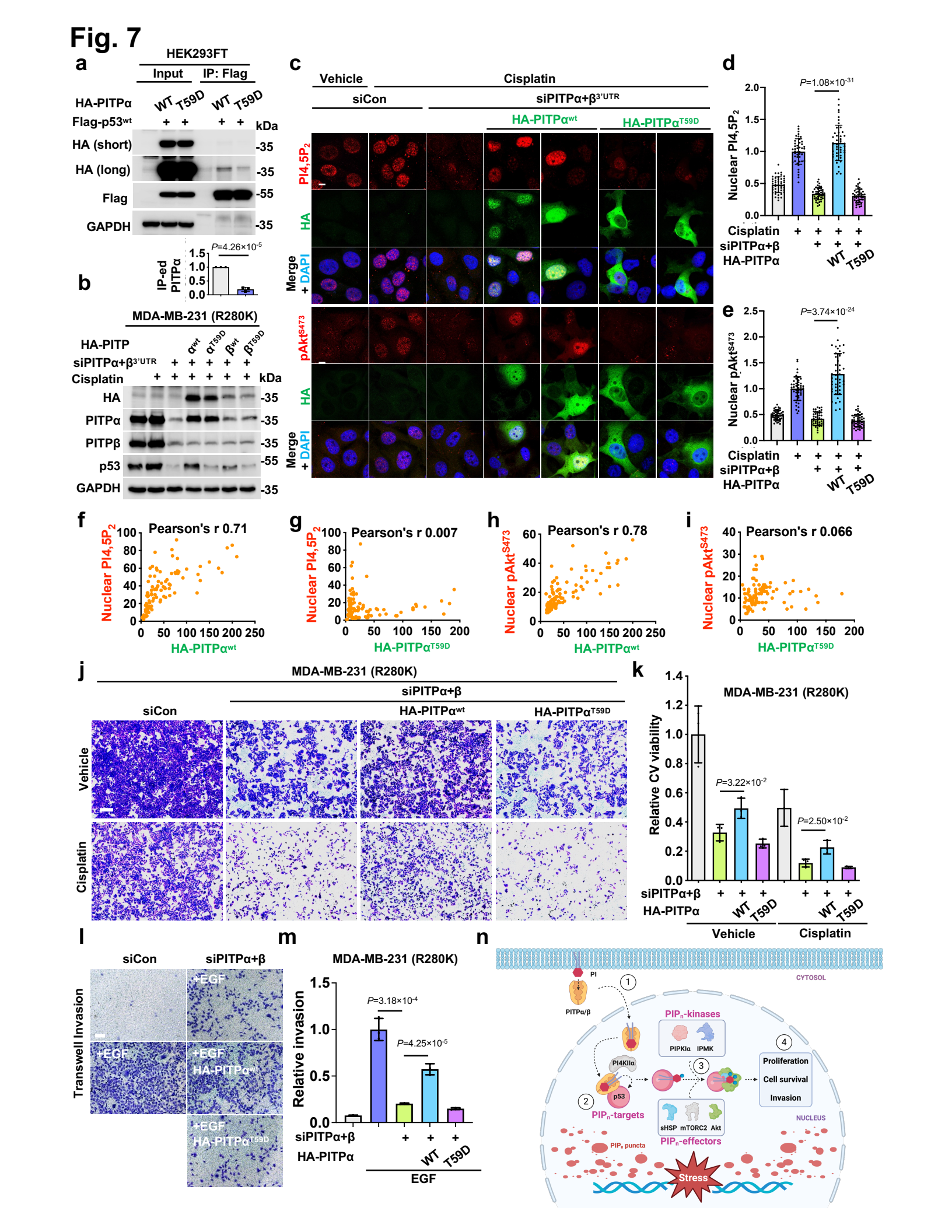
a
HEK293FT
Input
IP: Flag
HA-PITPα
WT
T59D
WT
T59D
Flag-p53wt
kDa
HA (short)
HA (long)
Flag
GAPDH
-35
-55
b
IP-ed PITPα
P=4.26×10-5
MDA-MB-231 (R280K)
HA-PITP
αwt
αT59D
βwt
βT59D
siPITPα+β3'UTR
Cisplatin
HA
PITPα
PITPβ
p53
GAPDH
c
Vehicle
Cisplatin
siCon
siPITPα+β3'UTR
HA-PITPαwt
HA-PITPαT59D
PI4,5P2
HA
Merge + DAPI
pAktS473
d
P=1.08×10-31
Nuclear PI4,5P2
Cisplatin
siPITPα+β
HA-PITPα
WT
T59D
e
P=3.74×10-24
Nuclear pAktS473
f
Pearson's r 0.71
Nuclear PI4,5P2
HA-PITPαwt
g
Pearson's r 0.007
HA-PITPαT59D
h
Pearson's r 0.78
Nuclear pAktS473
i
Pearson's r 0.066
j
MDA-MB-231 (R280K)
siPITPα+β
siCon
HA-PITPαwt
HA-PITPαT59D
Vehicle
Cisplatin
k
MDA-MB-231 (R280K)
Relative CV viability
P=3.22×10-2
P=2.50×10-2
siPITPα+β
HA-PITPα
WT
T59D
Vehicle
Cisplatin
l
siCon
siPITPα+β
Transwell Invasion
+EGF
+EGF HA-PITPαwt
+EGF HA-PITPαT59D
m
MDA-MB-231 (R280K)
Relative invasion
P=3.18×10-4
P=4.25×10-5
siPITPα+β
HA-PITPα
WT
T59D
EGF
n
PI
PITPα/β
CYTOSOL
PIPn-kinases
PIPKIα
IPMK
PI4KIIα
p53
PIPn-targets
sHSP
mTORC2
Akt
PIPn-effectors
PIPn puncta
Proliferation
Cell survival
Invasion
NUCLEUS
Stress

Extended Data Fig. 1

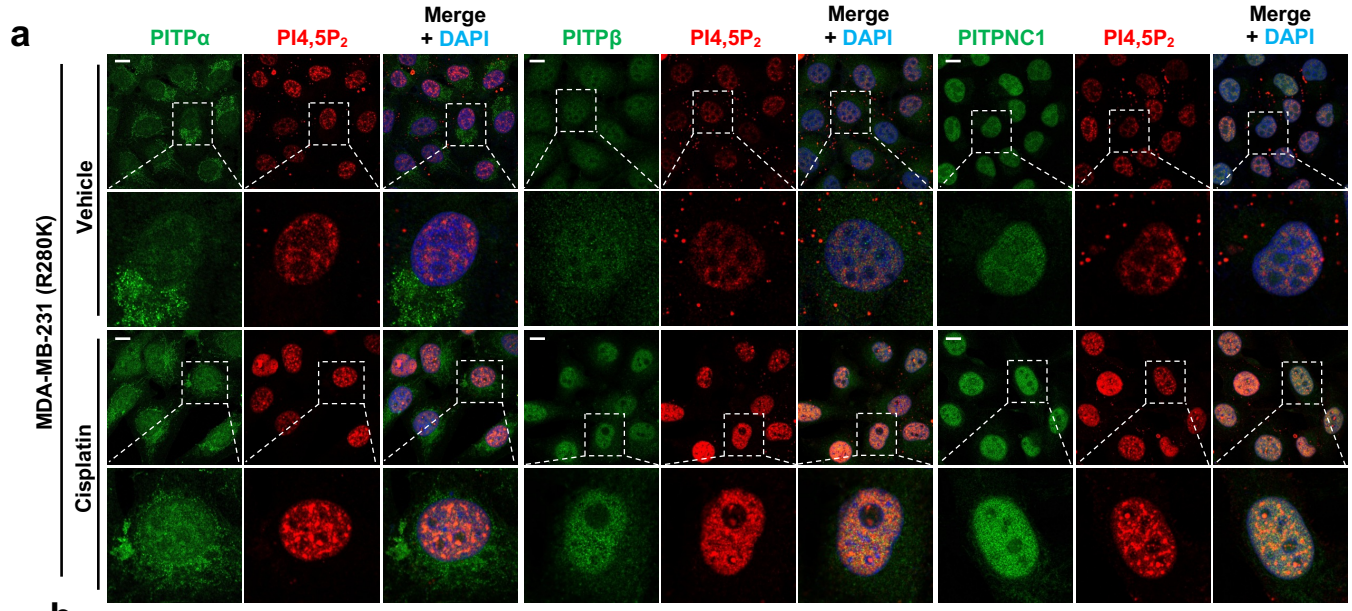

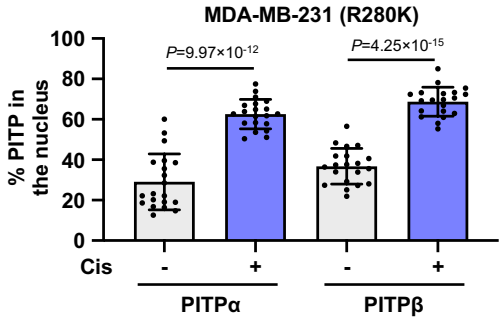

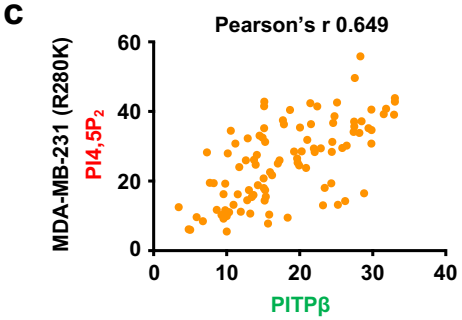

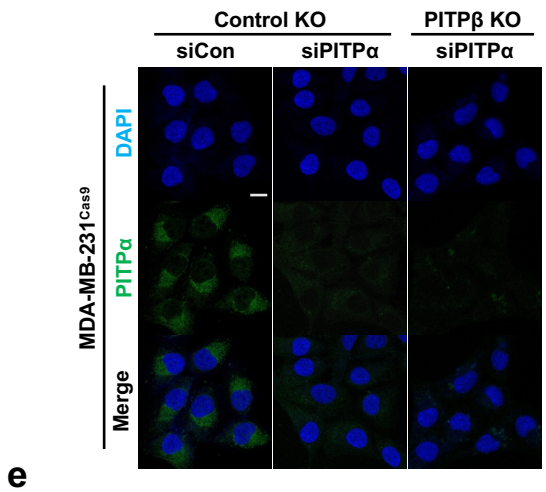

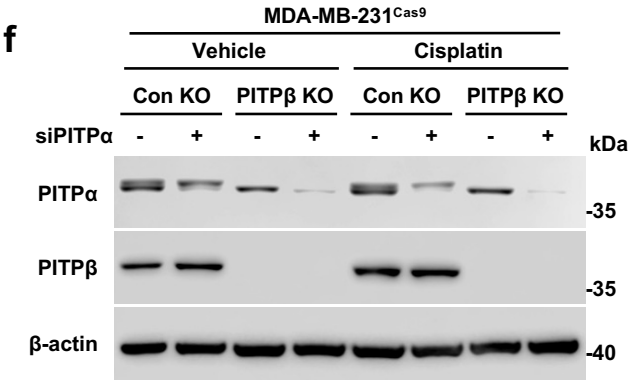

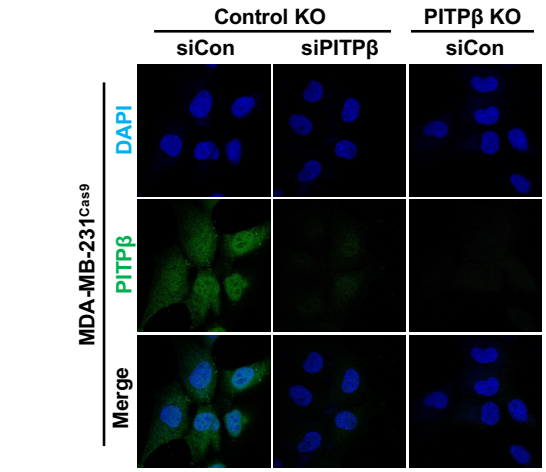

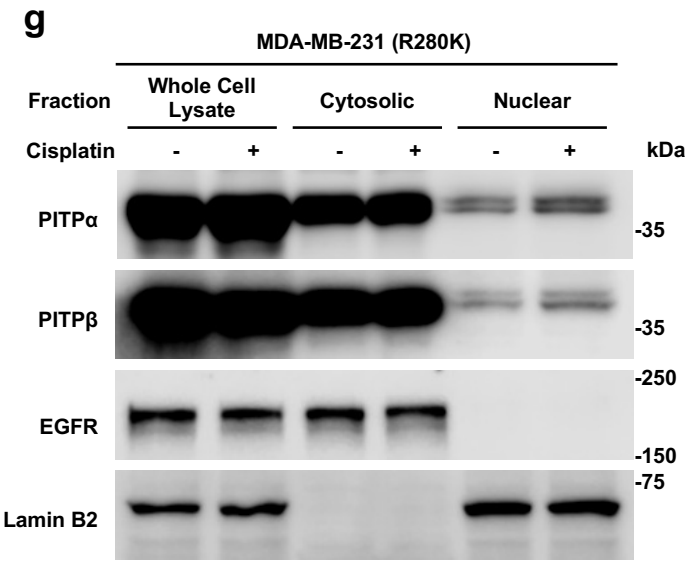

Extended Data Fig. 2

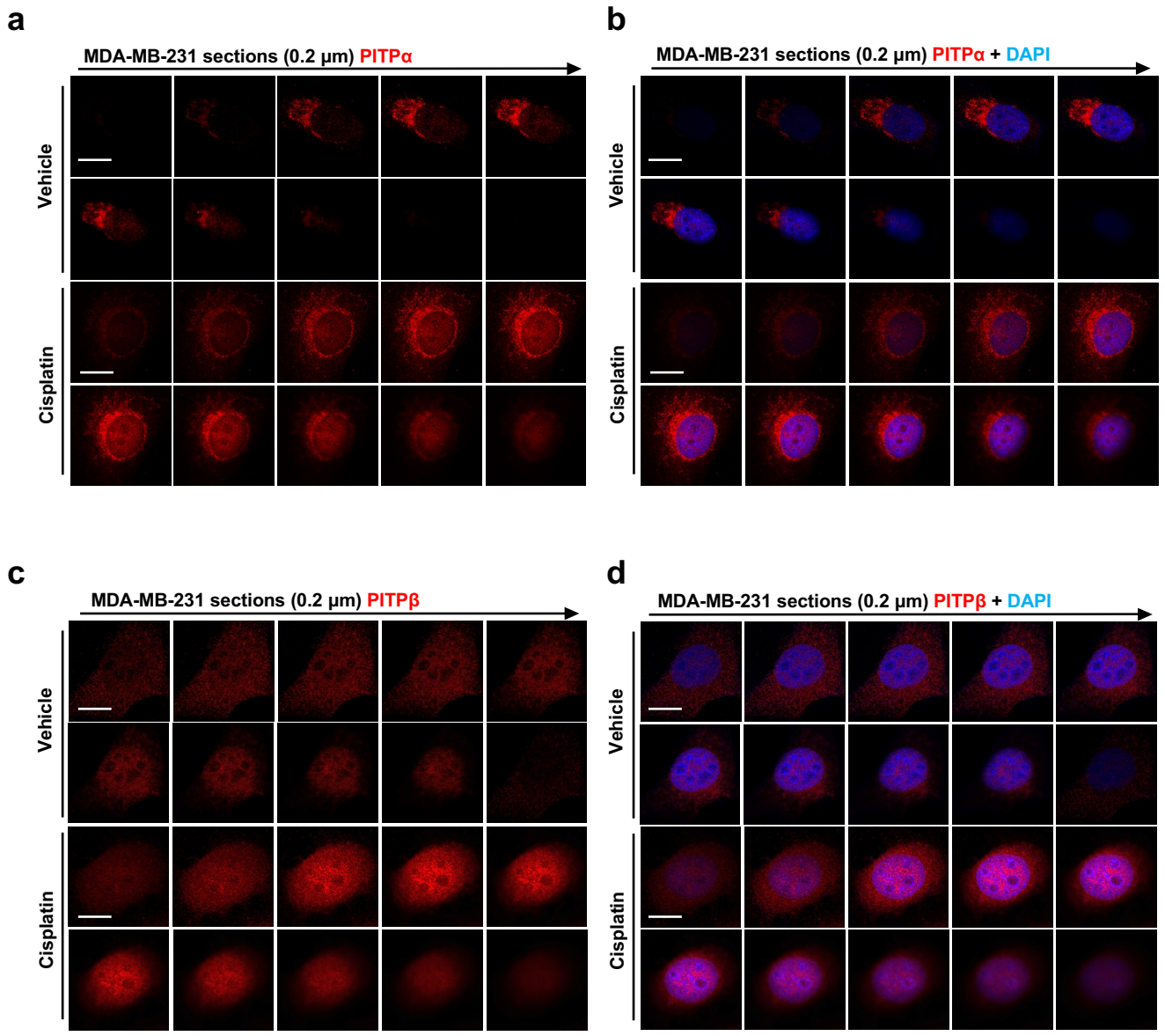

Extended Data Fig. 3

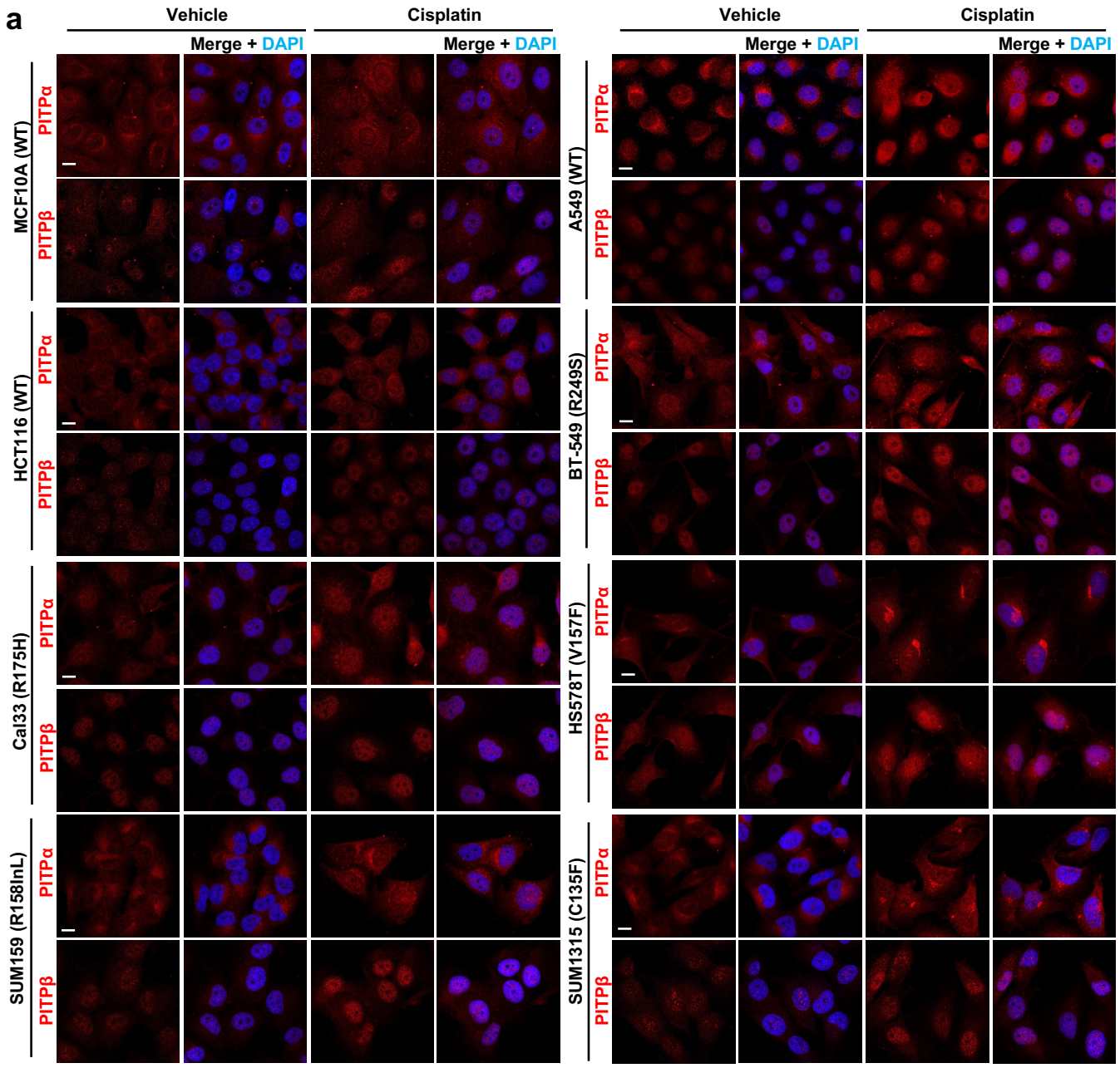

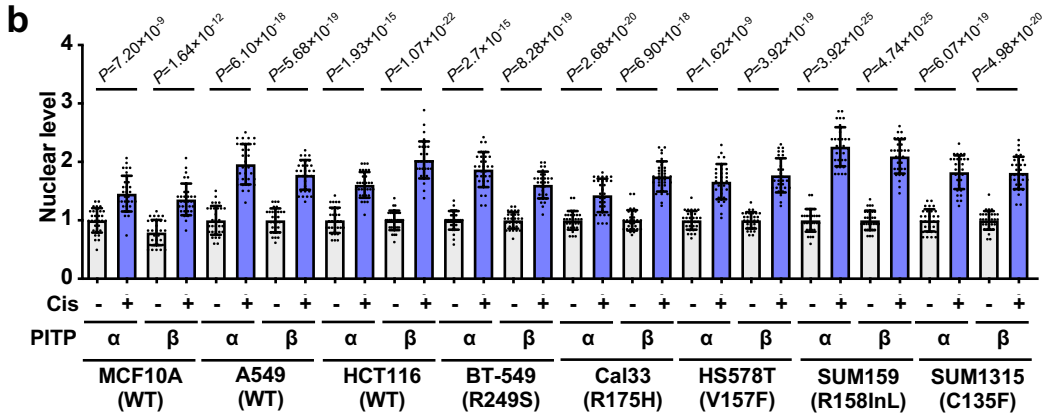

Extended Data Fig. 4

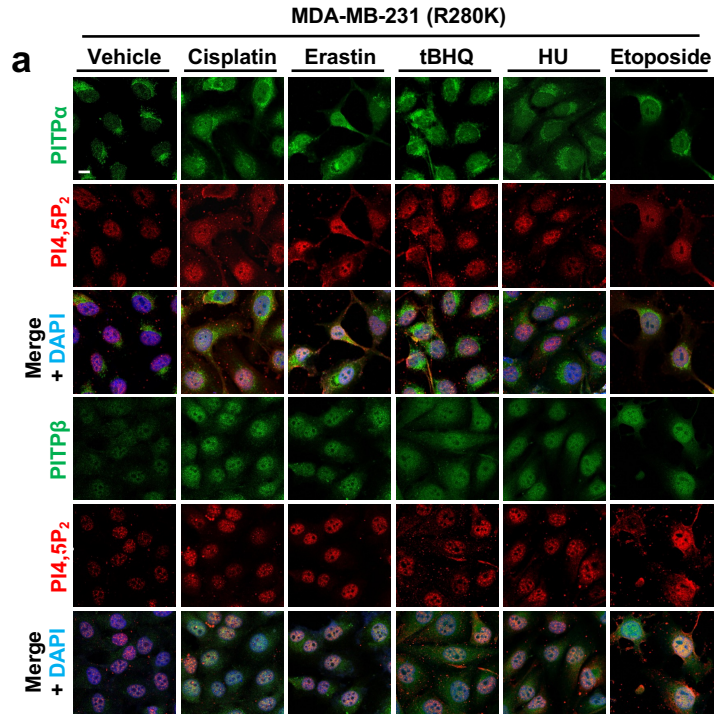

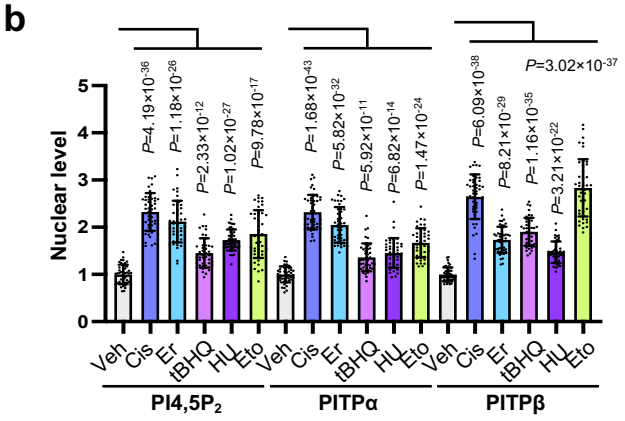

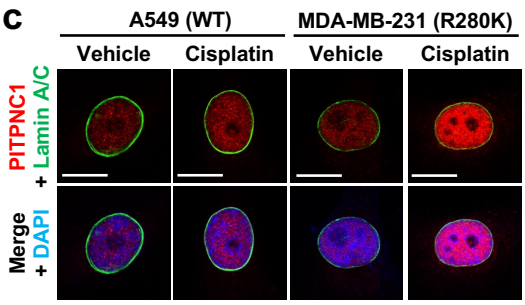

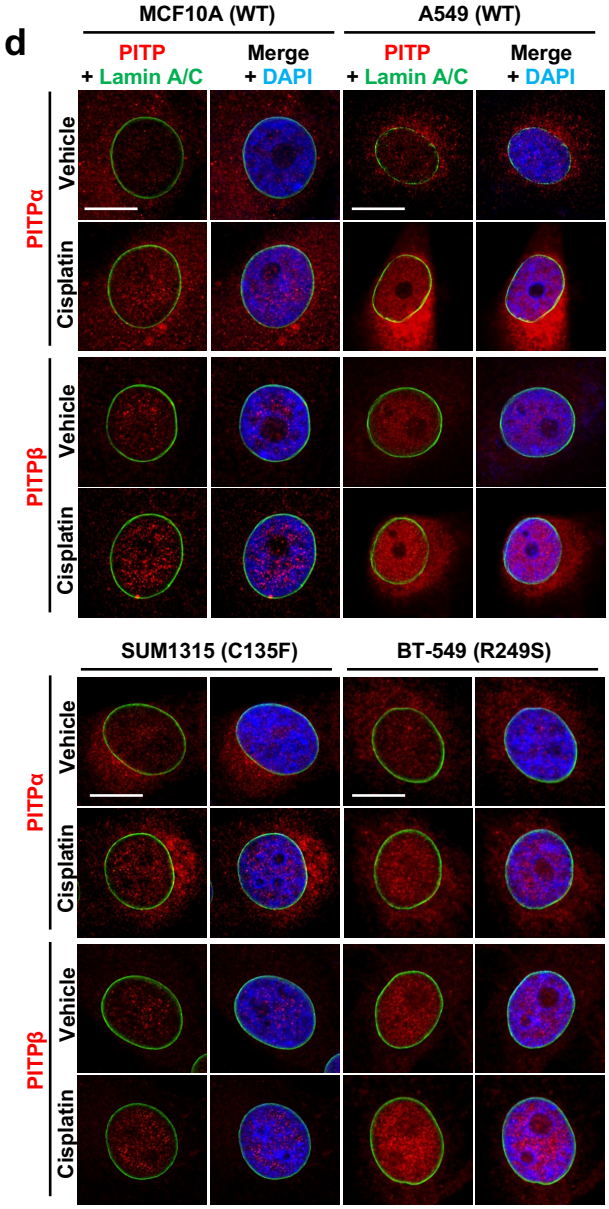

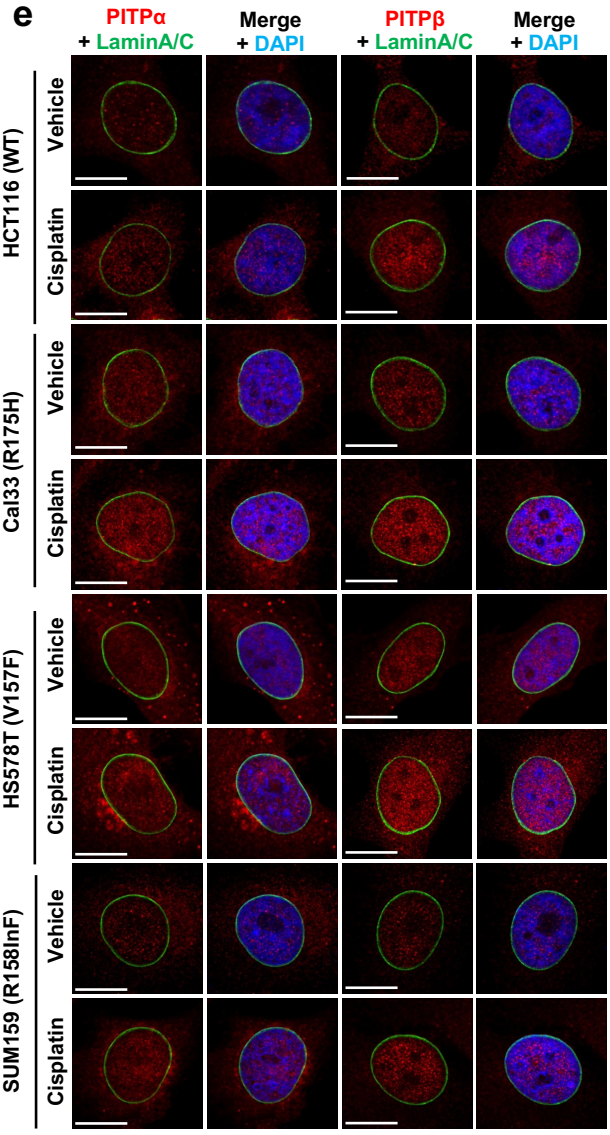

Extended Data Fig. 5

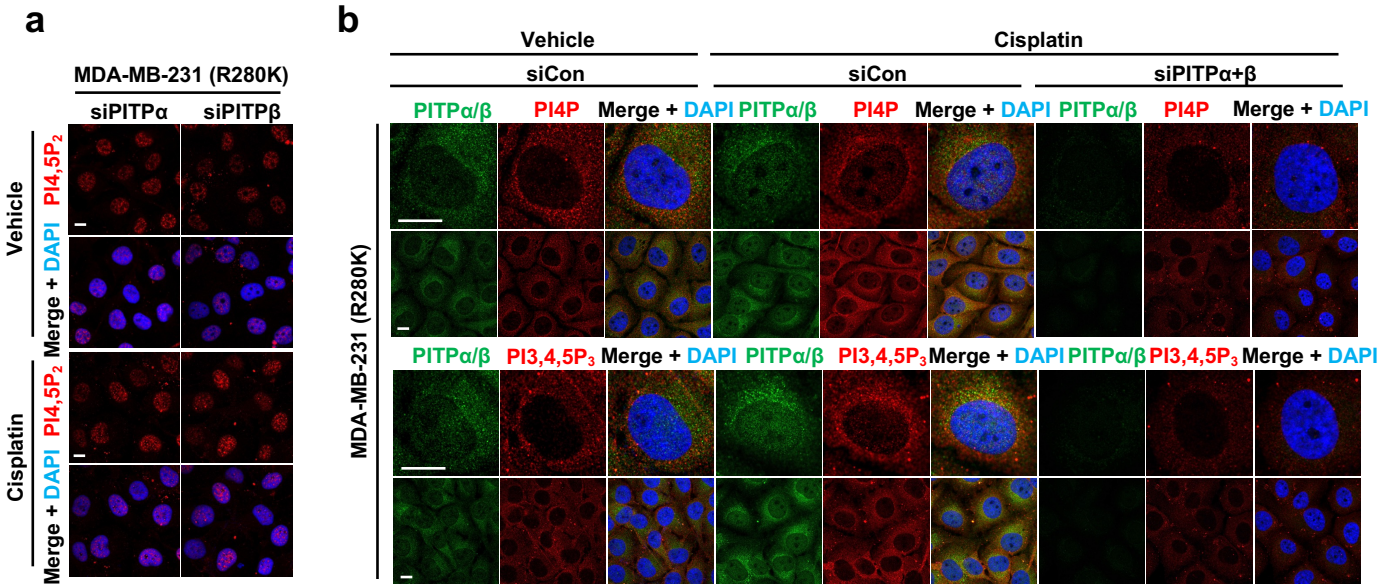

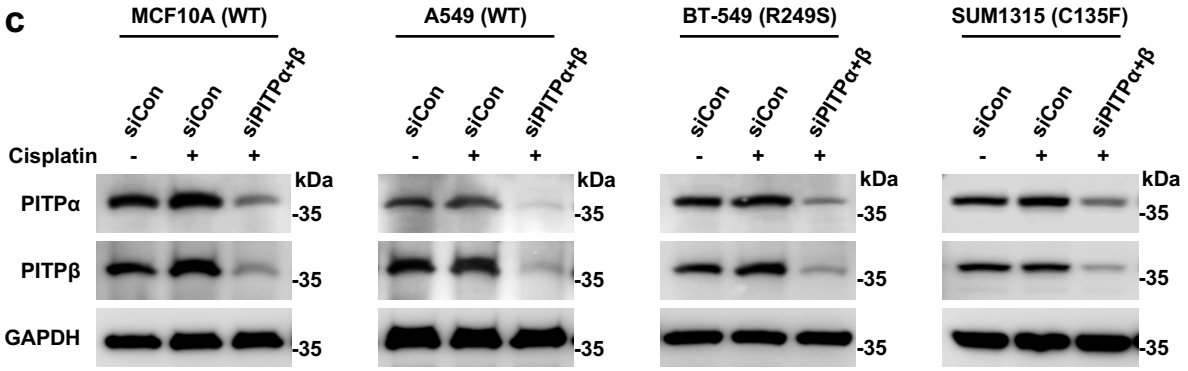

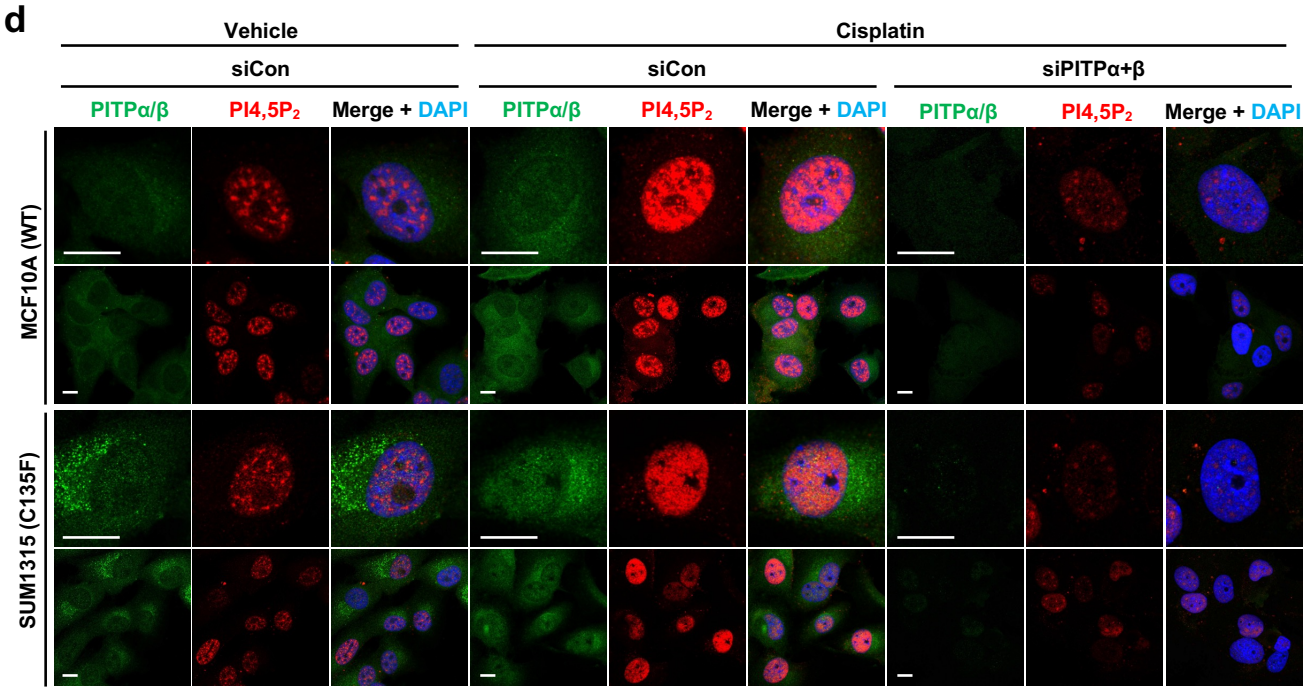

Extended Data Fig. 6

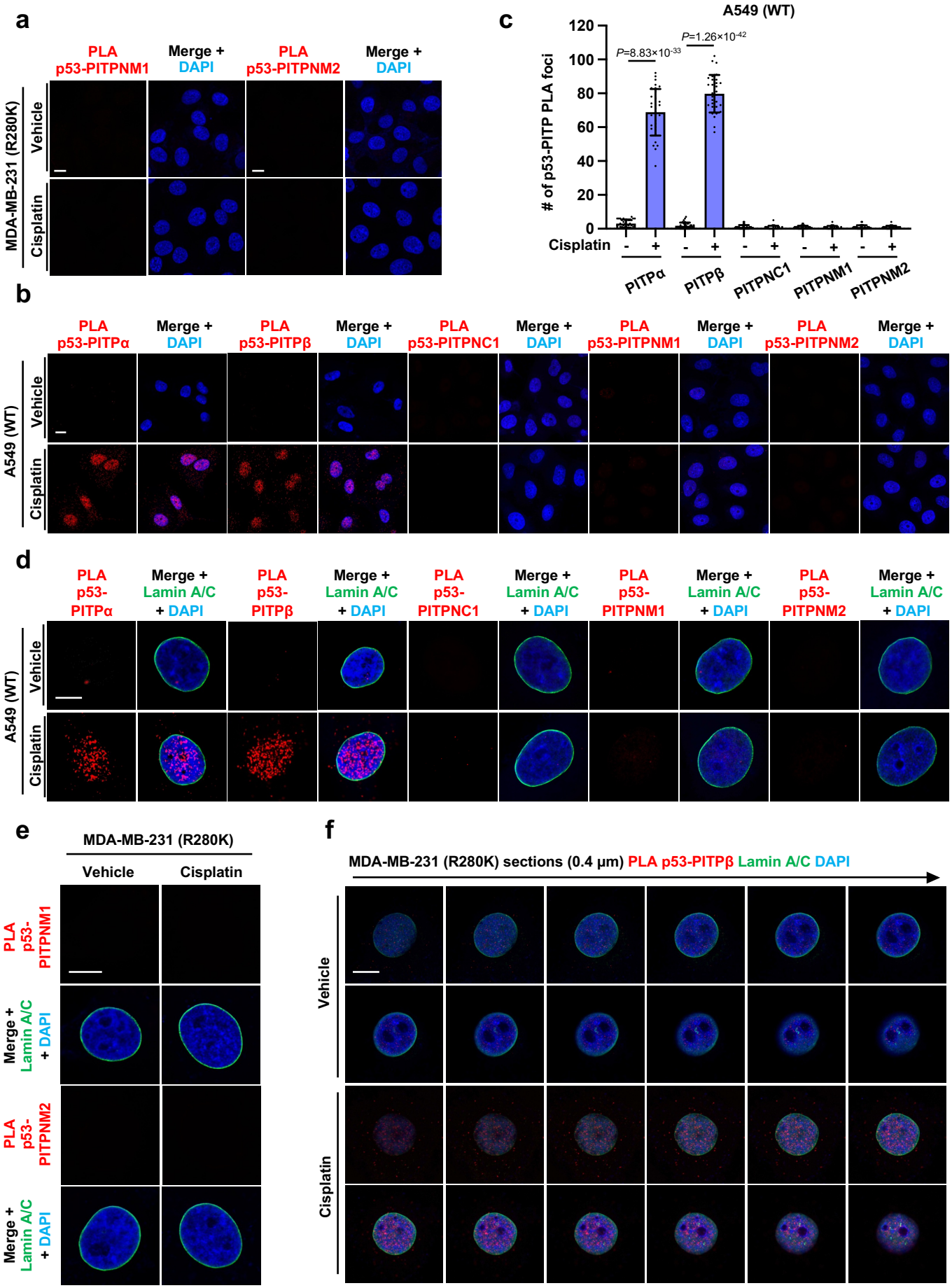

Extended Data Fig. 7

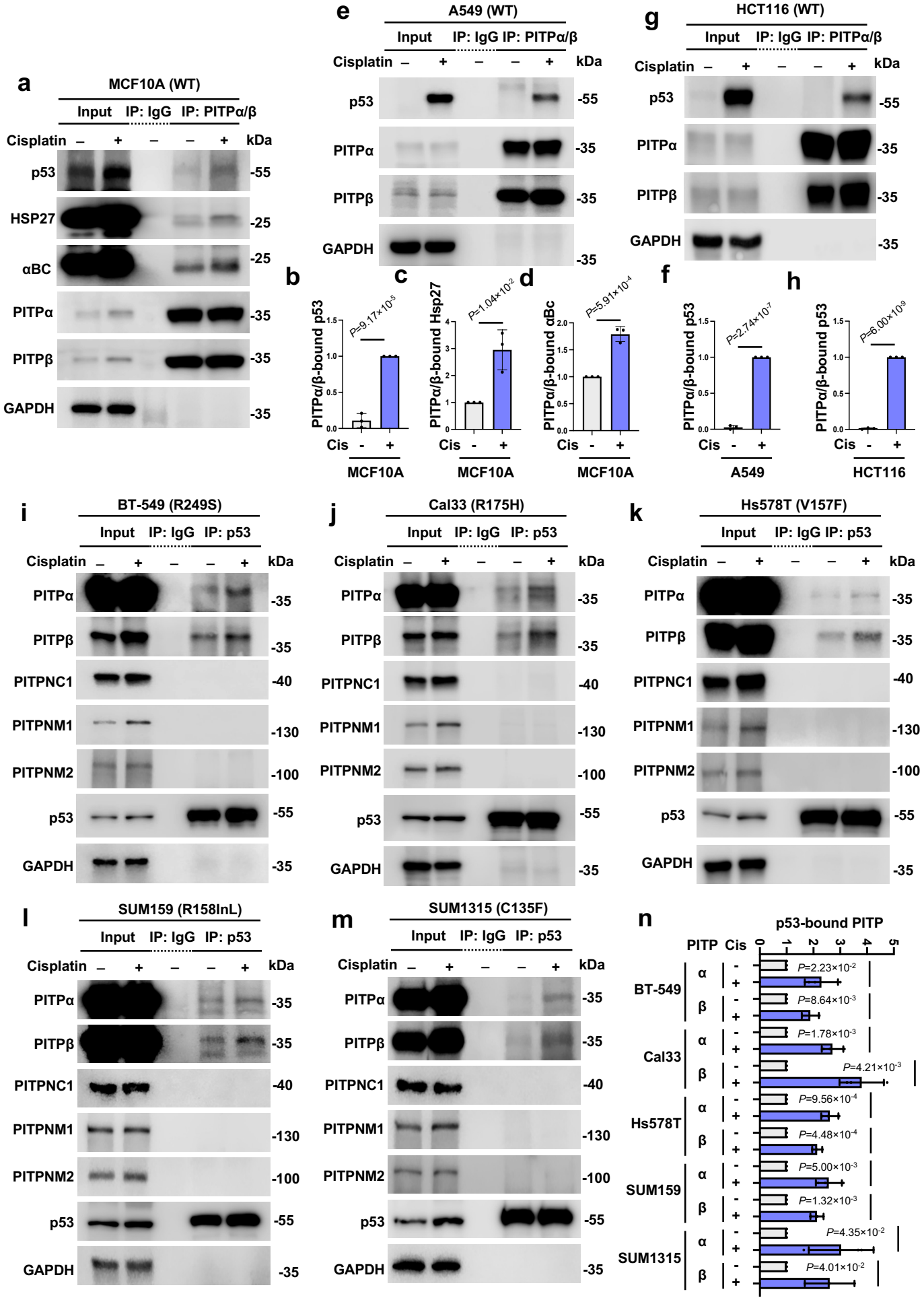

Extended Data Fig. 8

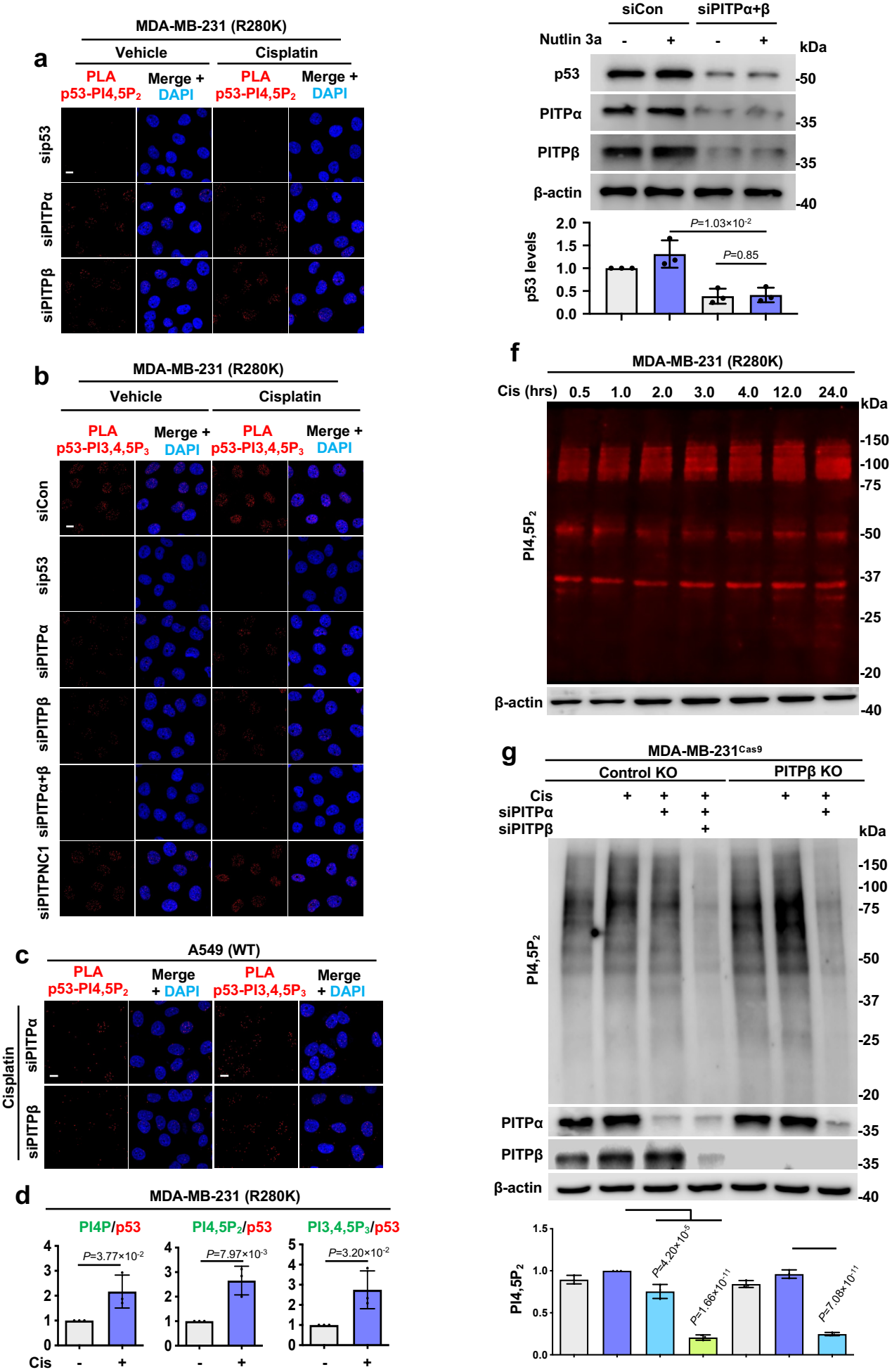

Extended Data Fig. 9

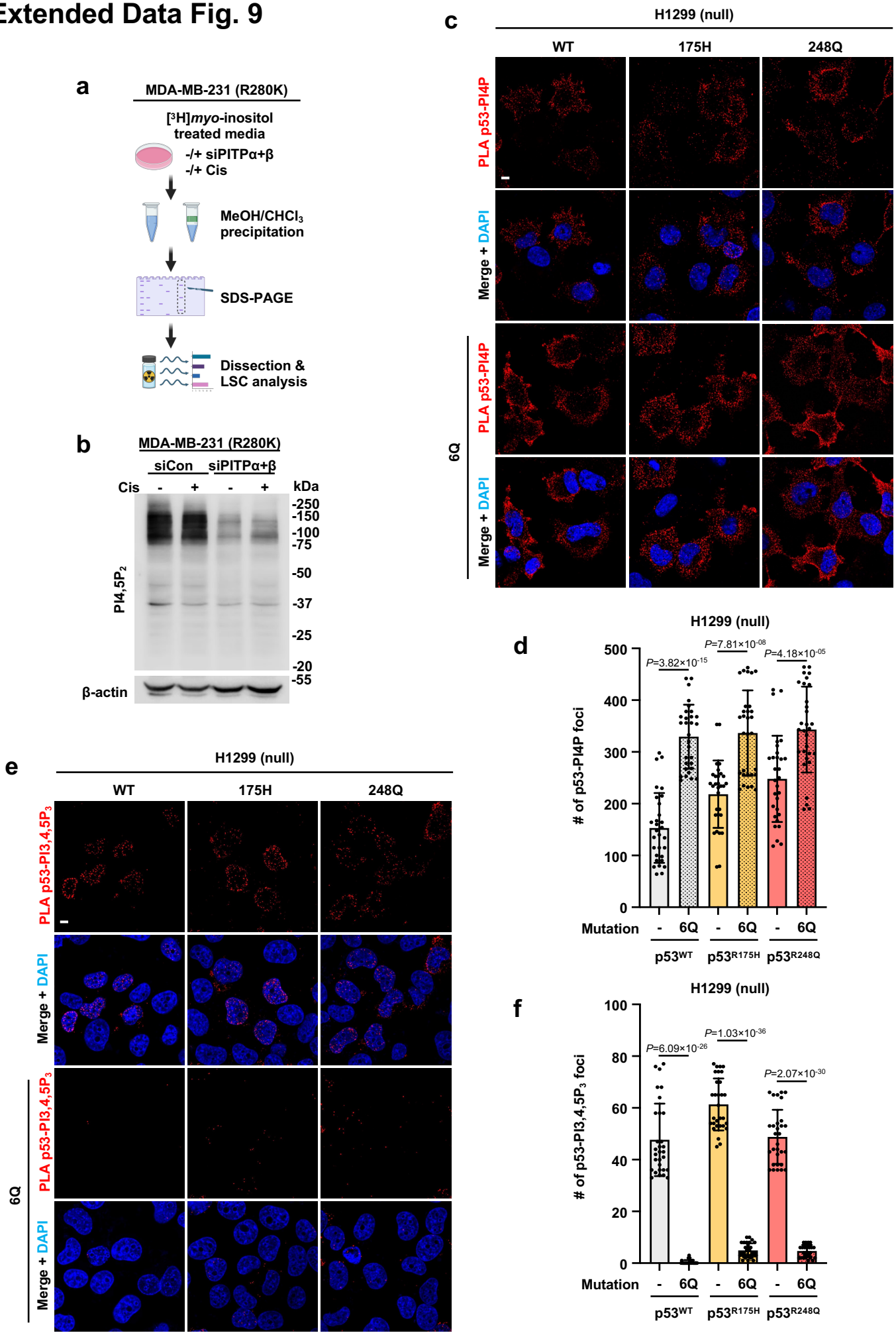

Extended Data Fig. 10

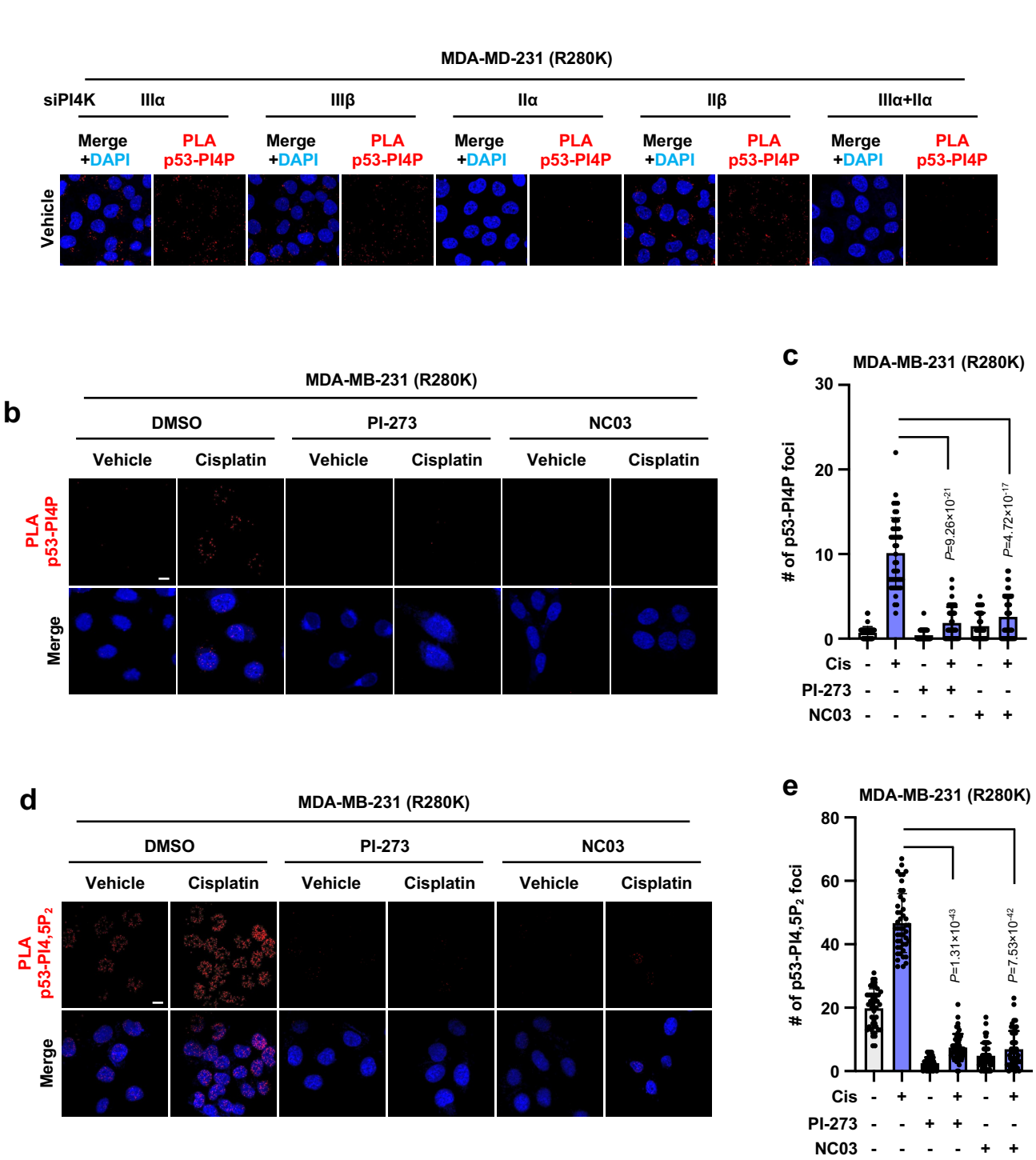

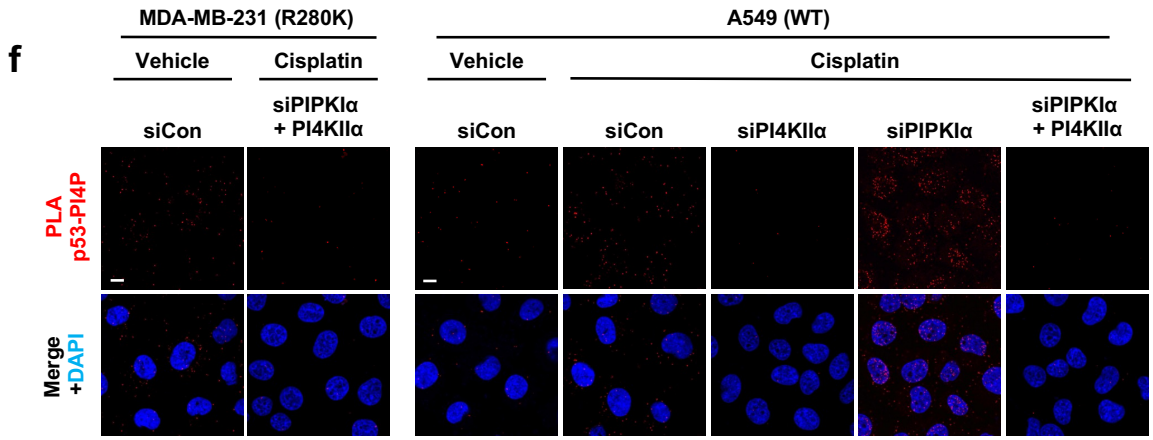

Extended Data Fig. 11

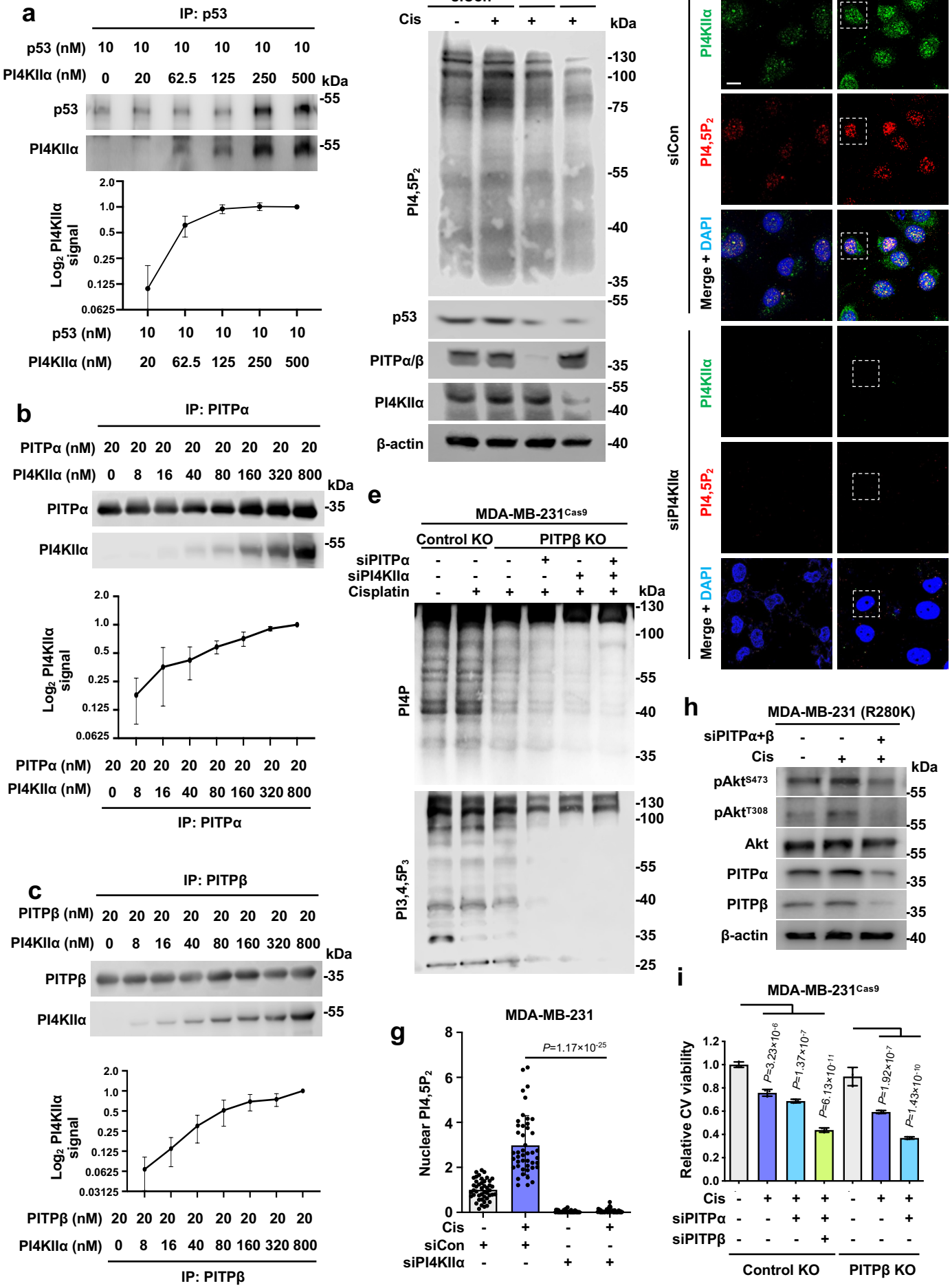
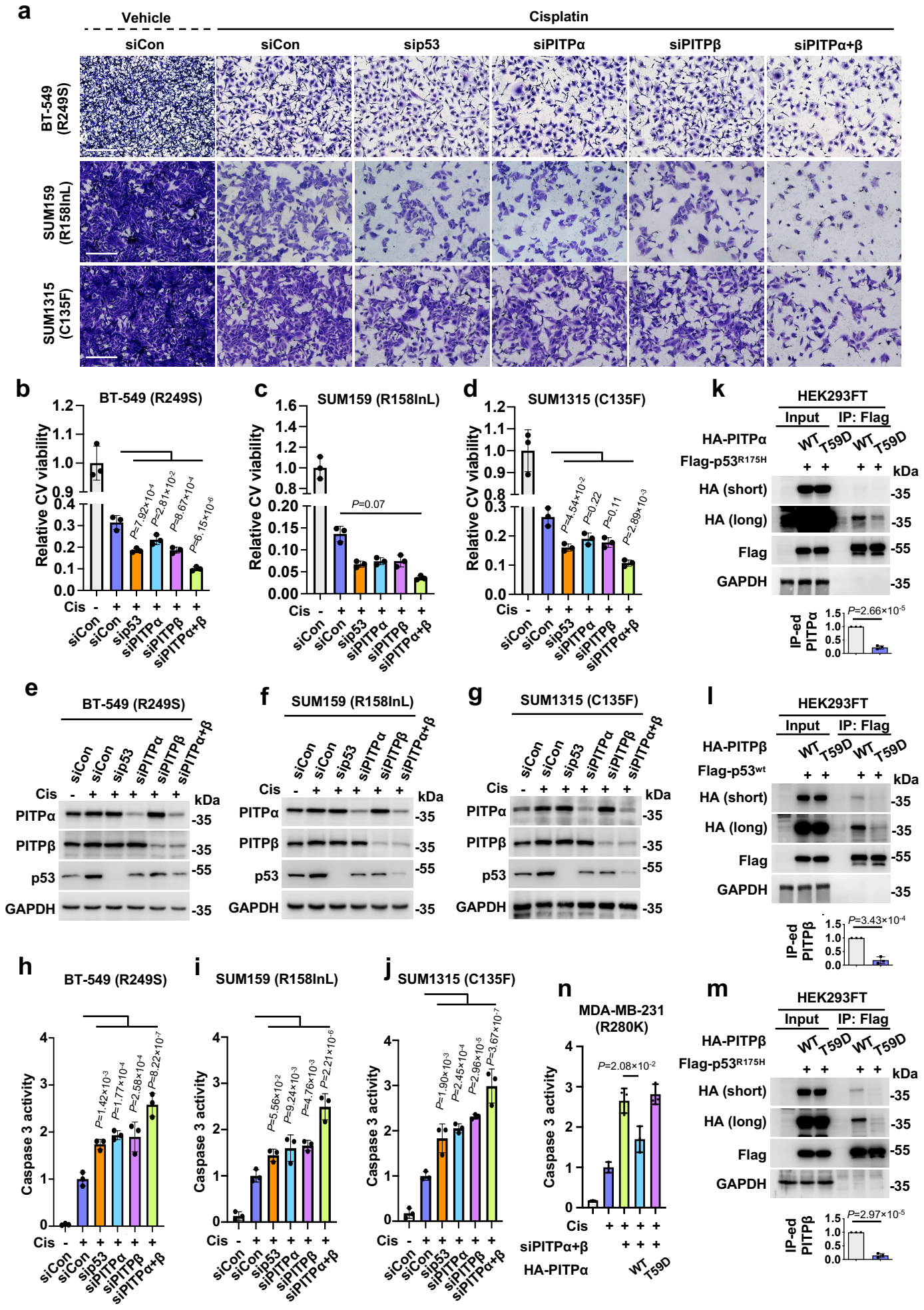
Extended Data Fig. 12